Title
Spatiotemporal Organization of Signaling Proteins on the Cell Membrane Studied by Spatially Patterned Supported Lipid Bilayers

Author
Kai, Hiroyuki

Publication Date
2015

Peer reviewed|Thesis/dissertation

Spatiotemporal Organization of Signaling Proteins on the Cell Membrane Studied by Spatially Patterned Supported Lipid Bilayers

By

Hiroyuki Kai

A dissertation submitted in partial satisfaction of the

requirements for the degree of

Doctor of Philosophy

in

Chemistry

in the

Graduate Division

of the

University of California, Berkeley

Committee in charge:

Professor Jay T. Groves, Chair
Professor Naomi S. Ginsberg
Professor Matthew B. Francis
Professor Luke P. Lee

Spring 2015

Spatiotemporal Organization of Signaling Proteins on the Cell Membrane Studied by Spatially Patterned Supported Lipid Bilayers

By

Hiroyuki Kai

Abstract

Spatiotemporal Organization of Signaling Proteins on the Cell Membrane Studied by Spatially Patterned Supported Lipid Bilayers

by

Hiroyuki Kai

Doctor of Philosophy in Chemistry

University of California, Berkeley

Professor Jay T. Groves, Chair

Membrane proteins in the cell are dynamically organized to process the information from the environment and can precisely regulate cell signaling and functions. The spatiotemporal dynamics of proteins can be investigated by means of fluorescence microscopy to elucidate the mechanism of cell signaling. In addition, a fluid lipid bilayer on a flat glass surface with two-dimensional mobility of lipid molecules, called supported lipid bilayer (SLB), has proved a powerful tool to investigate cell-cell interactions and reconstitute membrane protein functions in vitro.

The T cell is activated by an antigen presenting cell (APC) when a T cell receptor (TCR) is engaged by a major histocompatibility complex (MHC) on the APC. To precisely regulate T cell activation, the T cell organizes membrane proteins and other signaling molecules into particular spatial organization. We applied spatial patterning technologies to the SLB to probe and modulate spatiotemporal dynamics of the T cell signaling, and investigated its mechanism by fluorescence microscopy. In Chapter 2, the SLB embedded with a regular array of gold nanoparticles (nanodot array) was used to probe T cell receptor (TCR) microclusters on the T cell membrane. This nanodot array probes membrane protein assemblies below the diffraction limit of light in living cells by a mechanical means, which complements super-resolution microscopy. In Chapter 3, the spatiotemporal dynamics of Linker for Activation of T cells (LAT), another important protein in T cell signaling, was investigated by localized stimulation to the T cell using a polymer-patterned SLB. This method effectively separated the sites of T cell activation far apart from each other, and elucidated the LAT dynamics upon T cell activation more clearly than ever.

ESCRT proteins play an essential role in membrane budding and scission, and it is suggested that they use membrane curvatures to regulate their functions. In Chapter 4, we made a cover glass with nano-hollows of $\sim$100 nm in depth and $\sim$200 nm in diameter, and investigated the interaction between the SLB on the nano-curvature and ESCRT proteins. Highly selective accumulation of ESCRTs into the part of SLB with nano-curvature was observed, which indicated the ESCRTs sense the artificial nano-curvature just as they do in vivo. This

experimental platform opens up possibilities for precise kinetic studies on ESCRTs in vitro.

Acknowledgement

First of all, I thank my advisor Professor Jay T. Groves for having me in the research group, allowing me to explore many interesting things in biophysical science, and mentoring me with great patience. Not only science, I also enjoyed rock climbing activities with him in lab retreats in Yosemite. (To tell the truth, all of my rock climbing experiences were with Jay.)

I also thank other faculty committee members of my qualifying exam and dissertation, Professor Naomi S. Ginsberg, Professor Matthew B. Francis, Professor Luke P. Lee, and Professor Evan R. Williams, for giving me valuable comments on my research, presentation, and dissertation.

I also thank all my current and past colleagues in lab. Especially, I thank Dr. Niña Caculitan for working with me on an interesting project as well as encouraging me in the early stage of my graduate school. I thank Eulanca Liu for working with me as well as teaching me experiments. I thank Dr. Nicole Fay for teaching me protein cloning, working with me on several projects, and helping me learn biology before my qualifying exam. I thank Dr. Il-Hyung Lee and Professor James Hurley for bringing an interesting project to me, which ended up a fruitful collaboration in which we benefited from each other. I thank Helen Sun for working with me on experiment. I also thank Professor Theobald Lohmüller, Dr. Christopher Rhodes, and Dr. Wan Li for teaching me and having discussions with me about nanofabrication. I thank Dr. Samuel Lord for building great and easy-to-use microscopes in the lab. Without those microscopes he built, the majority of my experiment would have not been done. I thank Dr. Hsiung-Lin Tu for talking with me in the empty lab in the late night.

I thank Ms. Laurie Mason, an assistant to Professor Jay T. Groves, for her kind support throughout my graduate work. She helped me have my graduate work run smooth.

I also thank my former advisors, Professor Takuzo Aida, Professor Kazushi Kinbara, and Dr. Kentaro Tashiro, for their support and encouragement when I decided to study in the US six years ago. Without them, I would not be here now.

Finally I thank my father Yoshihide, my mother Kyoko, and my brother Yoshiaki, for their constant support and understanding on my graduate study abroad in the US, and Kaori Takano for her warm encouragement and support.

Contents

List of Figures

Chapter 1

General Introduction

Cells use a network of interacting proteins to process the signal from the environment to function properly. It has become widely accepted that not only the components and bulk quantity of proteins, but also the dynamic spatial arrangement of signaling molecules, are important parameters in cell signaling. T cell activation and ESCRT machinery are two remarkable examples of biological systems that take advantage of the characteristic environment of the cell membrane.

1.1 T cell signaling

1.1.1 T cells in an adaptive immune system

An adaptive immune system protects our body from foreign pathogens based on the memory of past infections. This vertebrate-specific immunity is governed by communication between multiple kinds of cells in the body (Figure 1.1). Antigen presenting cells (APCs) such as dendritic cells and macrophages capture pathogen and present peptide fragments of the pathogen (antigen) to the helper T cell (we called it just "T cell" throughout this dissertation) through a major histocompatibility complex class II (MHC-II), and once the T cell is presented with the antigen, it triggers the T cell activation signaling pathway, and leads to the secretion of cytokines to proliferate themselves by IL-2[1] and stimulate other cells such as macrophages and B cells by IFN-γ,[2] IL-4,[3] etc.

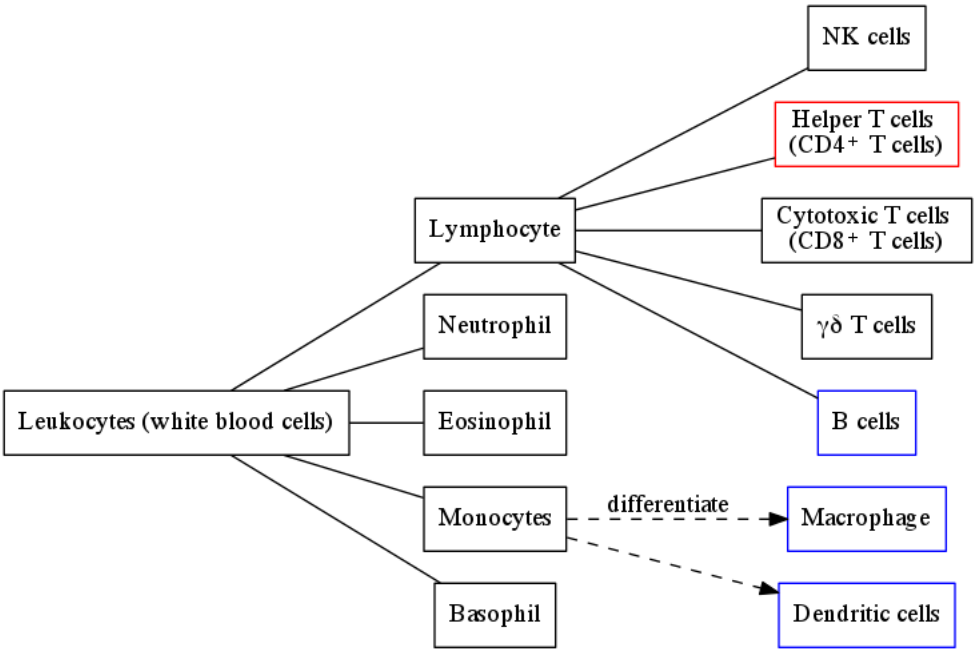

Figure 1.1: Cell types in the family of white blood cells. $CD4^+$ T cells (shown in red) are activated by antigen-presenting cells such as B cells, dentritic cells, and macrophages (shown in blue).

1.1.2 Antigen recognition by TCR

Presentation of antigen to the T cell by the APC occurs in a juxtacrine (i.e. contact-dependent) manner: MHC-II bearing an antigen peptide, called peptide-MHC complex (pMHC), binds to the T cell receptor (TCR) on the surface of the T cell (Figure 1.2). The TCR distinguishes peptide sequences to decide whether it gets activated or not. The remarkable fact about T cell activation is that it has extremely high sensitivity and selectivity towards antigen, and the T cell can distinguish two peptides with just a single amino acid residue difference to have dramatic difference in the signaling outcome.

The TCR undergoes somatic recombination during development, which gives diversity to TCRs in multiple clones of T cells, and every TCR recognizes different subset of peptides, and only those peptides activate that specific clone of T cells. T cells that respond to "self" peptides are removed during negative selection in the thymus. Tyrosines of the cytoplasmic region of TCR (immunoreceptor tyrosine-based activation motif, or ITAM) are phosphorylated upon the binding by pMHC with the antigen peptide, and this phosphorylation is critical in T cell activation, although how the binding of pMHC to TCR results in phosphorylation of TCR's ITAM is still unknown.

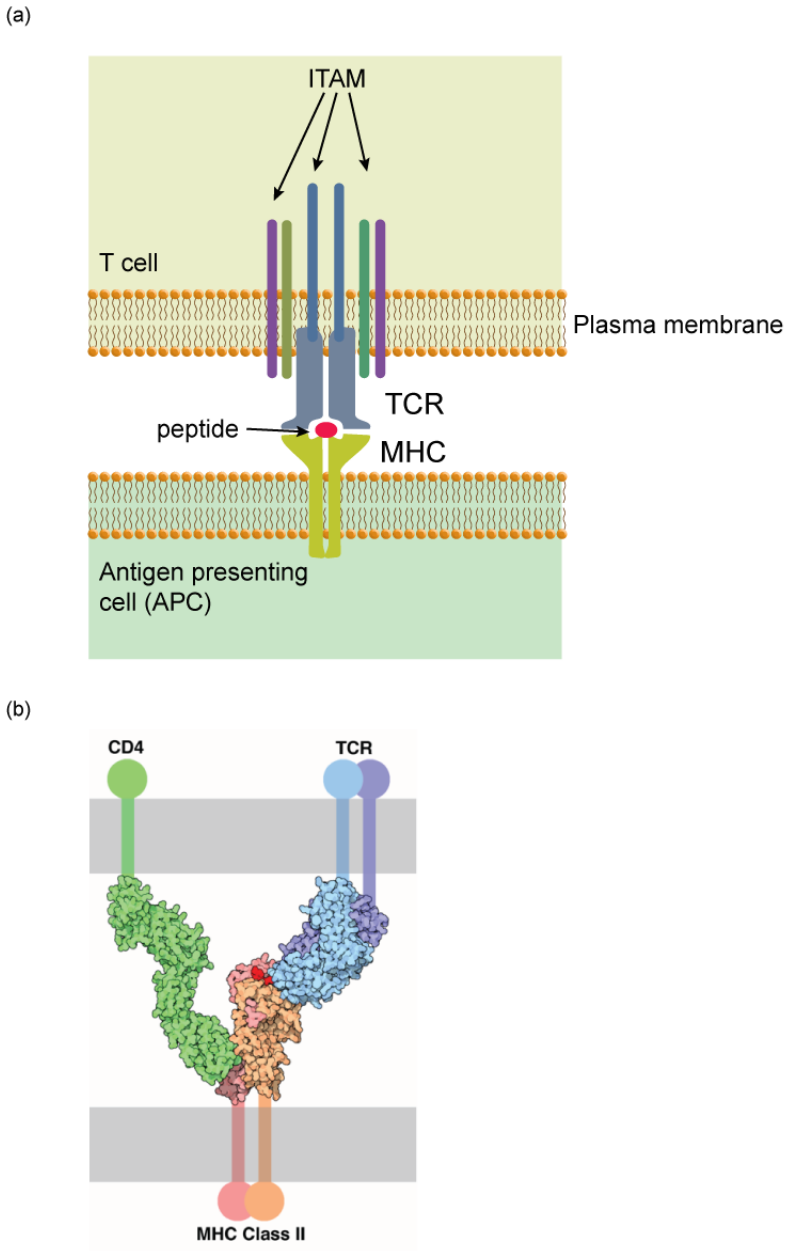

Figure 1.2: Antigen presentation to the TCR by the APC. (a) Schematic of T cell-APC contact. (b) Crystal structure of the part of TCR-MHC complex. Adapted from D. S. Goodsell, "T-Cell Receptor", *RCSB Protein Data Bank*[4] (http://www.rcsb.org/pdb/101/motm.do?momID=63). This structure lacks the transmembrane and cytoplasmic regions, and does not give information on binding-induced structural change of TCR.

1.1.3 TCR triggering and signaling cascade

TCR engagement by pMHC and phosphorylation of the ITAM of the TCR is the first step of T cell activation.[5] Once the TCR is phosphorylated, many other proteins are activated in the signaling pathway (Figure 1.3). These proteins physically associate with each other to convey the information of activation in the cell. Zap70 (zeta-chain-associated protein kinase 70) is recruited to the phosphorylated TCR cytoplasmic chain, and Zap70 further phosphorylates LAT (linker for activation of T cells), and LAT forms a cluster with other signaling proteins such as Sos, SLP-76, PLC-γ, etc.

1.1.4 Methods for T cell signaling study

Various techniques are used to study the mechanism of T cell signaling. The global protein expression level in the cell is of a primary interest. Immunoblotting (Western blotting) separates proteins in cell lysate based on molecular weight and charge by SDS-PAGE and stains the protein of interest by an antibody to quantify the protein. Phosphorylation level of proteins can also be quantified by using a phosphospecific antibody. As the T cell signaling pathway contains kinases and their substrates, immunoblotting is a common method to study their activities.

To study the role of the protein of interest in signaling, a genetic approach is used to introduce a mutation to the protein. A T cell line (e.g. the Jurkat cell[6]) that lacks a specific protein was supplied with external gene that encodes a mutated version of that protein.[7] Using this setting, the function of that mutated protein can be studied. To suppress protein expression in primary T cells, silencing (RNAi) can be used.[8–11]

Genetic transduction is used to introduce external gene to a cell. Retroviral transduction uses retrovirus with the gene of interest generated by packaging cell lines such as Phoenix cells[12] and Plat-E cells.[13] Fusion proteins of the protein of interest and a fluorescent protein are routinely used to visualize localization of proteins in the live cell by fluorescence microscopy.[14] Recent advances in super-resolution microscopy enabled to observe the spatial localization of signaling molecules in sub-diffraction limit size regime.[15,16] The endogenous protein is usually left intact in imaging studies with transduced fluorescent proteins.

There are a few common indicators to quantify the level of T cell activation. The secretion of cytokines, especially IL-2, is a common indicator of activation. Enzyme-Linked ImmunoSorbent Assay (ELISA) is used for quantifying IL-2 secretion from T cells. ELISA quantifies the concentration of a protein in solution using specific binding by an antibody. Single-cell analysis of cytokine secretion by T cells has also been achieved be separating cells and surrounding media into microwells.[17,18] Another important indicator of T cell activation of intracellular flux of Ca^{2+}ion from the nucleus to cytosol.[19–21] In addition, the

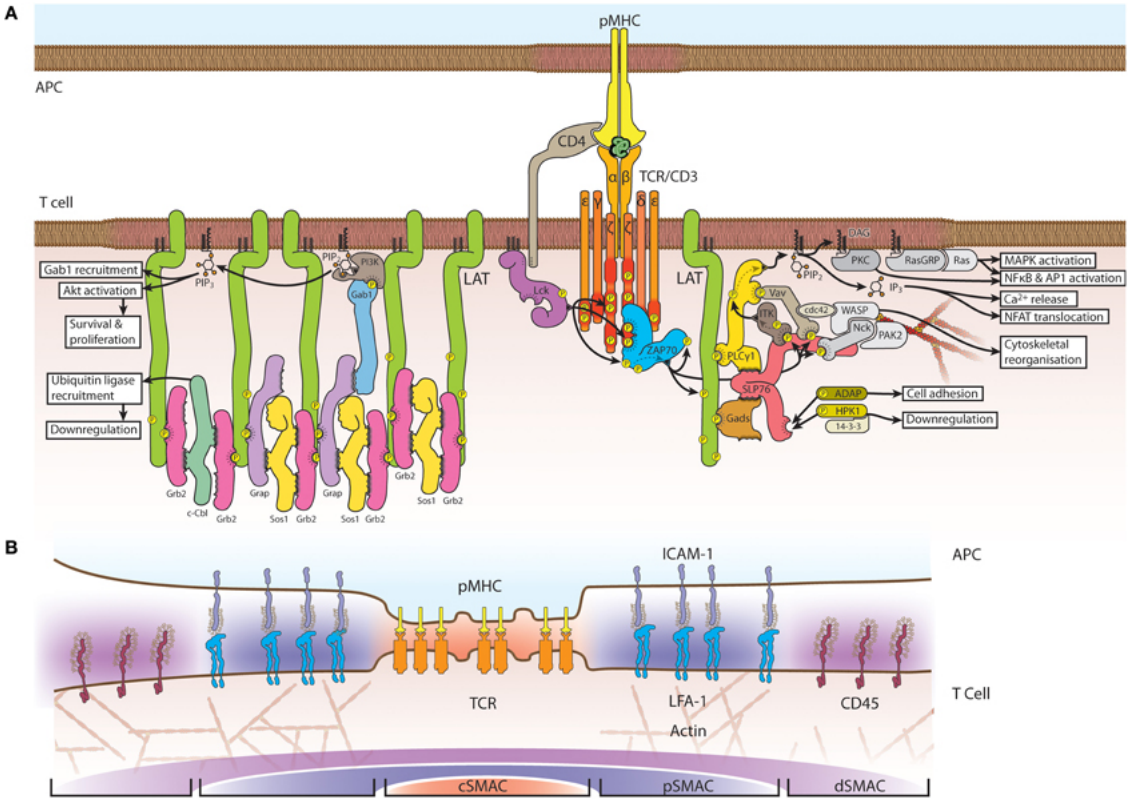

Figure 1.3: After TCR engagement with the pMHC on the APC, the T cell undergoes a cascade of activation steps. Figure as originally published in Jérémie Rossy, David J. Williamson, Carola Benzing, and Katharina Gaus. The integration of signaling and the spatial organization of the t cell synapse. *Frontiers in Immunology*, 3, November 2012.

phosphorylation of Erk,[22,23] translocation of NFAT that is dependent on Ca^{2+} flux,[24] etc. can be used as indicators of T cell activation.

1.1.5 T cell models

Jurkat T cell lines (immortalized human leukemic T cells) have been used as a model T cell system due to several advantages.[6] It is easy to maintain (cells infinitely grow), and gene modification to manipulate proteins by mutant selection is possible.[7] Jurkat cells were found to lack two lipid phosphatases, PTEN and SHIP, which might affect the TCR signaling by constitutive activation of the PI3K pathway of T cell signaling.[25–28] Despite this limitation, Jurkat T cells have been useful for mutation studies in T cell signaling.

TCR transgenic mice were created and used in T cell studies.[29] In a specific species of transgenic mouse, all T cells have the same single clone of TCR, which means all the T cells

from that mouse species responds to the antigen in the same manner. TCR transgenic mice made it possible to study the response of TCR to antigen in a manner closer to real T cells in vivo than Jurkat T cell lines, although it requires a considerable amount of time and expenses to establish a new kind of transgenic mouse. Primary murine T cells can be cultured from spleen and lymph nodes of a TCR transgenic mouse. Recently, TCR retrogenic mice have been developed.[30,31] This technology can be a complementary method to express specific TCRs in vivo.

1.2 Model membrane systems

1.2.1 Model membrane systems for studying membrane proteins

While membrane proteins are confined on the two-dimensional plane of a lipid bilayer, they can move along the surface of the cell membrane. This laterally confined movement gives a unique environment to membrane proteins. To study membrane proteins in biologically relevant environment and under control, several experimental platforms have been developed.

Giant unilamellar vesicles (GUVs) of lipid molecules are used for studying membrane-associated proteins.[32–40] In addition, instead of embedding membrane proteins in artificial vesicles, vesicles can be extracted from a native cell membrane as giant plasma membrane vesicles (GPMVs).[41–44]

1.2.2 Supported lipid bilayers

The model membrane systems described above all have spherical structures that are suspended in solution. As an alternative mode of model membrane, a flat bilayer of lipid molecules that is continuous in two dimensions can be made on the flat glass surface, and this is called supported lipid bilayer (SLB) (Figure 1.4).[45–48] Small unilamellar vesicles (SUVs) of lipid molecules are made by sonication[49] or extrusion of multilamellar vesicles (made just by suspending lipid molecules in water) through a porous membrane,[50–53] and when the SUVs are incubated with the cleaned glass surface, they spread onto the glass surface to form a flat, two-dimensional bilayer of lipid molecules by self-organization. There is a thin water layer of 1-2 nm in thickness between the lipid bilayer and the glass surface, which was measured by neutron reflection.[54] The SLB can be combined with total internal reflection fluorescence microscopy (TIRFM) to obtain high-resolution images in a real time manner, which makes this platform especially appealing. Another advantage of the SLB is that patterning techniques on the glass can be applied to control spatial arrangement of molecules on the SLB.

1.2.3 Mechanism of SLB formation

The proposed mechanisms of SLB formation are reviewed in detail by Richter and colleagues.[47] The self-organization of SUVs into the SLB occurs through a few steps - vesicle adsorption, rupture, and spreading into the planar bilayer structure. The simplest theory to justify SLB formation is described as the balance between stabilization by interaction between glass and lipid molecules (energetically favorable) and the cost of rigid structure formation (loss of entropy, unfavorable) upon the formation of a flat bilayer. This simple view, however, turned out to be insufficient, as adsorbed vesicles can be stable in commonly employed conditions for SLB formation.

Quartz crystal microbalance with dissipation monitoring (QCM-D) can monitor the process of SLB formation in a real time manner. QCM-D measures the mass of molecules adsorbed on the glass surface, and it can distinguish different surface states - the glass surface without vesicles, the surface with vesicles attached but not ruptured, and the surface with a bilayer.(Figure 1.4(b)), as water in SUVs is also measured as attached mass. In contrast, surface plasmon resonance (SPR) measures change in a refractive index near the surface, which quantifies the total amount of lipid molecules that are adsorbed on the surface. By combining these two experimental methods along with computer simulation, it was shown that isolated vesicles on the glass are stable and it undergoes rupture only above certain density threshold.[55] It is proposed that deformation of vesicles upon adsorption destabilizes vesicles, and the destabilization is enhanced under the condition with densely adsorbed vesicles.[56]

Vesicle charge is considered as the primary parameter that governs SLB formation, and hydrophilicity of the solid surface is also important to obtain a fluid SLB. From our experience, a glass coverslip cleaned with piranha solution (H_2SO_4/H_2O_2 3:1) should be used within 1 day after the piranha cleaning to obtain a fluid SLB consistently.

1.2.4 Characterization of SLBs

Fluidity of the SLB can be measured by fluorescence recovery after photobleaching, (FRAP) and fluorescence correlation spectroscopy (FCS), and single particle tracking (SPT). In FRAP, the small area of the SLB is irradiated with excitation wavelength of fluorescent lipids to bleach them. After bleaching, the fluid SLB can recover fluorescence of that bleached area by lateral diffusion of fluorescent lipid molecules. This easy method measures the global fluidity of the SLB, and you can also obtain diffusion coefficients from the FRAP measurement.

FCS uses the temporal fluctuation of fluorescence intensity in a small excitation area, and it determines diffusion coefficient by measuring how fast a molecule moves out from the excitation area. SPT tracks the movement of molecules over time and determines the diffu-

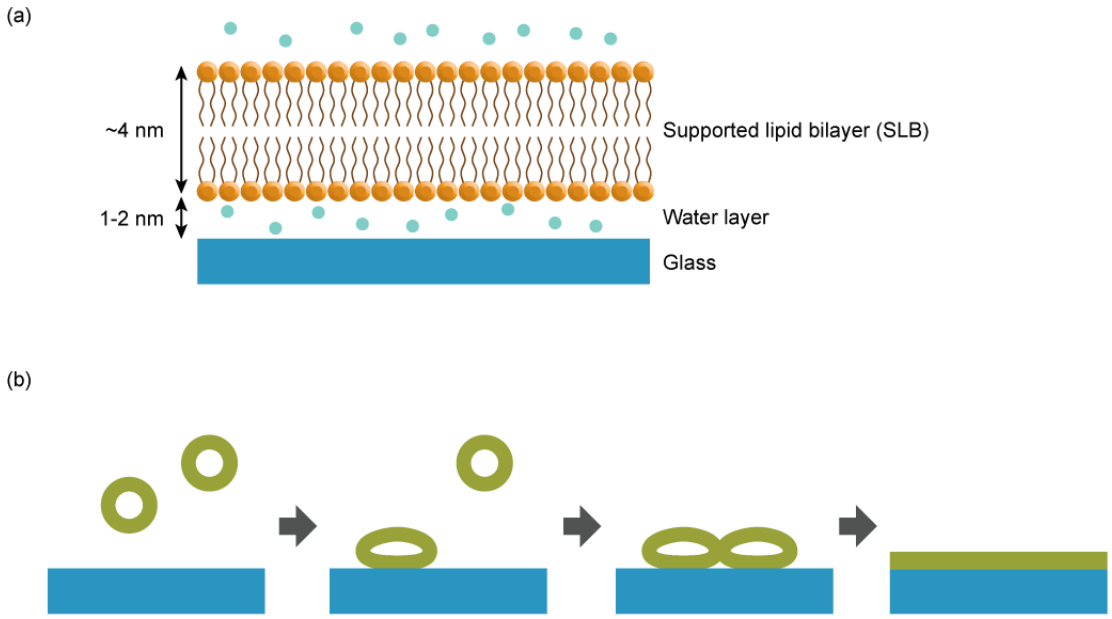

Figure 1.4: Supported lipid bilayer (SLB). (a) A schematic of the structure of a SLB. (b) The proposed mechanism of SLB formation. Vesicles adsorb to the glass surface, and they fuse together and rupture onto the glass when the density on the surface becomes high enough.

sion coefficient from mean squared displacement/time relationship derived from Langevin equation of Brownian motion.

The SLB can have defects (areas with no fluid lipid molecules) in some cases, and defects could potentially affect some applications.[57] Defects can become too small to be observed by normal fluorescence imaging, and AFM observation is desirable to better characterize those tiny defects. From our experiences, those possibly existing tiny defects have never been a problem for our application of the SLB for T cell studies.

1.2.5 Patterning technologies for SLBs

There are various technologies to fabricate patterns on the glass surface to form spatial patterns of the SLBs and proteins. (Figure 1.5)[58] Photolithography and e-beam lithography were used to impose the diffusion barrier on lipid molecules in the SLB.[59,60] Our group has been using this system extensively to investigate cell signaling and protein functions.[21,61–65] The diffusion barrier on the SLB was also made by using PDMS stamping, although the resolution is much lower than e-beam lithography.[66]

Photolithography, combined with plasma dry etching, was also used for creating topographic patterns on the glass and the SLB on top of that.[67] Self-assembly of polymer and colloidal particles is used to create a regular hexagonal array of gold nanoparticles on the glass surface, and this pattern of gold nanoparticles can be combined with the SLB.[68]

The glass surface can be coated with materials that lipid molecules do not adsorb to. This coating process, called passivation, is useful for patterning a SLB. A part of the passivation layer can be removed with desired shape by photolithography by a photomask, and the SLBs can be formed on the area where the passivation layer is removed. A monolayer of poly(l-lysine)-grafted poly(ethylene glycol) (PLL-g-PEG) is used to passivate the glass surface,[69,70] and this passivation surface can be removed by deep UV exposure with a photomask. This method has been successfully used for forming a SLB on the glass surface with a lithographically patterned surface. From our experience, patterns of $\sim$2 μm feature size can be readily made with this method. Parylene was also used as an alternative material to passivate the surface.[71]

1.2.6 SLBs as a platform to study cell signaling

The SLB mimics physiological environment of a laterally fluid cell membrane, and proteins can be attached to a lipid molecules in covalent and noncovalent manners, where proteins maintain their mobility. The SLB has proved a powerful tool to study a cell-cell junction and juxtacrine signaling[61,63,72] due to its compatibility with highly sensitive microscopy such as

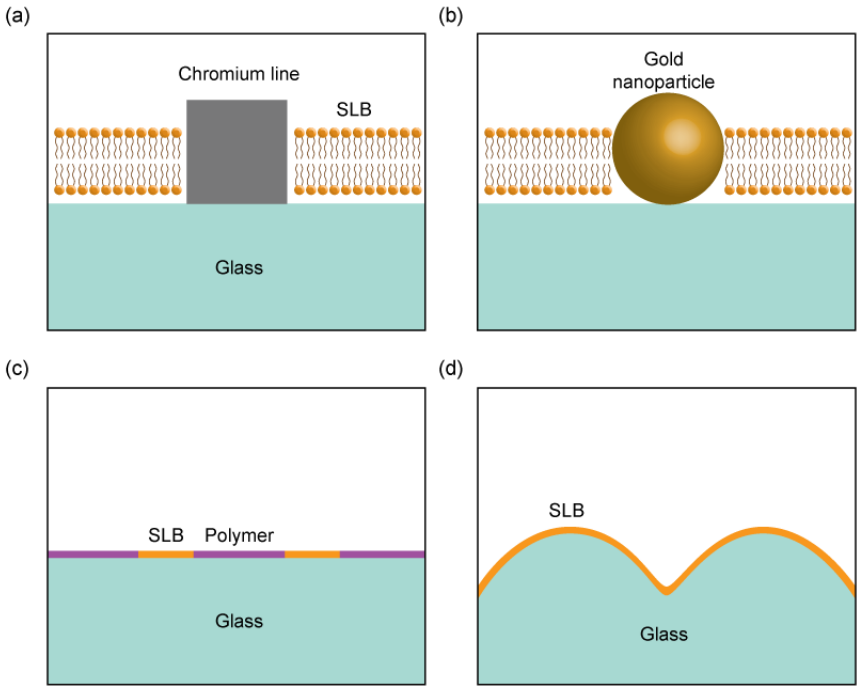

Figure 1.5: Various patterning technologies for the SLB. (a) Chromium lines for diffusion barriers. (b) A gold nanoparticle array. (c) Patterning by a polymer passivation layer. (d) Topographic patterning of glass. Note that (a) and (b) are drawn in higher magnification than (c) and (d)

TIRFM[73] and spectroscopies such as FCS.[74] Another advantage is its applicability to various surface patterning technologies as described above.

In addition to observing the spatiotemporal dynamics of signaling proteins on the live cell, it is also possible to study membrane proteins in vitro on the SLB.[75] Compartmentalized SLBs made by lithographic patterning described above can be considered as a SLB microarray.[76] The single-molecule kinetics of lipid-anchored GTPase was investigated on the compartmentalized SLB.[65]

It is important to note that there are a few discrepancies between a SLB and a real cell membrane. Cells that interact with proteins on the SLB do not experience dynamic feedback from their counterpart, which may become important in some cases. In addition, cell-cell junctions in vivo are not flat, and their shape is constantly fluctuating in three dimensions. Three dimensional topology of the cell-cell junction and curvature of the membrane play a role in some cases in cell.[77–86] Nonetheless, SLBs have been proved a powerful tool to discover new biological phenomena of cells and proteins and investigate them in great detail in vitro.

1.3 Spatiotemporal organization in T cell signaling studied on the model cell membranes

The SLB is compatible with various fluorescence microscopy techniques. Total internal reflection fluorescence microscopy (TIRFM) uses evanescent waves to excite fluorescent molecules only within $\sim$200 nm from the coverslip surface.[87–89] This is suitable for studying signaling on the cell membrane, as the cell membrane and signaling proteins that interact with ligands on the glass coverslip surface are in this region of thin illumination, and it reduces background noise thus improves a signal-to-noise ratio.

There is significant interest in the mechanism by which the T cell achieves high performance. Since the first discovery of characteristic concentric superstructures of membrane proteins, called immunological synapse (IS),[72,90] at the interface between the T cell and an antigen presenting cell (Figure 1.6), there has been significant progress in understanding of spatiotemporal regulation of signaling proteins. cSMAC (central supramolecular activation cluster) exists at the center and contains TCR/pMHC. cSMAC is surrounded by pSMAC (peripheral supramolecular activation cluster), which contains ICAM-1/LFA-1. The IS was originally thought as the site of T cell activation, but later it turned out to have a down-regulatory role as the TCR is dephosphorylated at cSMAC[91,92] and lysosomal compartments exist near the cell membrane of the cSMAC.[92] Ligands to T cells (pMHC and ICAM-1) can be either immobilized on the glass surface or tethered on the laterally fluid SLB, but the SLB has the advantage for observation of movement of molecules as it does not impose un-

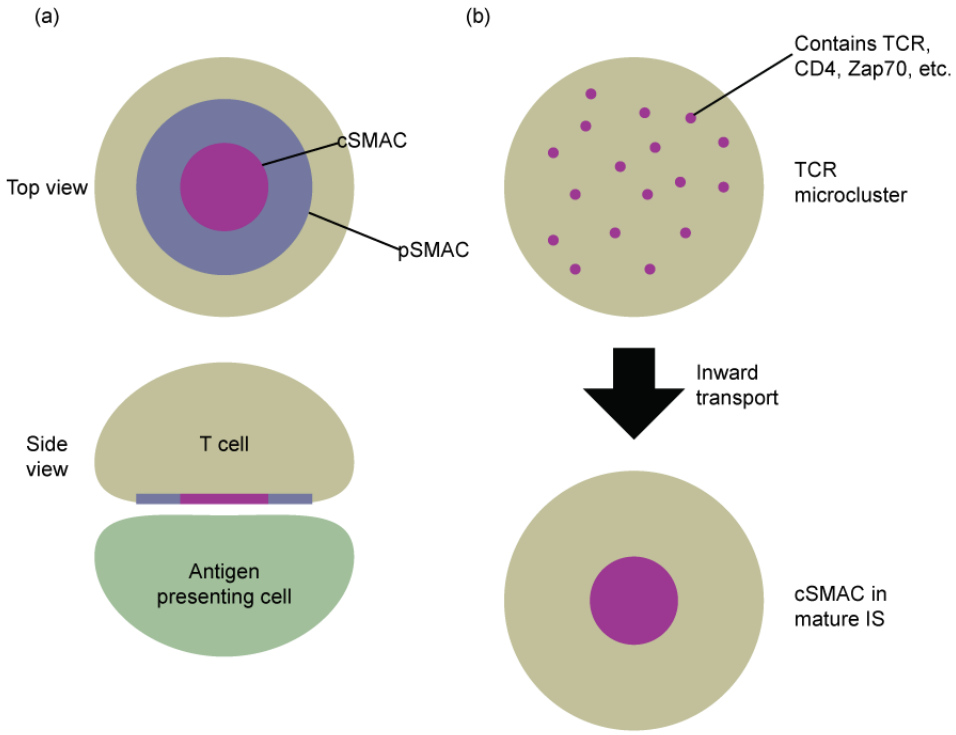

Figure 1.6: The immunological synapse (IS) and TCR microclusters. (a) At the T cell-APC contact surface, the cells form a concentric structure of protein assemblies called immunological synapse (IS) with two primary regions, cSMAC and pSMAC. cSMAC at the center contains TCR/pMHC, and pSMAC at the periphery contains LFA-1/ICAM-1. (b) TCR microclusters are formed at the entire contact surface, and they are centripetally transported towards the center of the contact surface to form cSMAC.

necessary constraints on the lateral transport of membrane proteins. The live cell imaging of T cells on the SLB with stimulatory ligands revealed the formation of small clusters on the entire contact surface between the T cell and the stimulatory SLB in a few seconds of contact, followed by lateral inward transport on the cell membrane to form a cSMAC. These small clusters of proteins containing TCR, called TCR microclusters, are thought to be a basic signaling unit of early T cell signaling.[93–95]

Mechanism of TCR microcluster formation is still unclear, but there are multiple hypotheses that explain it.[94–96] The ITAM of TCR is associated with the cytoplasmic side of a cell membrane and occupies the neighboring area, and this prevents multiple TCRs from form a tightly packed cluster. The TCR ITAM undergoes structural change upon the TCR engagement with antigen and phosphorylation of the ITAM, so that the ITAM is dissociated from the cell membrane, and multiple TCRs can assemble into a cluster by their weak *cis*

interactions. Clustering of multiple TCRs makes a defined gap of $\sim$14 nm between the T cell and the APC, and can possibly exclude CD45, a phosphatase with a large extracellular domain, and this "kinetic segregation" can change the balance between phosphorylation of Lck and dephosphorylation by CD45 to lead to stable ITAM phosphorylation. Also, theoretically it is energetically more favorable to have a smaller number of larger clusters than a larger number of smaller clusters because each cluster causes membrane deformation which is energetically unfavorable.[97,98] It should be noted, however, the phosphorylation of TCR ITAM seems to be unnecessary for microcluster formation. Once the TCR microclusters are formed, they are transported centripetally in a myosin-dependent manner, which suggests the role of actomyosin cytoskeleton in TCR microcluster transport.

LAT is an adaptor protein (i.e. a protein that does not have enzymatic activity but binds to other proteins to regulate signaling), and it is downstream of TCR microclusters. Upon TCR activation, the LAT forms visible clusters, and the LAT in the cluster is largely phosphorylated. Although the relationship between LAT phosphorylation and clustering is under debate, it is known that LAT mutation at tyrosine residues inhibits LAT cluster formation. As LAT accumulates signaling proteins, and LAT movement can be decoupled from TCR, it is interesting to observe the spatiotemporal dynamics of TCR and LAT clusters and correlate these two.

Chapter 2

Size-based chromatography of TCR microclusters

This chapter is partially reproduced from a previously published journal article: "Size-Based Chromatography of Signaling Clusters in a Living Cell Membrane."[99]

2.1 Introduction

2.1.1 T cell activation and TCR microclusters

The T cell is a key component in adaptive immune system that finds foreign pathogens in a body and exclude them. The T cell receptor (TCR) complex is made of $\alpha, \beta, \gamma, \delta, \varepsilon$ transmembrane subunits and cytoplasmic ζ chains. The T cell is activated when the TCR is bound by a major histocompatibility complex (MHC) bearing an antigen peptide (called pMHC) on the antigen presenting cell (APC). The engagement of TCR with pMHC causes phosphorylation of cytoplasmic tyrosines (immunoreceptor tyrosine-based activation motif, or ITAM) of TCR by a kinase Lck through an unclear mechanism. Once the ITAM of TCR is phosphorylated by Lck, another kinase Zap70 binds to the TCR and the Zap70 further phosphorylates tyrosines of a linker for activation of T cells (LAT). T cells have remarkable sensitivity and selectivity towards antigen. Submicron-scale assembly of TCR and other proximal signaling molecules, called microcluster, is considered a scaffold to facilitate the sensitivity and selectivity of TCR against antigens.[92,94,100] TCR microclusters are formed immediately after the stimulation of the T cell by pMHC, a ligand to TCR, or anti-CD3, in a cytoskeleton dependent manner,[101] .

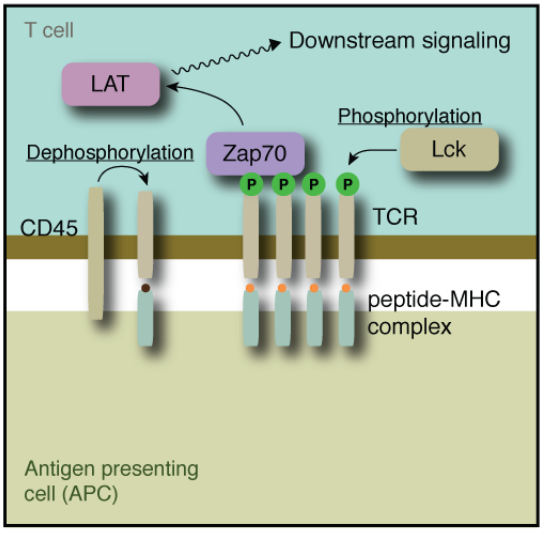

Figure 2.1: A simplified picture on the mechanism of initial T cell activation. Lck phosphorylates the cytoplasmic chain of TCR when the TCR is bound by pMHC. Zap70 binds to phosphorylated TCR, and then phosphorylates LAT, an adaptor protein that is localized to the cell membrane.

2.1.2 Elucidating the structure of diffraction limited TCR microclusters

As the spatial arrangement of TCR and proximal signaling molecules in the TCR microcluster is thought to be an important factor for TCR triggering, there have been studies to elucidate the structure of the TCR microcluster by superresolution microscopy. Although these powerful methods are becoming increasingly common to yield precise spatial arrangement of proteins inside signaling microclusters, it is still not straightforward to distinguish multiple clusters in a close proximity as those clusters can be the order of a few proteins, as well as those are dynamic entities. To investigate microclusters as a dynamic, functionally relevant unit of protein assembly, we embedded a regular array of gold nanoparticles ("nanodot array") onto the SLB as microcluster-size-dependent mechanical perturbation onto TCR microclusters and measured effects on the lateral transport of TCR microclusters (Figure 2.2).

2.1.3 Probing TCR microclusters by a gold nanodot array

Supported membranes functionalized with intercellular adhesion molecule-1 (ICAM-1) and peptide-loaded major histocompatibility complex (pMHC) proteins can effectively replace the antigen-presenting cell (APC) to form a hybrid immunological synapse with a living T cell.[72] As TCR on the T cell engage their antigen pMHC ligands on the supported membrane,

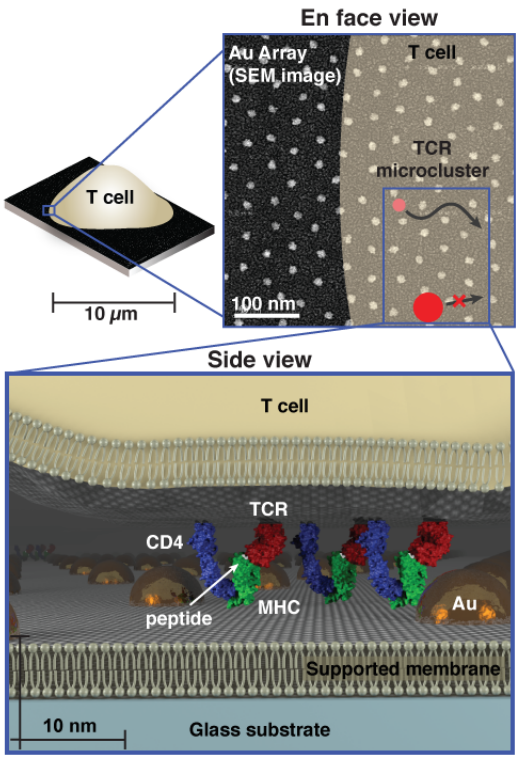

Figure 2.2: A schematic of nanodot array for mechanical perturbation on the lateral transport of TCR microclusters.

they assemble into signaling microclusters,[102–105] which indirect estimates suggest range in size from 70 to 500 nm[102,106](Figure 2.3). Within a matter of seconds after formation, the TCR microclusters become coupled to actin retrograde flow and are centripetally transported to the center of the junction to form the classical immunological synapse.[21,104,107] Physical structures, such as patterns of metal lines or arrays of gold nanodots (described here), can be fabricated onto the underlying substrate to define geometric restrictions on molecular transport in the supported membrane.[68,108] These substrate-imposed constraints are selectively transmitted to the living cell through receptorligand interactions to induce what we refer to as a spatial mutation.[21,61,63] In the case of the nanodot array, TCR cluster transport is impeded if the clusters are too large to percolate between individual nanoparticles in the array (Figure 2.2).

We employ a relatively straightforward method of block copolymer nanolithography to produce ordered arrays of gold nanoparticles (510 nm diameter) with highly controlled (relative standard deviation $<$20%) interparticle spacings ranging from 40 to 180 nm (Figure 2.5).[68,109–112] Interparticle spacings are controlled by the deposition and the specific polymers used in the gold micelle solution (Figure 2.4). Nanodot arrays can be readily fabricated over cm^2 areas, and supported membranes subsequently assembled on the substrate exhibit free mobility (D $\sim$ 1 μm^2/s)[68,113] throughout the array (Figure 2.6).

2.2 Methods

2.2.1 Nanodot fabrication

Gold nanodot arrays were fabricated by block copolymer micelle nanolithography.[68] Amphiphilic block copolymer (Polymer Source, PS-PVP) was dissolved in toluene (varied amount; Figure 2.4). Chloroauric acid (varied amount; Figure 2.4) was weighed quickly by a plastic spatula so that reaction of chloroauric acid with metal was avoided and absorption of water was minimized. After overnight stirring on a 40 °C hotplate, chloroauric acid was dissolved completely and the solution turned yellow. The resulting solution of gold salt/polymer micelles was kept in the dark at room temperature, and it remained intact for more than 1 year. A glass coverslip (40 mm diameter, 0.17 mm thickness; Bioptechs) was sonicated in IPA/water for 30 minutes, rinsed with a stream of MilliQ water, immersed into piranha solution for 5 minutes, rinsed with MilliQ water, and dried with a flow of nitrogen. The gold salt/polymer micelles solution was cast on the dried glass coverslip by slowly moving up the coverslip half of which was immersed into the solution, so that the half of the coverslip was cast with the solution. The coated glass coverslip was irradiated with oxygen plasma in a plasma cleaner (PDC-32G, Harrick Plasma) operated at 18 W for 90 minutes. The resulting nanodot array was characterized by scanning electron microscopy (SEM) to obtain the statistics of interparticle spacings of the nanodot array (Figure 2.5).

Reference	Activating Surface	# ag pMHC	Method	Microcluster analysis	TCR labeling	Size of TCR domains	#TCRs/domain	# cells tested
Yokosuka et al, *Nat. Imm.* 2005	Bilayer with GPI-anchored ICAM-1 and pMHC	density was "2.3-fold higher than that on activated B cells"; varied peptide in solution (0.8 μM, 4 μM, 20 μM, 100 μM)	Total internal reflection fluorescence microscopy	Fluorescence intensity based analysis relative to single eGFP molecule	CD3ζ-EGFP	not mentioned	After >10 min: 40-110 at periphery, 110-290 near cSMAC	~10
Campi et al., *JEM*, 2005	Bilayer with GPI-anchored ICAM-1 and pMHC	40 pMHC/μm²	Total internal reflection fluorescence microscopy	H57 binding sites by FACS show ~140 TCR/μm² on cell; Microclusters 2x the avg. intensity of pMHC at 50 mol/μm²; therefore 140 TCR/microluster initially	H57 anti-TCR f_{ab} fragment	0.35-0.5 um²	After a few min: 140	>20
Varma et al., *Immunity* 2006	Bilayer with GPI-anchored ICAM-1 and pMHC	varied from 0.2 pMHC/μm² to 20 pMHC/μm²	Total internal reflection fluorescence microscopy	Fluorescence intensity method as before, but after 30 min	H57 anti-TCR f_{ab} fragment	not mentioned	After 30 min: 11 TCR for 0.2 pMHC/μm²; 17 TCR for 20 pMHC/μm²	25
Lillemeier et al., *Nat. Imm.* 2010	Immobilized ICAM-1, B7-1, and pMHC on poly-L-lysine	18,500-21,500 pMHC/μm²	high speed photoactivated localization microscopy	probability density peaks	CD3ζ-PSCFP2	35-70 nm radius	70to 300	15-20
Lillemeier et al., *Nat. Imm.* 2010	Bilayer with histidine-tagged ICAM-1, B7-1, and pMHC	30 pMHC/μm²	high speed photoactivated localization microscopy	probability density peaks	CD3ζ-PSCFP2	35-70 nm radius	70 to 200	15
Lillemeier et al., *Nat. Imm.* 2010	Immobilized B7-1, and pMHC on poly-L-lysine	18,500-21,500 pMHC/μm²	Transmission electron microscopy	Ripley's *K*-function analysis	Anti-CD3ζ-Au particle	40-300 nm radius	7 to 30	25-30

Figure 2.3: Summary of past studies that investigate TCR domain size.

Average spacing obtained	Molecular weight of polymer		Concentration of polymer [mg/mL]	Loading ratio	Dip-coating speed [mm/min]
	M_n (PS)	M_n (PVP)			
40-50 nm	7.9×10^4	3.7×10^4	5	0.5	42
81 nm	1.1×10^5	5.2×10^4	6		36
120 nm	1.1×10^5	5.2×10^4	4		24
143 nm	1.1×10^5	5.2×10^4	4		12
171 nm	1.1×10^5	5.2×10^4	2		24

Figure 2.4: Conditions used for the fabrication of gold nanoparticle arrays to achieve various interparticle spacings. Polymers used: Polymer Source P4633-S2VP (for 40-50 nm spacings) and P5922-S2VP (for >80 nm spacings). A few samples from each batch of fabricated substrates were imaged by scanning electron microscopy (SEM) and analyzed to determine the average nanodot spacing. Values for the average spacing can fluctuate from different batches of fabrication using the same condition.

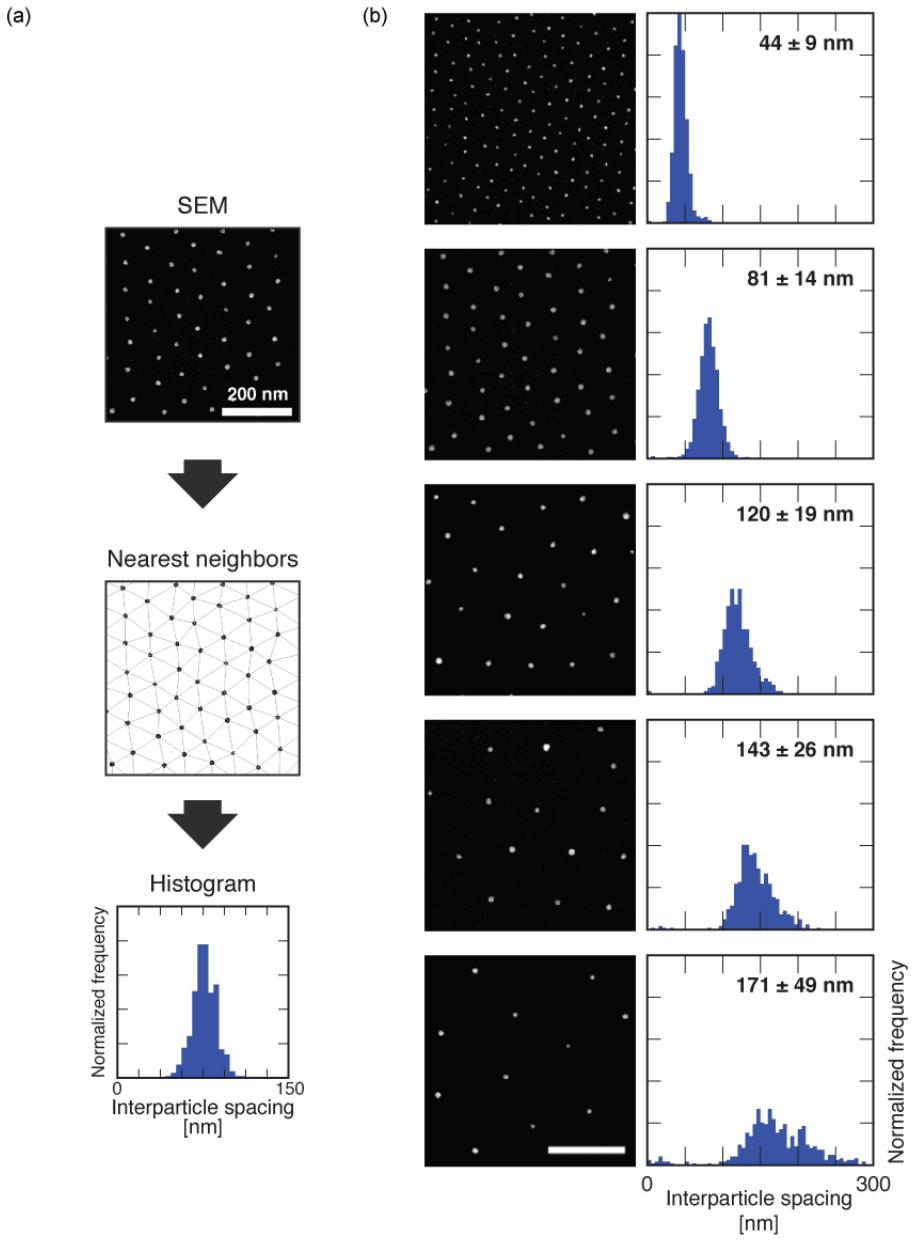

Figure 2.5: Scanning electron microscopy characterization of gold nanodot arrays. (a) Schematic for the analysis of gold nanodot spacing from SEM images. Scanning electron microscopy (SEM) images were analyzed using nearest neighbor detection by the Delaunay triangulation algorithm. The distribution of distances was collected to produce a histogram. (b) Histogram analyses for nanodot arrays at various spacings. SEM images of nanodot arrays (left) and histograms for the distribution of distances (right). Calculated mean and standard deviation of interparticle spacings are shown. Scale bar: 200 nm.

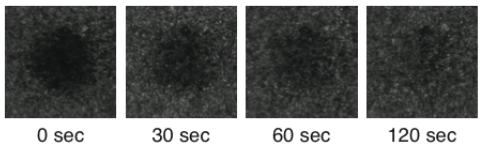

Figure 2.6: The supported membrane is fluid on the nanodot array. Fluorescence recovery after photobleaching (FRAP) images of Alexa fluor labeled MCC peptide bound to MHC proteins presented on the supported membrane with the nanodot array prior to T cell addition. Supported membranes consist of a continuous phospholipid bilayer that coats the surface of a solid substrate, such as silica or some polymers. A thin water layer separates the membrane from the underlying substrate, allowing free lateral mobility of lipids and membrane-linked proteins.

2.2.2 Primary T cells

RVC media for T cell culture was prepared by mixing DMEM (500 mL), FBS (50 mL), L-glutamine (5 mL), Pen/Strep (5 mL), NEAA (5 mL), MEM (5 mL), Arg/Asp/Folic Acid (5 mL), sodium pyruvate (5 mL), HEPES (1.19 g), and mercaptoethanol (1.73 µL), and filtered with a sterile filter. Murine primary T cells were cultured from spleen and lymph nodes taken from AND transgenic mice (JAX laboratory). Collected organs were smashed and filtered through 70 µm cell strainers, and T cells from lymph nodes and spleen were suspended in 10 mL RVC media separately. Suspended T cells were centrifuged with 500 x g for 5 minutes, and media was aspirated. T cells from lymph nodes were resuspended in RVC (10 mL). ACK lysing buffer (5 mL) was added to T cells from spleen to resuspend and incubate for 3 minutes, and RVC (5 mL) was added. These two cell batches were centrifuged with 500 x g for 5 minutes, and media was aspirated, and suspended in RVC (10 mL total) and combined together to filter through a 40 µm cell strainer. Cell density was counted, and the suspension was diluted to 10M cells/mL. The T cells were primed by adding MCC (2 mM stock, 2 µM working). Media was changed every 2 or 3 days with IL-2 (48 U/mL working). The T cells were used between Day 5 (4 days after harvesting organs) and Day 16.

2.2.3 Flow chamber preparation

A flow chamber with an isothermal heater (FCS2, Bioptechs) was used for all cell imaging experiment. The SLB with pMHC and ICAM-His was prepared according to the standard method as described previously except for the following modifications. A glass coverslip was patterned with gold nanodots as above, and the surface was cleaned and activated by oxygen plasma instead of piranha solution before SLB formation. It was confirmed that piranha solution immediately removes gold nanodots in the glass surface (data not shown)

and piranha solution is not applicable.

2.2.4 Fixed cell imaging

Anti-TCR Fab fragment was labeled with Alexa Fluor 568-NHS ester using an antibody labeling kit (Life Technologies) to prepare anti-TCR Fab/Alexa Fluor 568 conjugate (Anti-TCR Fab-568). Primary T cells between Day 5 and 14 were centrifuged at 500 x g for 2 minutes, and anti-TCR Fab-568 (1 μL) was added to a cell pellet to incubate on ice for 20 minutes. It is known that Anti-TCR Fab does not interfere with TCR-pMHC binding.[102] The flow chamber prepared above started to be warmed to 37 °C with an isothermal heater 20 minutes before T cell injection. T cells were injected into a flow chamber, and the chamber was kept at 37 °C for 20 minutes. The T cells were fixed by 2% paraformaldehyde in imaging buffer for 10 minutes at room temperature, and the chamber was rinsed with imaging buffer (2 mL).

2.2.5 Image analysis

Epifluorescence images of T cells fixed 20 minutes after injection were analyzed by extracting variance of a radial profile (2) from every cell, a scalar quantity that shows the degree of spread of TCR microclusters over the cell surface (Figure 2.12) To cross-validate the effectiveness of σ^2 as a metric of microcluster spread, we also calculated other quantities from radial profiles and images(Figure 2.13). In every ratio of agonist/null, the population data was compared with cells on a plain bilayer (=without nanodots) with the same agonist/null ratio (Figure 2-5(a)).

2.2.6 Live cell imaging for tracking TCR microcluster movement

TCR of T cells were stained with anti-TCR Fab-568 as in the fixed cell imaging above, and the stained T cells were injected into a flow chamber. TIRF images were obtained with 500 milliseconds exposure with a 1 second frame interval for 10 minutes. Time lapse images were analyzed by u-track software[114] or a Matlab script to obtain trajectories of microclusters. Parameters of analysis were adjusted to give optimal tracking trajectories judged by eye.

2.2.7 Calcium imaging

Calcium influx was measured by fura-2-acetoxymethyl ester dye (Fura-2 AM; Molecular Probes) as described previously.[21] T cells were incubated with 1 M Fura-2 AM in FBS-free media for 15 minutes at room temperature and incubated with serum rich media at 37C for 20 minutes. Cells were then labeled with anti-TCR Fab-568 as above. Intracellular calcium flux was monitored with excitation wavelengths of 340 and 380 nm and emission of 510 nm using a 40x objective with S7 CoolSnap K4 camera as before . Time course of Fura-2 340/380 fluorescence intensity ratio of every cell was analyzed by Imaris software and the intensity profiles were plotted as heatmaps by a MATLAB script.

2.3 Results

2.3.1 Live cell tracking of TCR microclusters on a gold nanodot array

Nanodot arrays differentially restrict long-range transport of TCR microclusters as a function of the interparticle spacing within the array. As TCR engage pMHC loaded with activating agonist peptide moth cytochrome C (MCC; ANERADLIAYLKQATK) in the supported membrane, signaling clusters form, and their movement was tracked on live cells by total internal reflection fluorescence (TIRF) microscopy (Figure 2.7). On a 171 nm spaced array with an average agonist pMHC density of 80 molecules/μm^2 (Figure 2.10), most TCR clusters successfully percolate through the array. The final positions of continuously tracked clusters are circled on both the track plot (top) and final frame (bottom) in (Figure 2.7(a)) On a 40 nm array with the same agonist pMHC density, clusters exhibit some centripetal transport but most become trapped while still in peripheral positions (Figure 2.7(b)). In general, agonist pMHC is observed to colocalize with TCR, irrespective of whether they are freely moving or trapped (Figure 2.7(b), (d) and Figure 2.8). Leukocyte function associated antigen-1 (LFA-1) bound to ICAM-1 can still form a ring pattern, as is characteristic in a mature immunological synapse (Figure 2.9). This suggests that LFA-1:ICAM-1 complexes are less affected by the physical constraints imposed by the nanodot arrays. In addition to the larger lateral size of TCR microclusters, as compared with LFA-1:ICAM-1 clusters,[62] the closer apposition of the two cell membranes dictated by the short length of the pMHC:TCR complex[115–117] is likely to also contribute.

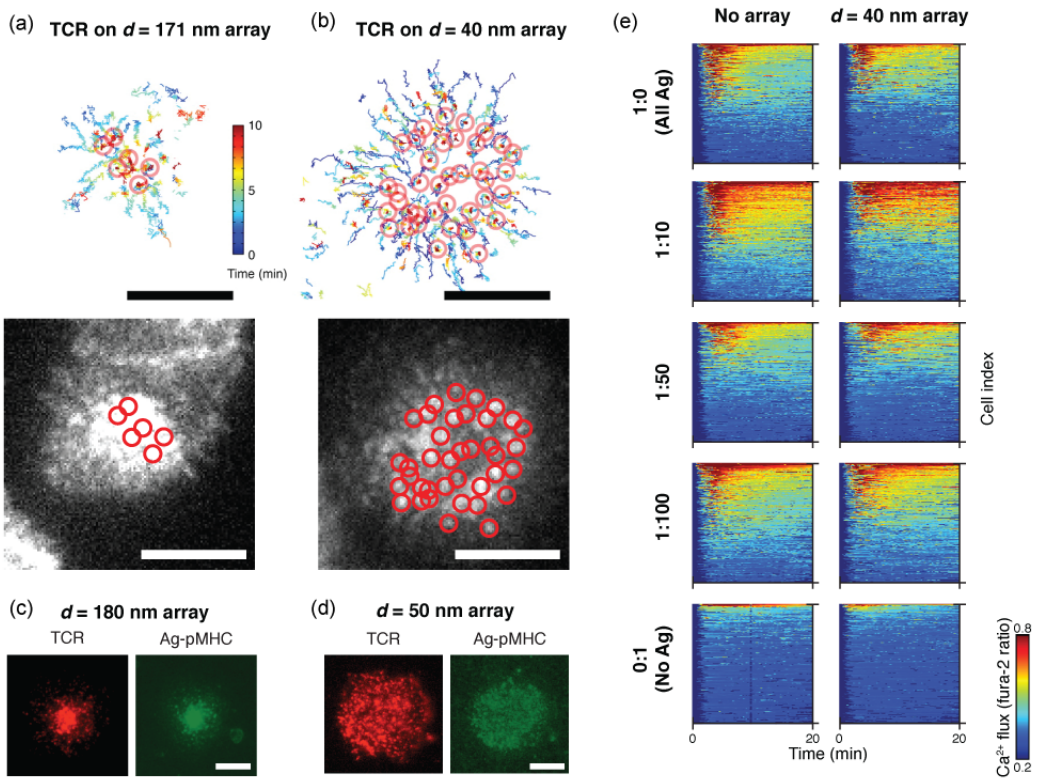

Figure 2.7: Signaling cluster chromatography of live T cell membranes. (Top a, b) Individual trajectories of TCR microclusters in cells interacting with supported membranes containing nanodot arrays of (a) 171 nm or (b) 40 nm spacing. Color bar represents elapsed time (0-10 minutes). Open circles indicate final positions. (Bottom a, b) TIRF images of the cells after 10 minutes. (c, d) Epifluorescence images of TCR (red) on cells interacting with pMHC (green) presented on a SLB studded with 180 nm spacing (c) or 50 nm spaced (d) arrays. (e) Intracellular Ca^{2+} flux for cells presented with varying ratios of agonist (ag) to null peptide presented by pMHC on SLBs with or without the nanodot array; nanodot arrays do not interfere with T cell triggering. Scale bars: 5 μm.

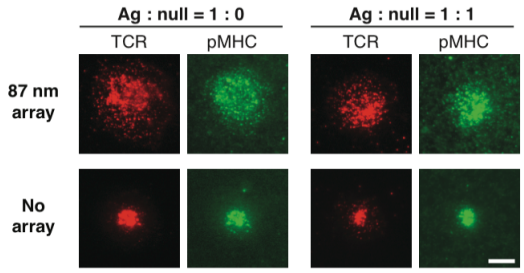

Figure 2.8: TCR and pMHC on and off the nanodot array. ICAM-1 still forms a partial ring on the nanodot array. Bright field and epifluorescence images of TCR and intercellular adhesion molecule-1 (ICAM-1) on a supported membrane embedded with or without a nanodot array. Scale bar: 5 μm.

2.3.2 Calcium signaling

Although the 40 nm spaced nanodot array impedes long-range transport of TCR clusters, no significant interference with signaling function was observed [1]. To quantitatively characterize the antigen specific triggering of T cells, we monitor intracellular Ca^{2+} flux using a Fura-2 dye reporter[21] while titrating the ratio of agonist peptide to a null peptide (T102E) at constant total pMHC density (80 molecules/μm^2). Null peptide-pMHC alone does not induce TCR triggering. The Ca^{2+} concentration (colorimetric scale) is plotted for each cell (y-axis) as a function of time (x-axis) (Figure 2.11) for at least 350 cells per condition in Figure 2.7(e). Agonist-null ratios from 1:0 to 1:100 all lead to comparable Ca^{2+} response in T cells on or off the arrays. When no agonist peptide is present, essentially no Ca^{2+} response is observed in either case.

2.3.3 Two-dimensional titration by nanodot spacings and antigen densities

T cells can respond to fewer than 10 individual agonist peptides.[21,118,119] However, morphological characterization of the immunological synapse and TCR signaling cluster phenomena is often performed at agonist pMHC densities in the range of 2000-1500 per cell.[72,103] Little is known about how the physical properties of TCR signaling clusters scale with antigen density or even if stable TCR clusters exist at the lowest level of antigens that can lead to T cell triggering.[21,104] This is especially important given that, under most physiological condi-

[1] We know from prior studies that interference with TCR cluster movement can induce minor perturbations on cell signaling.[61,62] However, our experiments aim to map the boundary of conditions at which frustration first occurs in order to map the size of the TCR cluster. Thus, from the point of view of the experiment, there is no need to interpret what happens in the T cell after the TCR cluster transport has been impeded.

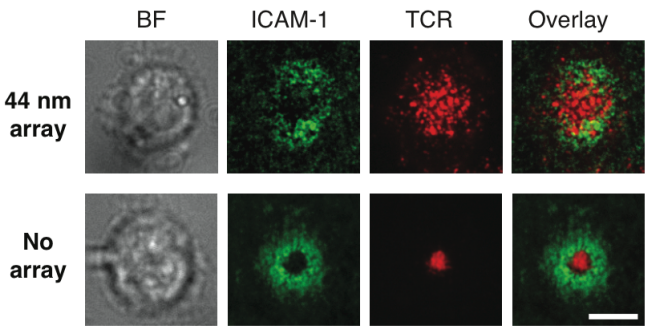

Figure 2.9: ICAM-1 still forms a partial ring on the nanodot array. Bright field and epifluorescence images of TCR and intercellular adhesion molecule-1 (ICAM-1) on a supported membrane embedded with or without a nanodot array. Scale bar: 5 μm.

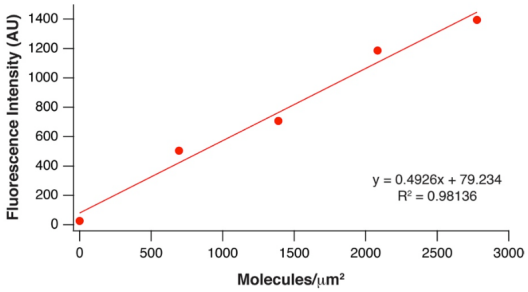

Average Intensity MCC-C-AF568 (AU)	125.27
Texas Red/Alexa Fluor 568 correction factor	1.1195
Calculated bilayer [MCC-C] (molecules/μm²)	83.54

Figure 2.10: Calibration of the density of MCC-loaded MHC molecules on the supported membrane. Quantitative fluorescence analysis was used to determine the surface of MCC-loaded MHC molecules. (a) The surface density calibration standard was generated using supported membranes doped with Texas Red at various concentrations. (b) The concentration of Alexa Fluor 568 labeled MCC- loaded MHC on the bilayer (83 molecules/μm^2) was calculated using the equation derived from (a) and values shown in (b).

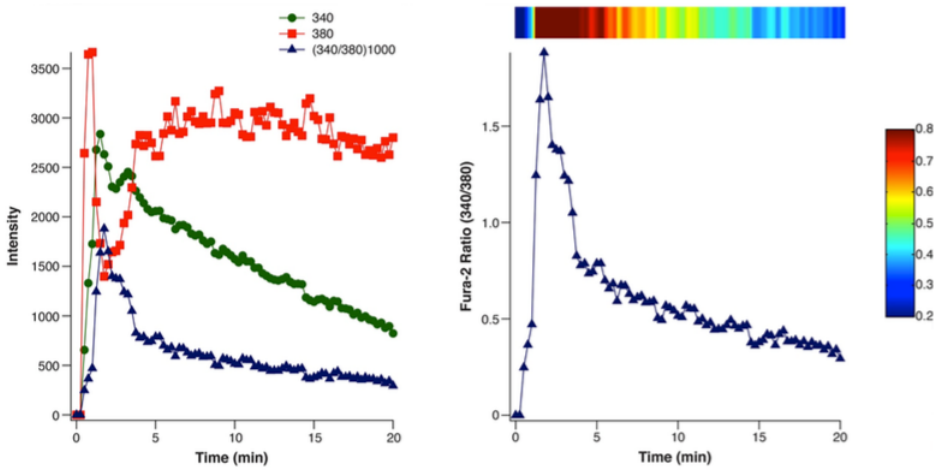

Figure 2.11: Quantification of calcium flux. (a) Calcium flux for a single cell on a bilayer. Curves for Fura-2 AM excitation at 340 nm (green) and 380 nm (red), both with emissions collected at 510 nm. The calculated curve for the Fura-2 ratio (340/380) is shown (blue). (b) Curve of the Fura-2 ratio (blue) and corresponding heat map trace for a single cell. A heat map for all the Fura-2 ratio traces is generated to display all the Ca2+ flux data for a large number of cells per condition.

tions, antigen is present on cell surfaces at extremely low levels. Here we apply the nanodot array chromatographic strategy to probe the physical properties of TCR signaling clusters as a function of antigen density.

The relative frustration of TCR cluster transport induced by the nanodot array can be quantified using a radial profile analysis as depicted in Figure 2.12. The measured TCR density is converted into a normalized radial probability distribution. We compute the variance, σ^2, of the symmetrized probability distribution to provide a scalar measure of the degree of frustration (see Section 2.2.5). In an uninhibited immunological synapse, the radial transport of TCR toward the geometric center of the junction leads to low variance while a completely frustrated system exhibits high variance. This analysis allows comparison of cells as well as analysis of cell-cell variation within an ensemble unbiased by labeling efficiency or cell size.

Results from a two-dimensional titration experiment in which antigen density and nanodot array spacing are independently varied are illustrated in Figure 2.14 and 2.15. As before, the total pMHC density is fixed at $\sim$80 molecules/μm^2, and the ratio of agonist to null peptide is titrated. Five different nanodot array spacings, ranging from 40 to 171 nm, as well as unpatterned membranes were examined, and a minimum of 39 cells was analyzed for each combination of conditions. Representative images with color-coded borders corresponding to population average data (Figure 2.12) are depicted in a matrix layout in Figure 2.14. As antigen is titrated to lower densities, the TCR clusters are able to percolate through progres-

sively smaller nanodot arrays. Appreciable TCR transport was observed even on the 40 nm spaced arrays at agonist-null peptide ratios of 1:50 and below. These data reveal that the effective size of TCR signaling clusters varies continuously with antigen density and that functional signaling clusters readily percolate through 40 nm spaced arrays at low antigen density.

2.4 Discussion

Structural studies of TCR and CD4 simultaneously bound to pMHC suggest that the lateral size of this complex in the T cell membrane is 10 nm in diameter.[120] Additionally, TCR-pMHC complexes require relatively close apposition of the two membranes.[115] Thus, the 10 nm high nanodots may sterically interact with other proteins associated with the TCR signaling cluster (Figure 2.2). As such, the physical footprint of the TCR cluster in the T cell membrane, more so than just the bound pMHC ligands in the supported membrane, is likely to define the effective cluster size as determined by percolation through the nanodot array. In support of this conclusion, we note observations of distinctly different behavior in a juxtacrine signaling system (ephrinA1-EphA2) that has a larger intercellular spacing (21 nm) .[121] In a hybrid live cell supported membrane junction, ephrinA1-EphA2 form signaling clusters that exhibit lateral transport in a manner reminiscent of TCR signaling clusters.[63,111,122] However, transport of EphA2 clusters is not impeded by the nanodot array, even when the clusters are visibly larger than the array spacing.[111] The EphA2 clusters appear to be able to pass over the nanodot array. Only when some of the ephrinA1 ligand is directly affixed to the gold nanodots is any impedance imposed on the EphA2 clusters.

If TCR complexes within a cluster are assumed to pack in a rough lattice with a 10 nm unit cell, a cluster with 10 TCR would have a diameter of 30 nm and might therefore be expected to percolate through the array. The useable space between nanoparticles in the array is less than the interparticle spacing (e.g., 30 nm for the 40 nm array, accounting for the nanoparticle size itself). Nanodot array chromatography does not necessarily provide a direct caliper for the size of the TCR cluster since other properties, such as the dynamics of the TCR cluster, are naturally convolved with the percolation measurement. Nevertheless, this type of ambiguity is inherent to essentially all forms of size chromatography without significantly reducing their utility.

Collective consideration of results from the experiments described here reveals the physical nature of the TCR signaling cluster to be distinctly dependent on the amount of antigen encountered by the cell. At high antigen densities, they reach sizes that exhibit difficulty percolating through supported membrane-embedded nanodot arrays with interparticle spacings as large as 120 nm. At lower antigen densities, but still well above the threshold for triggering intracellular Ca^{2+} flux, TCR clusters can move through nanodot arrays with interparticle spacings as small as 30 nm. At these lower antigen densities, TCR clusters appear to

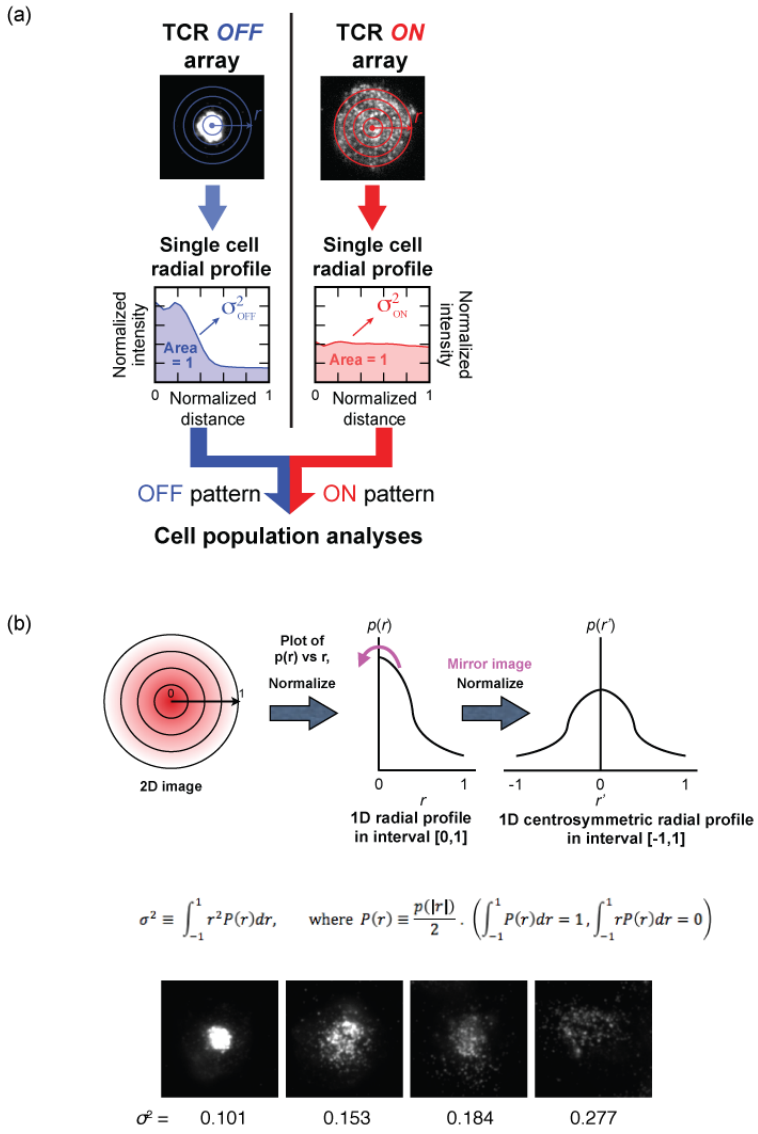

Figure 2.12: Quantitative analysis of the perturbation on TCR microcluster transport. (a) Schematic of the quantitative analysis method. Normalized radial intensity profile of the TCR image (radial probability distribution for TCR) for each cell off or on the array in the same sample. Variance of the distribution (σ^2), which corresponds with the degree to which TCR transport is frustrated, was calculated for each profile generated. Population level analyses are performed thereafter. (b) How the variance was calculated (top). σ^2 for example cell images (bottom). Larger σ^2 corresponds to more scattered TCR microclusters.

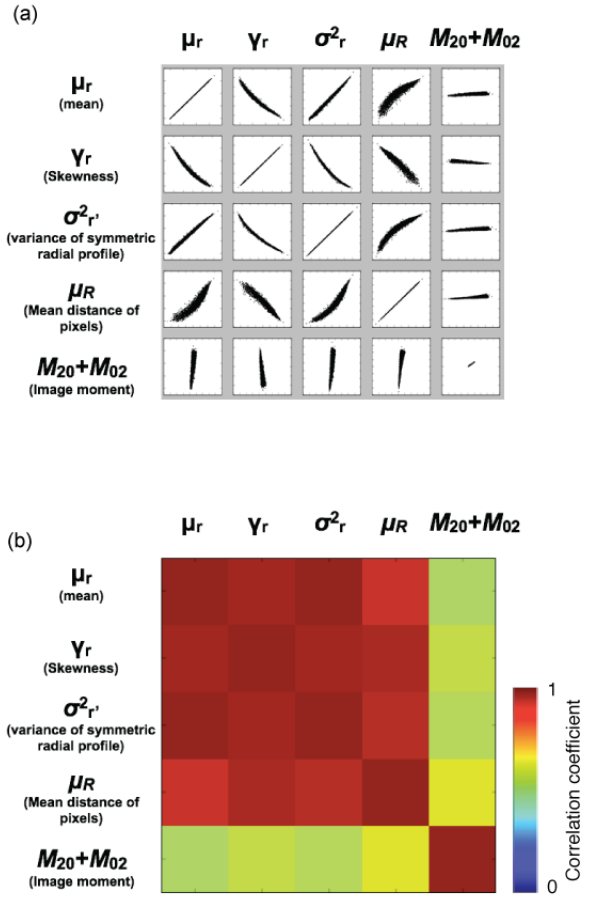

Figure 2.13: (a) Correlation between various metrics for TCR microcluster transport perturbation. 2D plots of a pair of metrics from every cell in all conditions combined. (b) The correlation matrix of metrics shows $\mu_r, \gamma_r, \sigma_r$, and μ_R are strongly correlated, which means they can be used interchangeably.

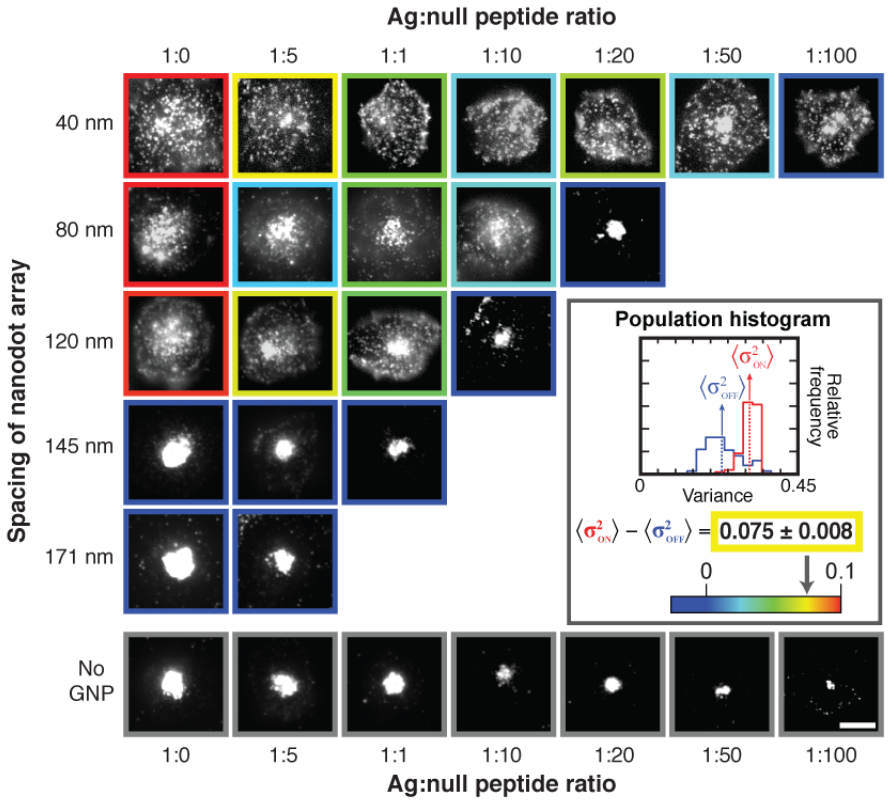

Figure 2.14: Representative cell images of two-dimensional titrations. TCR microcluster chromatography with the titration of nanodot spacing and ag-null peptide ratios. Cells are fixed 20 minutes after contact with the SLB according to the indicated conditions, and epifluorescence images of TCR are shown. (Inset) The distribution of variance was plotted in a histogram for the cell population. The degree of TCR cluster centripetal transport is quantified as the difference between the population variance on and off the array, and the calculated value is represented as the colored borders around each TCR image.

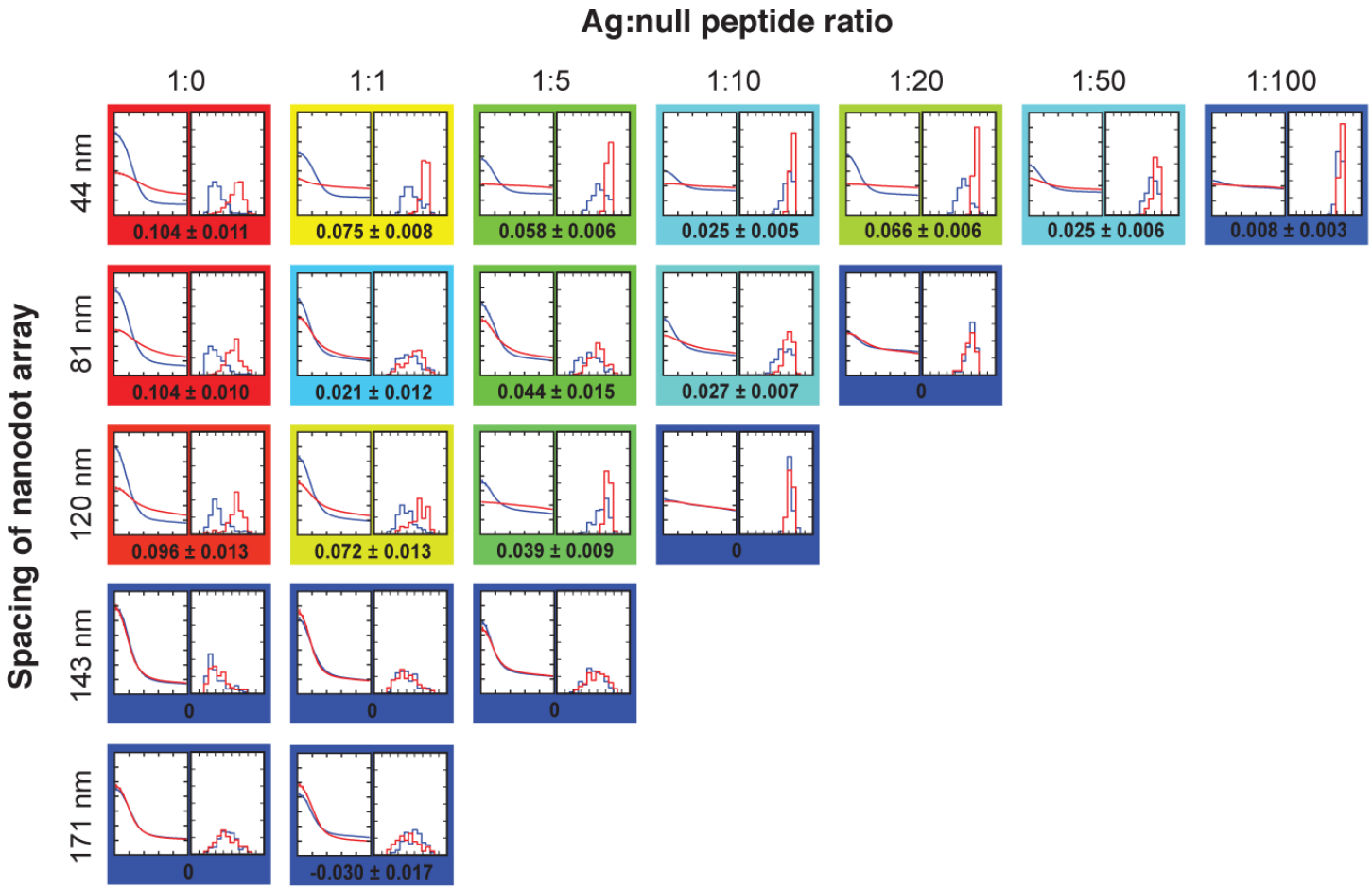

Figure 2.15: Cell population analyses of TCR microcluster transport as a function of nanodot array spacing and agonist peptide density on the SLB. The graph on the left is the average radial profile on (red) and off (blue) the array. The graph on the right is the population histogram generated per condition. The colored borders indicate the difference in variance off and on the nanodot array.

be small (<10 TCR), flexible, or dynamic. This observation necessitates a reconsideration of the concept of a TCR signaling cluster to account for such antigen-dependent variability. Downstream signaling reactions within the TCR cluster must either be independent of these physical properties or perhaps regulated by them. The supported membrane-embedded nanodot array platform provides a physical means to both probe and manipulate membrane assemblies, such as the TCR signaling cluster, while they are functioning in the membrane of a living cell.

Chapter 3

Clustering dynamics of LAT studied by localized activation

3.1 Introduction

3.1.1 LAT as a signaling hub in the T cell

Early T cell signaling has a cascade of phosphorylation events with a precisely regulated spatiotemporal dynamics (Figure 3.1).[94] Upon T cell receptor (TCR) engagement with peptide-major histocompatibility complex (pMHC), phosphorylation of TCR followed by binding of Zap70 (zeta-chain-associated protein kinase 70) to TCR occurs, and LAT (linker for Activation of T cell) is phosphorylated by Zap70. Phosphorylated LAT forms a cluster that contains SLP-76 (SH2 domain containing leukocyte protein of 76kDa), Gads (GRB2-related adaptor downstream of Schematic), Sos (Son of Sevenless), etc., and this signaling protein assembly triggers further downstream signaling such as calcium influx, Ras activation, etc. LAT is a transmembrane protein, and murine LAT contains 242 amino acids with only four amino acids in the extracellular domain.[123,124] and two palmitoylated cysteine residues near the transmembrane region (Figure 3.2). LAT is an adaptor protein that is bound by other enzymatic proteins, but LAT itself does not have any catalytic activity. The intracellular domain of LAT has nine tyrosines. Tyrosines of LAT are phosphorylated immediately after TCR activation, and phosphorylation of LAT is essential for T cell signaling. Mutating tyrosines of LAT causes the inhibition of association of LAT with PLC-γ1[123] as well as severe pathological conditions in T cell development and function[125,126] Once tyrosines of LAT are phosphorylated, LAT is bound by multiple other proteins through their SH2 domains, domains that recognize phosphorylated tyrosine selectively.[124,127] Grb2 and Sos1 are associated constitutively.,[128,129] and multivalency of LAT (multiple phosphotyrosines) and Grb2/Sos1 complex (multiple SH2 domains) can explain cluster formation by biochemical

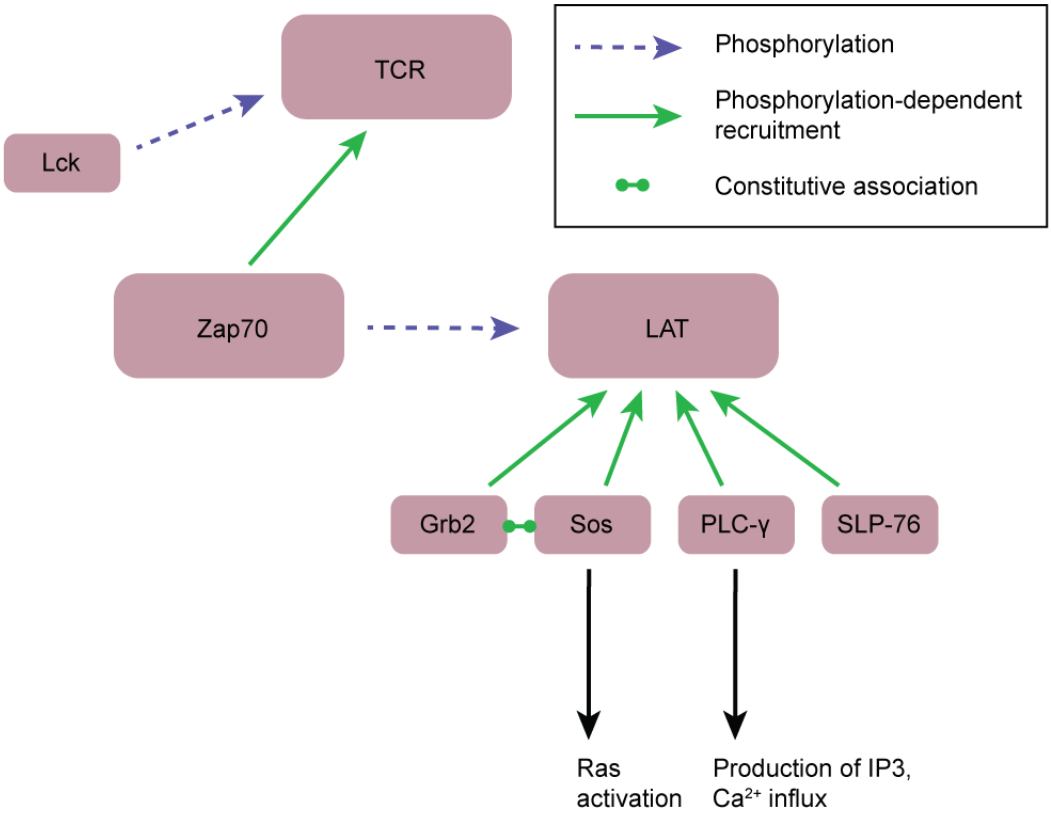

Figure 3.1: The early T cell signaling pathway around TCR and LAT.

experiment[129] and theoretical and computational studies[130,131]

3.1.2 Imaging studies of LAT dynamics on the cell membrane

Although it is clear that LAT is associated with important signaling proteins as a LAT signalosome, much remains to be solved about the precise mechanism of LAT cluster formation, the role of LAT clustering in signaling, and spatiotemporal regulation of cluster. Imaging techniques have yielded important findings on how LAT clustering is regulated upon T cell activation.[132–137] A typical setup to observe the dynamics of LAT is a glass coverslip coated with anti-CD3, which triggers TCR signaling, and the dynamics of fluorescent fusion proteins on the cell surface can be observed in a real time manner using fluorescence microscopy. LAT clusters, which are visible as blobs brighter than the background intensity on the cell membrane, appear immediately after the T cell is stimulated. Immunostaining of phosphorylated LAT (pLAT) visualizes spatial distribution of pLAT, and LAT is phosphorylated in the cluster. This indicates the phosphorylation of LAT is associated with the formation of

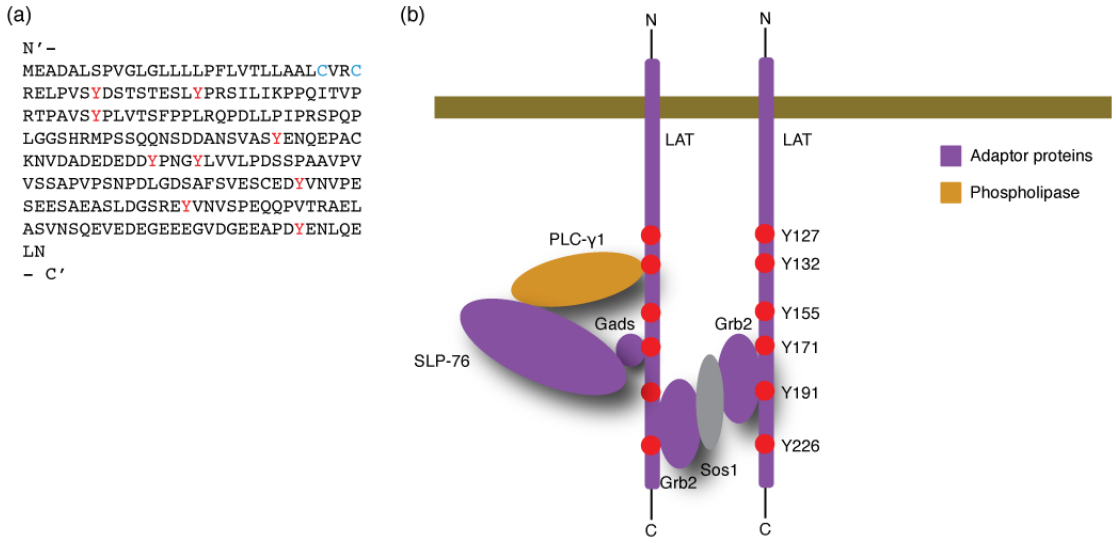

Figure 3.2: (a) 242 amino acid sequence of mouse LAT (UniProt ID: O5495). Tyrosines (Y) were shown in red, palmitoylated cysteine (C) in blue. (b) Simplified schematic of interaction of LAT with other signaling molecules in LAT signalosome.

visible LAT clusters.

In addition to the bulk spatial distribution of LAT, there have also been studies on mobility of LAT upon TCR triggering. LAT diffusion on the cell membrane slows down upon TCR triggering by anti-CD3 coated beads.[138] Vale and his colleague observed LAT dynamics on the cell membrane of a Jurkat T cell stimulated by immobilized ligands on glass, by means of single molecule tracking, and found that larger fraction of LAT molecules move between signaling protein clusters and trapped there,[139] which is reminiscent of Kusumi's "hop diffusion" model.[140]

3.1.3 Controversy on the origin of signaling active LAT

The size of clustering may be a governing factor for the regulation of signaling in LAT signalosome, because the microenvironment for signaling proteins may differ for LAT clusters of different sizes. Electron microscopy studies suggested the existence of nanoclusters of LAT even in a resting cell before TCR triggering.[141] High-speed PALM (superresolution microscopy) and fluorescence cross correlation spectroscopy (FCCS) was used to find that TCR and LAT form nanoclusters of the average diameter of 35-70 nm separately in a resting T cell and they concatenate upon activation.[106] There is also a report of the presence of visible

clusters of LAT by fluorescence microscopy in naive T cells even before the activation.[142]

Although LAT is largely localized to the plasma membrane, there is also a cytosolic pool of LAT as vesicles. Recent reports suggested that the involvement of subsynaptic vesicles of LAT in T cell activation.[143] The movement of cytosolic LAT vesicles was imaged, and it was found that LAT vesicles move in cytosol between the sites of SLP-76 clusters.[134] This suggests the involvement of cytosolic LAT in signaling, although it is not straightforward to associate this with the regulation mechanism of signaling, because SLP-76 is downstream of LAT and SLP-76 is considered to accumulate as a consequence of LAT phosphorylation. Super-resolution microscopy study found pre-existing LAT clusters are not phosphorylated, and indicated that subsynaptic vesicles of LAT are recruited upon activation and get phosphorylated.[144] Vamp7, one of SNARE proteins that facilitate the fusion of vesicles, was shown to be involved in the recruitment of LAT subsynaptic vesicles and subsequent phosphorylation, while the vesicles do not fuse to the cell membrane.[11] In contrast, experiment using CD4-LAT chimera that is localized to the cell surface indicated that 90% of phosphorylated LAT at 2 minutes after TCR activation originates from cell surface LAT.[145] This result indicates that the cell surface LAT plays a primary role in signaling at an early time point, although it does not exclude possibility of involvement of subsynaptic LAT in signaling in later time points. As Dustin pointed out,[146] the cell membrane is a highly irregular structure and those clusters that appear to be signaling-active subsynaptic LAT vesicles observed in these recent studies might be actually within the cell membrane. Nonetheless, those studies raised interesting possibilities that LAT can be regulated in a more complex manner than previously thought.

As discussed above, recently debated activation mechanisms of LAT can be classified into three different hypotheses (Figure 3.3). (1) LAT forms a cluster on the cell membrane upon phosphorylation following TCR triggering.[145] (traditional view) (2) LAT exists as a nanocluster even before TCR triggering, and LAT nanocluster and TCR nanocluster concatenate once the TCR is triggered[106] (3) LAT clusters are recruited from cytosol after TCR triggering.[144,147] These three mechanisms are not mutually exclusive, and possibly coexist in the T cell. However, each of these leads to completely different pictures of how signaling molecules are activated after TCR triggering, and it is important to elucidate the spatiotemporal dynamics of LAT activation and regulation.

One implication by apparently varied results reported recently is that it is important to not only understand the dynamics of LAT with spatial resolution in the cell membrane and cytosol, but also quantitatively map the dynamics to the time course of T cell activation, because T cells may combine different pathways involving the same protein at different time points.

3.1.4 Localized stimulation to T cells for observing the bulk live-cell dynamics of LAT

Although there have been studies on the dynamics of LAT upon TCR activation and its roles in T cell signaling, there has not been much investigation on the dynamics of LAT cluster size upon TCR activation. This is probably because many systems use immobilized ligands for stimulating TCR, and this imposes artificial constraints on the size of formed TCR microclusters. In addition, it is difficult to correlate individual LAT cluster formation with TCR activation by means of traditional homogeneous stimulation to the T cell, because density of TCR activation sites is too high and multiple signaling clusters on the T cell membrane readily coalesce in such an experimental setup. Observing LAT dynamics upon stimulation of TCR by ligands on the SLB in the way that each activation site is separated from each other will give insights into spatiotemporal dynamics of LAT as a function of TCR engagement and TCR microcluster formation. We set out to investigate the response of LAT upon activation of TCR by localized stimulation to the T cell using a spatially patterned SLB. The spatially patterned SLB was prepared by photolithographic patterning on a glass coverslip coated with PLL-PEG polymer,[148] and the patterned SLB with pMHC and ICAM-1 was used to locally activate the T cell and observe spatiotemporal dynamics of the LAT in the live T cell in a real time manner. In addition, as phosphorylatable tyrosines are necessary for the LAT to associate with other signaling molecules, mapping LAT phosphorylation with both spatial and temporal resolutions is of great interest. Previous studies did not observe correlation between stimulation time and phosphorylation in single cells with a statistically relevant sample size. We also employed time lapse live-cell imaging on the SLB to get statistics of live-cell LAT dynamics by capturing multiple live cells (Figure 3.4).

3.2 Methods

3.2.1 Patterning bilayers

Caution: piranha solution is highly reactive, and it causes an explosive reaction with organic solvents including isopropanol. Exceeding 3:1 ratio of H_2SO_4 and H_2O_2 can also be dangerous. You should have H_2SO_4 in a container first, and add H_2O_2 on top of H_2SO_4. Unless otherwise stated, ultrapure water from MilliQ was used as water for rinsing. A glass coverslip (40 mm, 0.17 mm thickness; Bioptechs) was cleaned by sonication in isopropanol/water (1:1 volume) for 30 minutes, rinsed with a stream of ultrapure water, cleaned with piranha solution (conc. H_2SO_4/H_2O_2 (30%), 3:1 volume) for 5 minutes at room temperature, rinsed with a stream of ultrapure water, and dried with a flow of nitrogen. The cleaned coverslip was put on a drop of PLL-PEG-biotin solution (0.1 mg/mL in 1x PBS, 20 μL; PLL (20 kDa) grafted with PEG (2 kDa) and PEG-Biotin (3.4 kDa); SuSoS, Switzerland) on a parafilm for

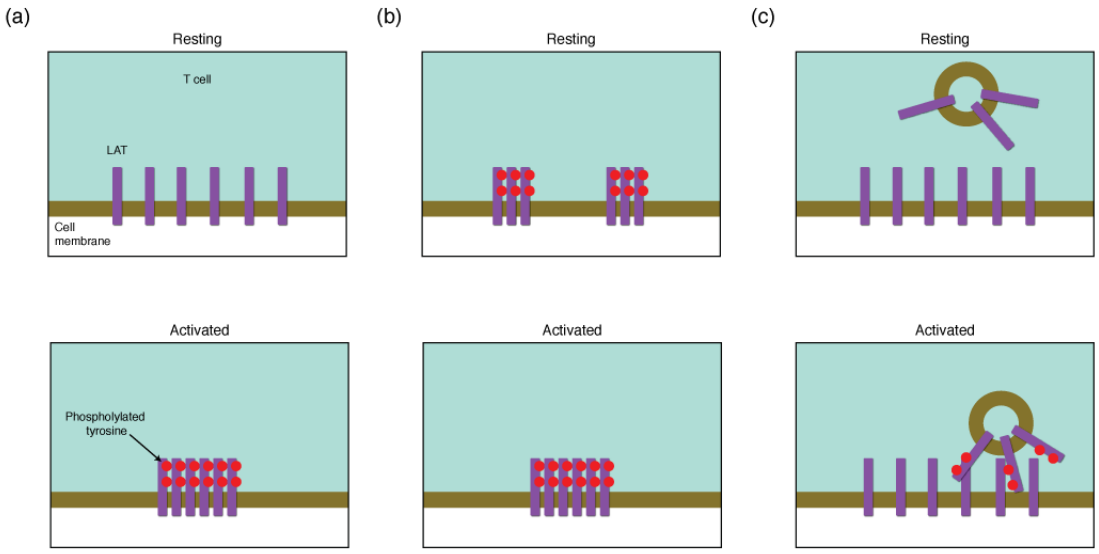

Figure 3.3: Three hypothetical mechanisms of LAT activation. (a) LAT forms a cluster upon phosphorylation following TCR triggering (b) LAT exists as a nanocluster even before TCR triggering, and LAT nanocluster and TCR nanocluster concatenate once the TCR is triggered. (c) LAT clusters are recruited from cytosol after TCR triggering.

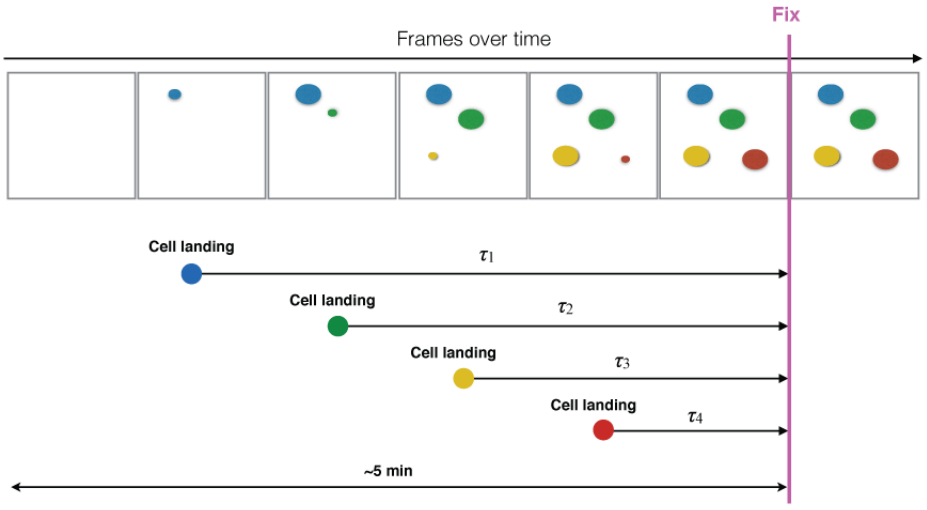

Figure 3.4: A schematic of time-lapse fixed cell imaging. Each cell is represented as an ellipse in color. With the sound assumption that cells do not move out of the field of view, this method captures cells with individual landing time with uncertainty of frame interval.

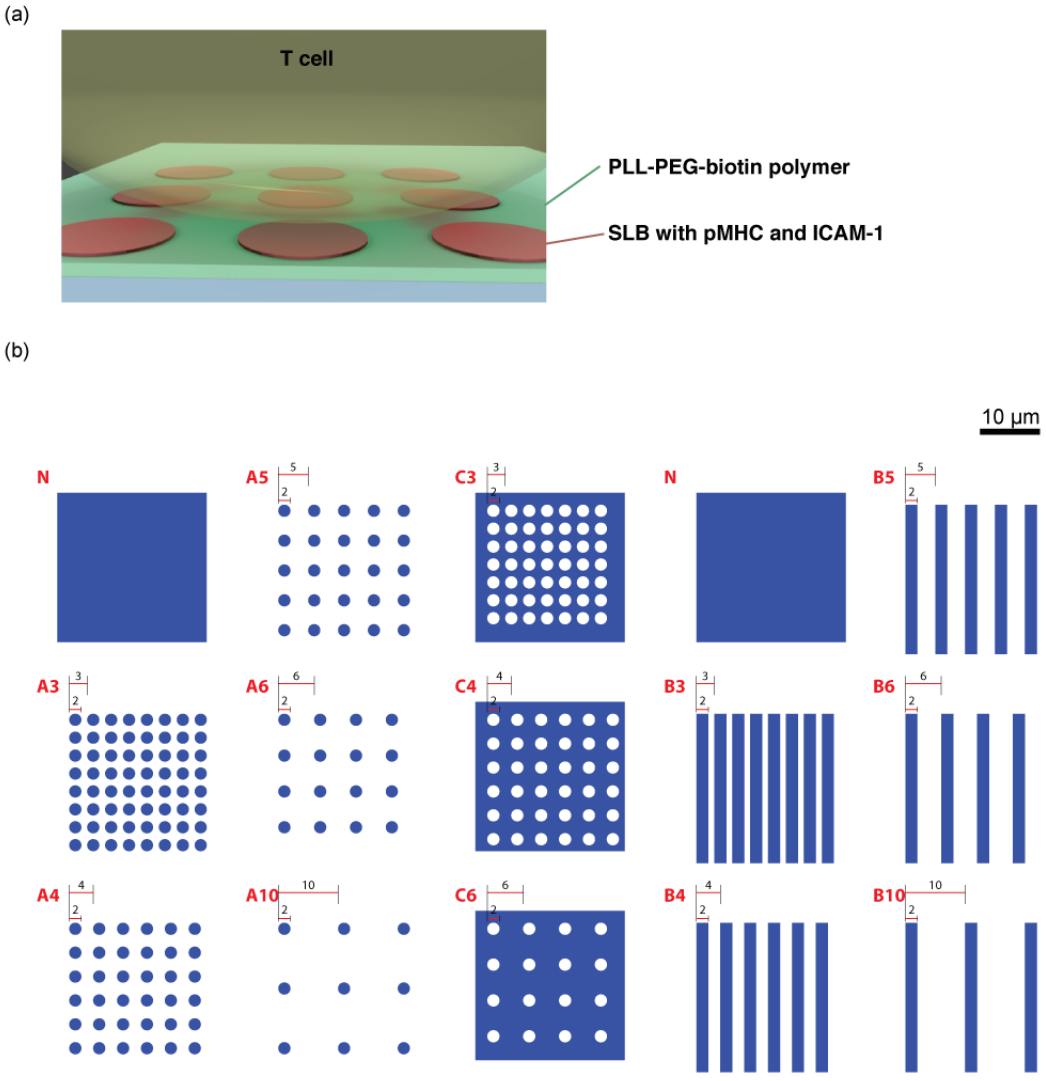

Figure 3.5: Patterning of a SLB by PLL-PEG-biotin polymer. (a) Schematic of polymer pattering and interaction between the patterned bilayer and T cell. The only limited area of T cell surface is activated by fluid ligands on the SLB, while the T cell maintains contact with the surface for the entire area. (b) Design of a photomask for deep UV lithography. The pattern is W 15 mm x H 9 mm, and it is made of 3 x 3 identical subpatterns of W 5 mm x H 3 mm. Each subpattern consists of 15 sections (W 1 mm x H 1 mm each) of different shapes.

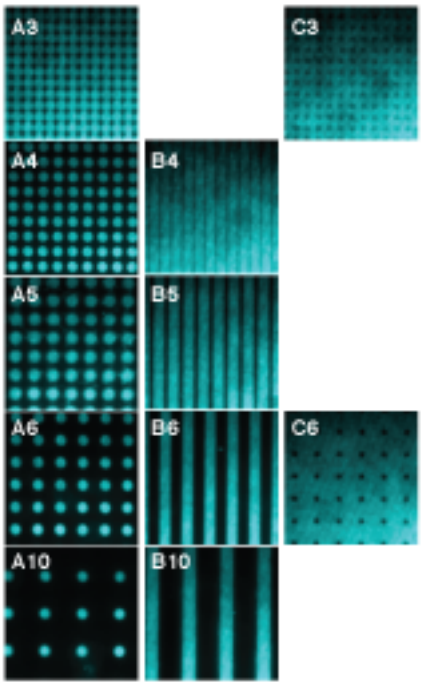

Figure 3.6: Fluorescence images of patterned SLBs. The SLB was made of DOPC/DOGS 98:2, and pMHC and ICAM-1 was incubated on the SLB. The peptide of pMHC (MCC-C) was labeled with Alexa Fluor 647-maleimide. B3 and C4 did not give a clear pattern (they looked homogeneous). Images were rotated by arbitrary angles for clarity.

15 minutes. The resulting polymer coated coverslip was rinsed with 1x PBS (1.5 mL) and water, and dried with a flow of nitrogen. The dried coverslip was put on a drop of water (6.8 μL; 5 μm calculated thickness) on a photomask (Figure 3.5 (b)). Deep UV exposure was carried out for 10 minutes with a UV ozone cleaner (Jelight UVO-Cleaner Model 342) machine followed by rinsing with water and drying with nitrogen. The patterned coverslip was used for making the SLB within 30 minutes.

3.2.2 Primary T cells with transduced LAT-EGFP

T cells were harvested from AND transgenic mice as in Chapter 1. The Phoenix cell line was maintained by splitting with x5 area dilution every 2-4 days in a 75 cm^2 cell culture flask, and 3-4 days before infection, they are seeded into a 175 cm^2 cell culture flask with x5 area dilution. On the day of harvesting mouse organs (Day 1), Phoenix cells were transfected with pCL-Eco and LAT-EGFP plasmids (87.5 μg each; 0.5 $\mu g/cm^2$ cell flask area) with Lipofectamine 2000 (1 $\mu L/cm^2$ flask area), and media of transfected Phoenix cells was changed to T cell RVC media. On Day 3, T cell media was changed to RVC of the Phoenix cell culture with 2 M cells/mL and 48 U/mL IL-2 and 4 μg/mL polybrene. The suspended T cells were put in a 24-well plate with 1.5 mL/well, and spun down with 1.3k x g for 1 hour at room temperature. The T cell media was changed every other day with 48 U/mL IL-2 afterwards. The T cells were used before Day 15.

3.2.3 Labeling of protein and peptide

TCR on live T cells was labeled with anti-TCR Fab labeled with Alexa Fluor 568-NHS ester using an antibody labeling kit (Life Technologies) on ice for 20 minutes right before cell injection. MCC-C peptide (0.5 mM) was labeled with a fluorescent dye with a maleimide functional group (Alexa Fluor 568-maleimide (AF568) or Atto 647N-maleimide (AT647N); 2.5 mM) in 1x PBNS buffer at room temperature for 2 hours, and kept at -20 °C in the dark.

3.2.4 Flow chamber preparation

A flow chamber with an isothermal heater (FCS2, Bioptechs) was used for all cell imaging experiment. The glass coverslip with PLL-PEG-biotin patterns was prepared as above. Small unilamellar vesicles (SUVs) of 1,2-dioleoyl-sn-glycero-3-phosphocholine (DOPC; Avanti Polar Lipids, #85035)/1,2-dioleoyl-sn-glycero-3-[(N-(5-amino-1-carboxypentyl)iminodiacetic acid)succinyl] (nickel salt) (DOGS; Avanti Polar Lipids, #79044) (98:2, 0.5 mg/mL) was made by sonication by a tip sonicator (Sonics and Materials VCX750, 35% amplitude, 2-3 W, 45 seconds x 2 with 10 seconds interval, ∼300 J total.). SUVs were used within a few

days after they were made. The assembled flow chamber was filled with 1x TBS (2 mL). The SUV solution (280 µL) was mixed with 10x TBS (70 µL) and injected into the flow chamber to incubate for 40 minutes to form a laterally fluid lipid bilayer on the coverslip surface. The flow chamber was rinsed with 1x TBS (2 mL), and $NiCl_2$ solution (100 mM in 1x TBS, 0.4 mL) was flowed in to incubate for 5 minutes. The flow chamber was rinsed with 1x TBS (2 mL), and imaging buffer (1x HBS + 1% FBS, 2 mL) was flowed in to block the surface for 15 minutes. A solution of ICAM-His, ICAM-biotin, and pMHC containing excess dye (0.4 mL) was injected to incubate for 40 minutes in the dark. The chamber was rinsed with imaging buffer (2 mL).

3.2.5 Live and fixed cell imaging

A flow chamber prepared above started to be warmed to 37 °C with an isothermal heater 20 minutes before T cell injection. T cells were injected into a flow chamber, and time lapse imaging was started immediately after cell injection. The stage was moved around among n grid positions (typically n = 8, 16, 64), to obtain time lapse images over multiple fields of view. This method enabled observation of live cells of the statistically relevant sample size. The cells were fixed afterwards (time varied) with 1% paraformaldehyde in imaging buffer (2 mL) for imaging fixed cells. Every cell in the fields of view have known duration of interaction with the SLB, τ (Figire 3.4)

3.2.6 Image analysis

LAT cluster intensity dynamics was measured by a line scan of fluorescence intensities on a series of time-lapse images on Jython scripts on Fiji software, and plotted by a Python script with Numpy and Matplotlib (Appendix B). Parameters for line scan and plotting (coordinates of lines and plotting color range) were manually set and recorded in tab-separated values (TSV) files, and those parameters were fed to the script (Figure 3.7). Common utility functions for image analysis were extracted into a separate Jython script (Listing B.3). This setup makes data analysis completely reproducible, and all parameters are recorded in a clear and concise manner.

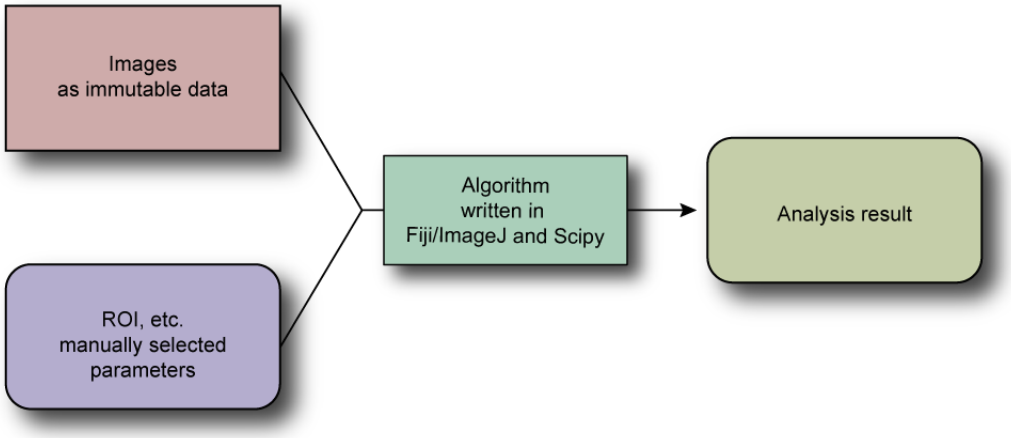

Figure 3.7: A schematic of image processing. Original images are immutable (i.e. not modified in place), and all operations including cropping, thresholding, etc. are done on memory by default. Intermediate image files can be saved if necessary, but even in that case, all the parameters of the operations are recorded and the analysis results are dependent only on the original images and parameters, not intermediate images. This "Single Source Of Truth" approach keeps image analysis simple and traceable.

3.3 Results

3.3.1 Adhesion of T cells on a patterned bilayer

The SLB was patterned with a photomask with various sizes of circles and stripes (Figure 3.5, 3.6). In the presence of ICAM-biotin, T cells formed a round and flat adhesion onto the surface of substrate with many kinds of patterns (Figure 3.8). For patterns with a wide gap between SLB patches (patterns A10, B10, etc.), some cells preferentially adhered to the region with the SLB, avoiding adhesion onto the PLL-PEG-biotin area. Although there is some fluorescent background signal on the PLL-PEG-biotin region, this is probably non-specific binding of excess AF568 dye, not labeled pMHC, because there is almost no background signal when the AF647 was used. Although there might be some residual amount of pMHC that bound to the PLL-PEG-biotin surroundings in a nonspecific manner, this is unlikely to affect signaling, as most of them are not properly oriented to interact with TCR.

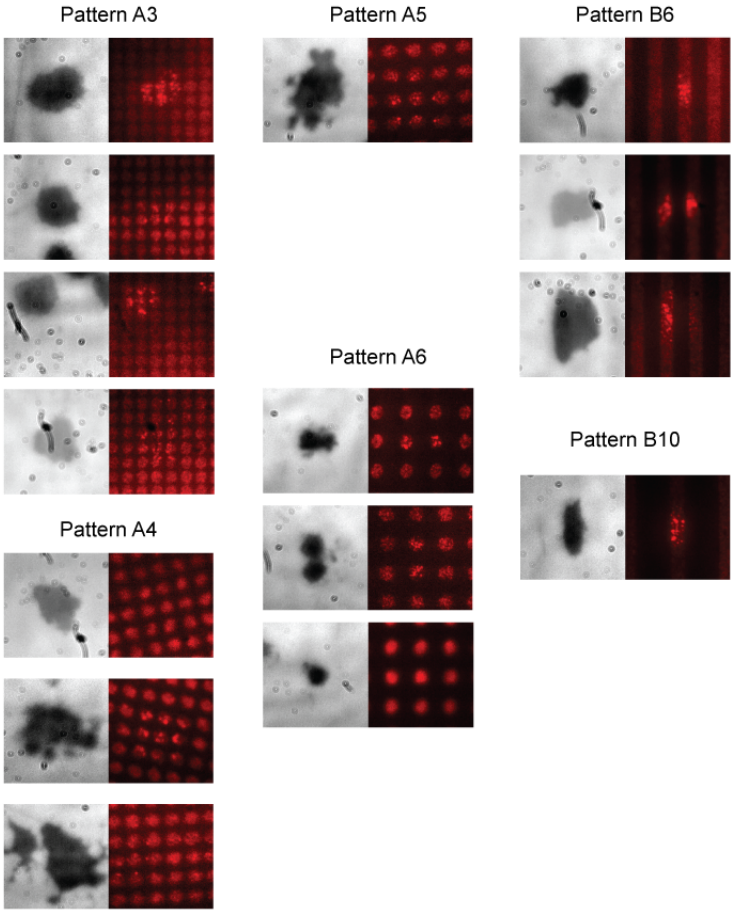

Figure 3.8: Adhesion of T cells to polymer patterned bilayers. T cells adhered to a SLB that was patterned with PLL-PEG-biotin. Very few cells adhered onto Pattern A10, and their contact areas were small (data not shown), presumably due to the low number of ICAM-1 that can interact with a T cell

3.3.2 Live cell imaging of LAT cluster formation on the SLB

LAT-EGFP cluster formation was observed by time-lapse imaging. Many cells on patterns A4, A5, and A6 showed the formation of large clusters that occupy each circular SLB patch. They appeared to grow bigger than TCR microclusters (Figure 3.9). Those LAT clusters typically appear within 2 minutes after the T cell starts spreading onto the SLB (Figure 3.10). Interestingly, the LAT clusters appeared only once for the majority of SLB patches, and they did not show bright clusters again at later time points. In stark contrast to LAT, TCR microclusters were persistent for more than 10 minutes of imaging (Figure 3.12, 3.13).

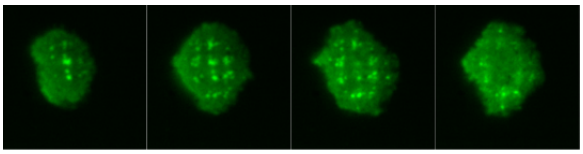

Figure 3.9: Time-lapse imaging of LAT clusters on the T cell membrane. Frame interval: 17 sec.

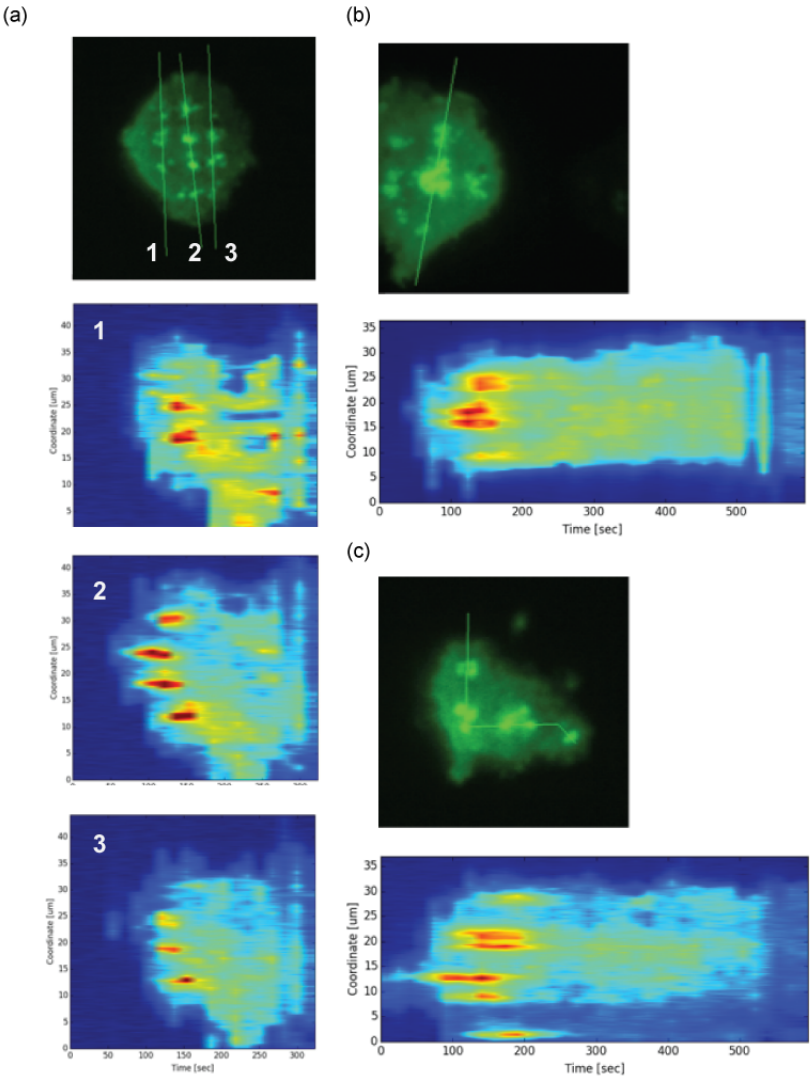

Figure 3.10: Temporal intensity change of LAT of T cells on a polymer patterned SLB. Three representative cells (a), (b), and (c) are shown. X axis: time, Y axis: coordinate along a scan line.

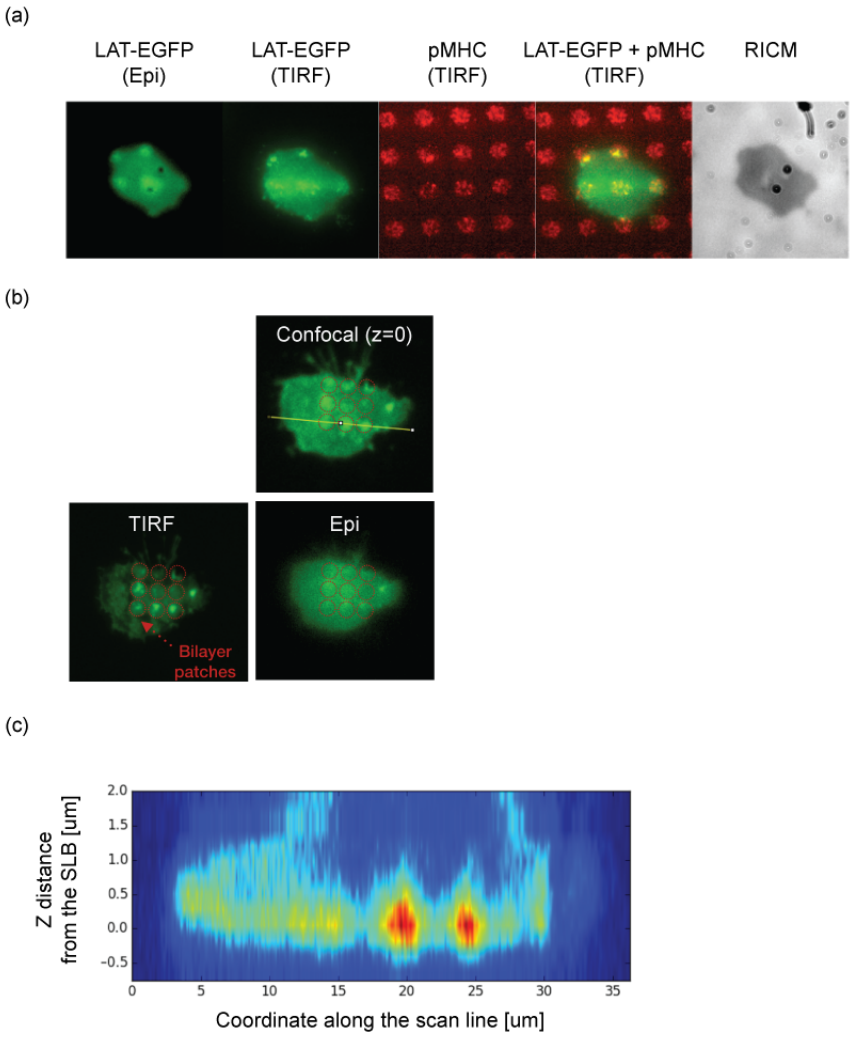

Figure 3.11: LAT-EGFP observed by epifluorescence and confocal microscopy. (a) Epifluorescene images and RICM image. (b) Confocal images (a different cell than (a)), and (c) a vertical slice by confocal microscopy images in (b). Cells were fixed at 4 min after cell injection.

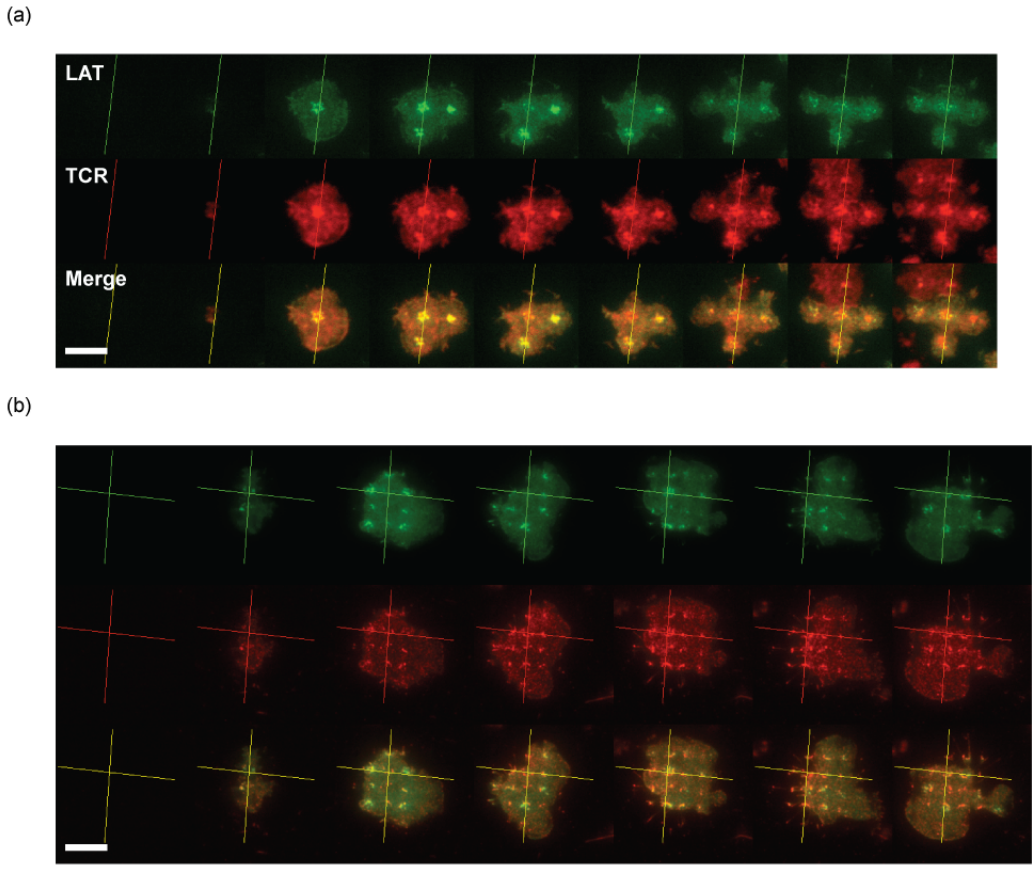

Figure 3.12: Two-color live-cell imaging of LAT-EGFP and TCR. (a) and (b) are two representative cells. Intensity profiles along the lines shown in images were taken, and plotted over time in Figure 3.13. Frame interval is 17 seconds. Scale bar: 10 μm.

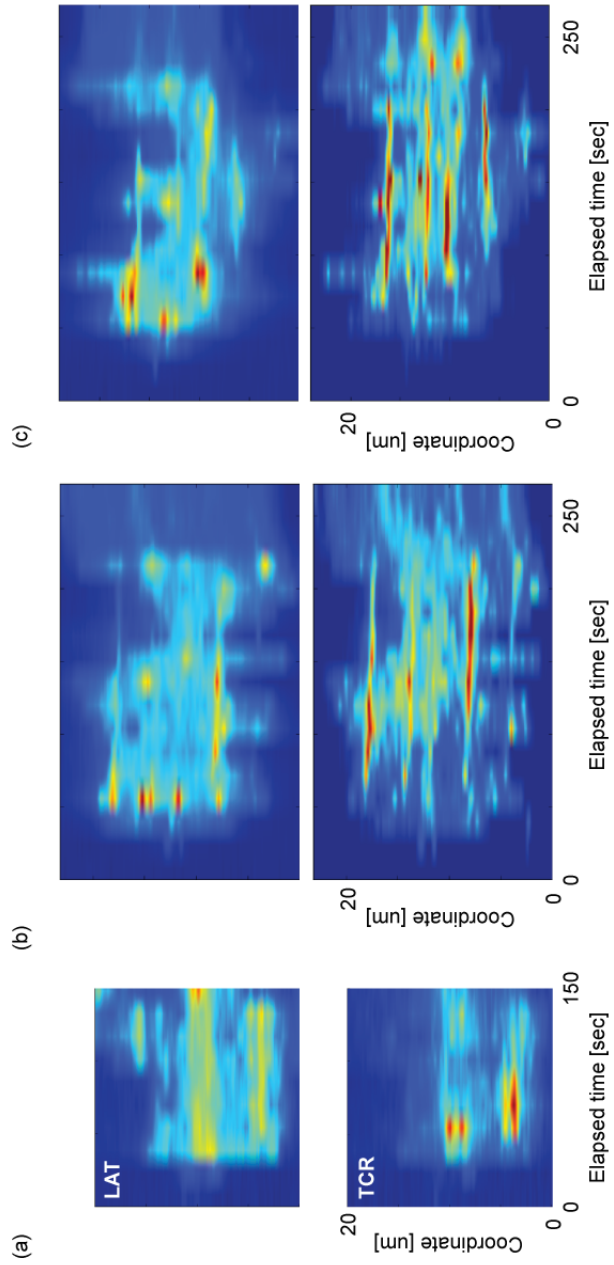

Figure 3.13: Intensity change of LAT and TCR. (a) is from Figure 3.12(a), and (b) and (c) are from Figure 3.12(b).

3.3.3 Confocal microscopy and epifluorescence microscopy of fixed cells

We used epifluorescence microscopy and confocal microscopy to confirm that the LAT clusters observed by TIRF microscopy above are indeed clusters of higher density of LAT, not the artifact by the difference of distance from the glass surface. The T cells were fixed at varied time points, and imaged in an unbiased manner using a square lattice grid of stage positions with 0.5 mm lattice interval (the number of positions: typically 60-144). Representative images are shown in Figure 3.11. Confocal microscopy images clearly showed that bright clusters of LAT are localized the cell membrane that interfaces with the SLB. Although the contrast of LAT clusters in epifluorescence images is lower than TIRF images because the there is background LAT from the cytosol and upper side of the cell membrane, there are still visible puncta of LAT at the SLB patches. We also confirmed that fixing cells does not cause artifact (false positive cluster) or break a cluster in TIRF images by real-time imaging of fixing process, though it causes significant decrease in overall intensity of LAT.

3.4 Discussion

Live-cell TIRF imaging revealed the distinct dynamics of LAT in the T cell. Bright LAT clusters appeared selectively on the SLB patches at the early time point (within 2 minutes) of cell landing, and they disappeared within 60 sec in most cases (Figure 3.9). The distribution of LAT sustaining duration in the same sample is small, although in some conditions LAT clusters were persistent and did not disappear over 10 minutes (data not shown). Nonetheless, majority of SLB patches produced a big, bright LAT cluster only once per patch, and once the LAT cluster dissipates, it does not appear again at the same patch. A similar one-time clustering phenomenon and dissipation of LAT was observed on a cover glass with immobilized ligands to TCR within 150 sec.[132]

Our results indicate the LAT clustering happens only one time from each TCR activation site more clearly than the previous studies, because TCR activation sites (the SLB patches) are well separated from each other, while the SLB maintains the ability of TCR to form a physiologically relevant cluster. Each TCR microcluster is capable of forming a LAT cluster only once after they are formed, and this implies there is a specific mechanism to turn off or regulate LAT clustering after initial triggering of LAT, beyond just a simple signaling pathway that is only dependent on TCR phosphorylation. If the LAT clustering was just a function of TCR phosphorylation and TCR microcluster formation, it would be possible to continuously generate LAT clusters from one TCR activation site. However, this is not the case in our observation.

It is noteworthy that time-lapse, multi-position imaging was combined with cell fixation to measure cell activation duration, τ, for many cells in the fields of view (Figure 3.4) in a single flow chamber. TIRF, epifluorescence, and confocal microscopy images were taken at the same fixed cell with known τ with the uncertainty of frame interval. This technique is useful for obtaining unbiased population statistics for cells with different τ. The immunostaining protocol employed in this study, however, has to be optimized for quantifying phosphorylation of LAT, as Alexa647-rabbit IgG secondary antibody had significant non-specific binding to proteins.

Chapter 4

In vitro reconstitution of dynamic ESCRT protein assemblies by a SLB with nano-curvature

This is a collaboration with Dr. Il-Hyung Lee in Professor James Hurley's group.

4.1 Introduction

The endosomal sorting complexes required for transport (ESCRTs) play an essential role in membrane scission by coordinated sequential reactions by ESCRT-I, ESCRT-II, and ESCRT-III.[149] ESCRT-I and ESCRT-II are involved in membrane budding (forming a local curvature on the cell membrane), and ESCRT-III plays a role in membrane scission at that curved surface of the membrane.

In vivo study of ESCRT machinery by deletion of a part of ESCRT pathway to elucidate the mechanism of ESCRT machinery was unsuccessful, because the formation internal vesicles was inhibited in those conditions.[150–152] In vitro studies helped understanding of ESCRT machinery. Electron microscopy studies revealed structures formed by ESCRT-III subunits.[153–156] Recently, there have been studies on the ESCRT system using an artificial membrane with curvature that ESCRT proteins assemble onto. Hurley and colleagues reconstituted the ESCRT-III function on giant unilamellar vesicles (GUVs), and observed membrane budding of GUVs by ESCRT-III with fluorescence microscopy.[35] GUVs provide a physiologically relevant environment for ESCRTs that is suitable for them to form a membrane budding. In another study, liposomes deposited on a solid surface were used as a scaffold to nucleate ESCRT-III filaments, and observed ESCRT-III nucleates selectively at the edge of

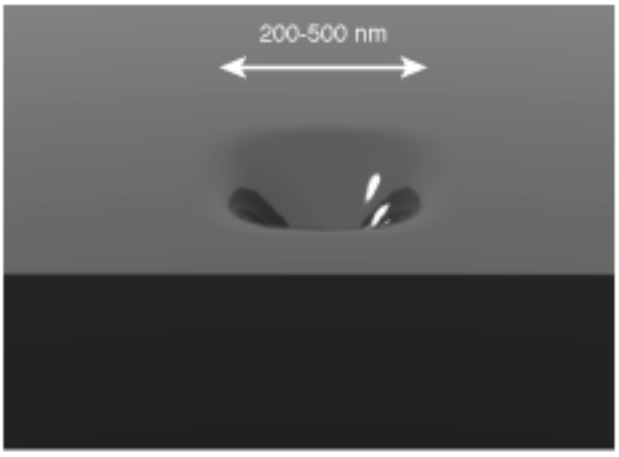

Figure 4.1: A schematic of a SLB with nano-curvature

the liposome with higher curvature.[157]

It is important to investigate the mechanism of ESCRTs in vitro in a physiologically relevant environment with the controlled curvature, as the curvature is thought to be an essential parameter for ESCRT machinery functions. We developed an experimental platform to impose pre-fixed nano-curvature on a membrane environment for ESCRTs. A glass coverslip with nano-hollows of $\sim$100 nm in depth and $\sim$200 nm in diameter (Figure 4.1) was fabricated, and a fluid supported lipid bilayer was deposited on top of that. This membrane with pre-fixed nano-curvature for ESCRTs was used to study the dynamics of ESCRTs assemblies. Geometry-selective assembly of ESCRTs was observed on this experimental system, which opens up possibilities for precise kinetics study on ESCRTs.

4.2 Methods

4.2.1 Fabrication of nano-curvature on a glass surface

Caution: piranha solution is highly reactive, and it causes an explosive reaction with organic solvents including isopropanol. Exceeding 3:1 ratio of H_2SO_4 and H_2O_2 can also be dangerous. You should have H_2SO_4 in a container first, and add H_2O_2 on top of H_2SO_4. A glass coverslip (25 mm diameter, 0.17 mm thickness, No. 1.5; Harvard Apparatus) was cleaned by sonication in isopropanol/water (1:1 volume) for 30 minutes, rinsed with a stream of ultrapure water, cleaned with piranha solution (conc. H_2SO_4/H_2O_2 (30%), 3:1 volume) for 5 minutes at room temperature, rinsed with a stream of ultrapure water, and dried with a flow of nitrogen. A thin film of chromium (6 nm thickness) as a conductive layer was deposited on the cleaned coverslip by an e-beam metal evaporator (Edwards EB3) with 0.1-0.5 nm/sec deposition rate. Nano-curvature on a glass coverslip was fabricated on the glass coverslip with a chromium film by a focused ion beam (FIB; FEI Quanta) operated at 30 kV and 1 nA using a cylindrical milling shape of 100 nm in diameter and 100 nm in depth. The thin chromium film was removed by immersing the coverslip in conc. HCl aq. and touching the surface with an aluminum wire (http://nanolab.berkeley.edu/labmanual/chap1/1.10miscetch.pdf; obtained on Feb 28, 2015), which peeled the chromium film within a few seconds as seen by eyes. The coverslip was rinsed with deionized water, and dried with a flow of nitrogen. The resulting geometry of representative samples was measured by atomic force microscopy (AFM; Asylum Research MFP-3D) at a tapping mode with 335 kHz frequency.

Acknowledgement: We thank Professor Peidong Yang and Dr. Chong Liu for AFM measurement.

4.2.2 Protein expression and purification

Protein expression and purification was done by Dr. Il-Hyung Lee according to the method previously reported.

4.2.3 Real-time imaging of ESCRT proteins on a SLB

ESCRT proteins were labeled with Atto 647N, Atto 488, or Alexa fluor 488, according to the standard methods. A glass coverslip with nano-curvature prepared above was cleaned by piranha solution, assembled into an open chamber (Attofluor Cell Chamber), and the SLB was formed on the glass surface according to the standard method with the composition of 81.995% POPC, 15% POPS, 3% PI3P, 0.005% DiD, and the proteins of interest were

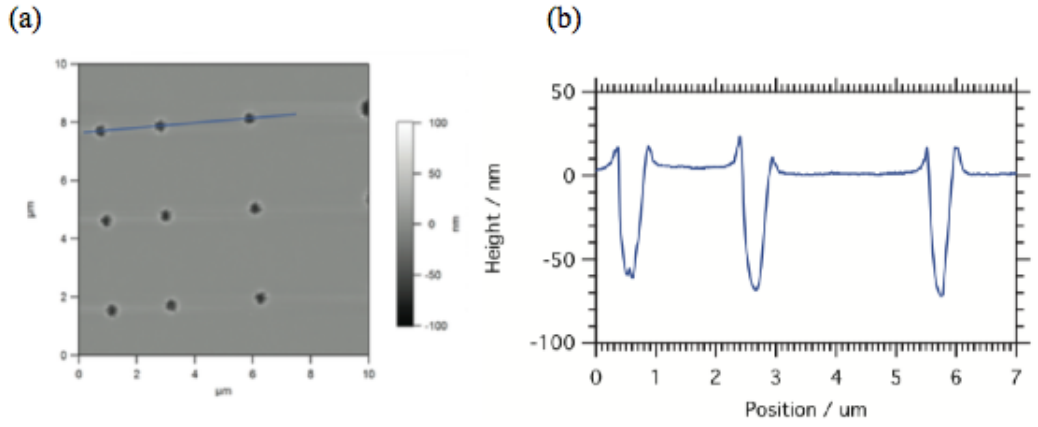

Figure 4.2: Topography of nano-hollows measured by AFM. (a) A height map. (b) A Line scan of height. Note that y axis is scaled larger to make the hollow shape visible more clearly.

injected into the chamber.

4.3 Results

4.3.1 Fabricated nano-curvature and formation of a SLB

Glass surface was successfully milled by FIB to have a massive array of nano-hollows with various sizes, typically ∼200 nm in diameter and ∼100 nm in depth. AFM images show the round edge of the hollow shape. The beam shape of FIB process was set to make a cylindrical shape with 50-500 nm in diameter and 50-500 nm in depth, and there is a considerable amount of broadening of the shape compared to the shape in the machine setting. The edge of cylindrical shape was smoothed because of this broadening, which turned out optimal for creating a continuous supported lipid bilayer on top of that. The laterally fluid SLB was formed on majority of the fabricated nano-hollows continuously, as demonstrated as FRAP (Figure 4.3).

4.3.2 Dynamic accumulation of CHMP4B into the nano-curvature

CHMP4B, a subunit of ESCRT-III proteins, showed strongly selective accumulation into the nano-hollows on the SLB (Figure 4.4), while the underlying SLB itself is still laterally fluid (Figure 4.3) and almost no accumulation into the nano-hollows (Figure 4.4(c)). CHMP4B

(a)

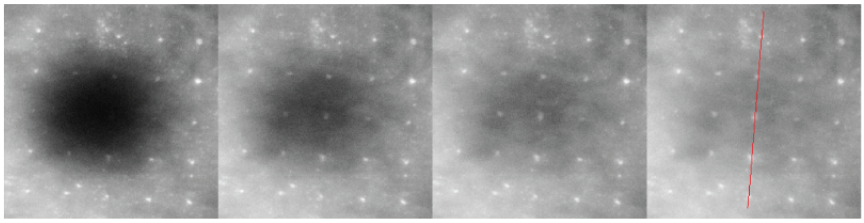

(b)

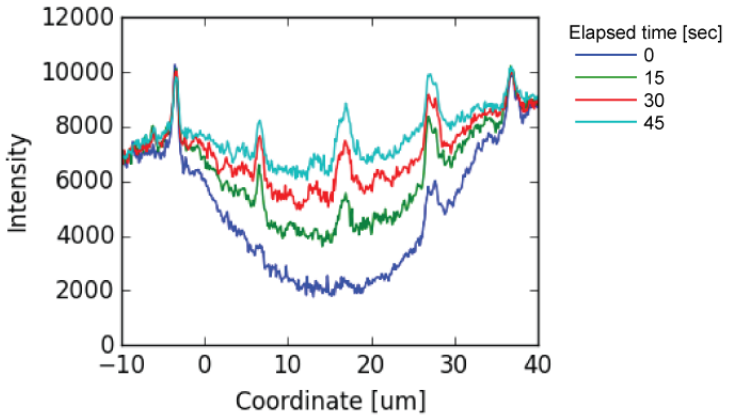

Figure 4.3: Fluorescence recovery after photobleaching (FRAP) on the nano-hollows. (a) Time lapse images, 15 sec interval. (b) Line scans of intensities of time-lapse images in (a).

fluorescence intensity was traced over time, and it showed intensity change that saturates over time (Figure 4.5). In addition, this result suggests the existence of a lagged phase or cooperativity for this accumulation process, because some traces showed a sigmoidal curve, although this has to be further confirmed. Interestingly, CHMP4B also accumulated into the nano-hollows in the absence of any other proteins (Figure 4.5, blue trace). ALIX, a membrane-associated accessory protein in ESCRT machinery, did not accumulate into the nano-hollows, which excludes the possibility of non-specific aggregation of membrane proteins into the nano-hollows.

4.4 Discussion

We developed an experimental platform to study curvature sensing proteins with a predefined nano-curvature geometry, and applied it to ESCRT-III protein assembly. CHMP4B, a subunit of ESCRT-III, is recruited selectively into the SLB on the nano-hollows. The similar selective recruitment into nano-hollows was observed for other ESCRT-III subunits (data not shown). ESCRT-III is involved to membrane scission after the membrane budding by ESCRT-I and ESCRT-II occurs, and this selective accumulation of CHMP4B into nano-hollows we observed indicates that CHMP4B senses the curvature to form a functional assembly. This platform is expected to be applied for further kinetic studies of ESCRT machinery to elucidate biological functions of this curvature-triggered assembly of ESCRT-III proteins.

It is noteworthy that we were able to make a continuous SLB on this nano-hollow with $\sim$200 nm in diameter. If the edge of a nano-hollow is too sharp, the SLB cannot form as a continuous surface. The edges of nano-hollows were round enough, as demonstrated by AFM topographic imaging (Figure 4.2).

Stamou and colleagues have developed an experimental platform using single vesicles to study curvature dependent functions of membrane proteins.[85,86] This system with single vesicle measurement enabled the precise measurement of membrane curvature/protein function relationship. As a general interest in nano-hollows we made for future applications, it is interesting to compare our system (nano-hollows) with Stamou's platform (liposomes). Advantages of our system are (1) Nano-hollows can be combined with TIRF microscopy to do precise measurement such as single molecule tracking. (2) Nano-hollows have a continuous SLB connected to a surrounding flat glass surface. This is a unique property of our system, which enables the study on the recruitment of membrane proteins into nano-hollows. Disadvantages of our system are that (1) the fabrication of nano-hollows is a time-consuming process. (2) There is always some intrinsic variation in nano-hollow shapes even with the same fabrication condition, and direct characterization of individual nano-hollow shape is not easy. In situ aqueous phase AFM will work for characterizing individual nano-hollow geometry during ESCRT assembly experiment.

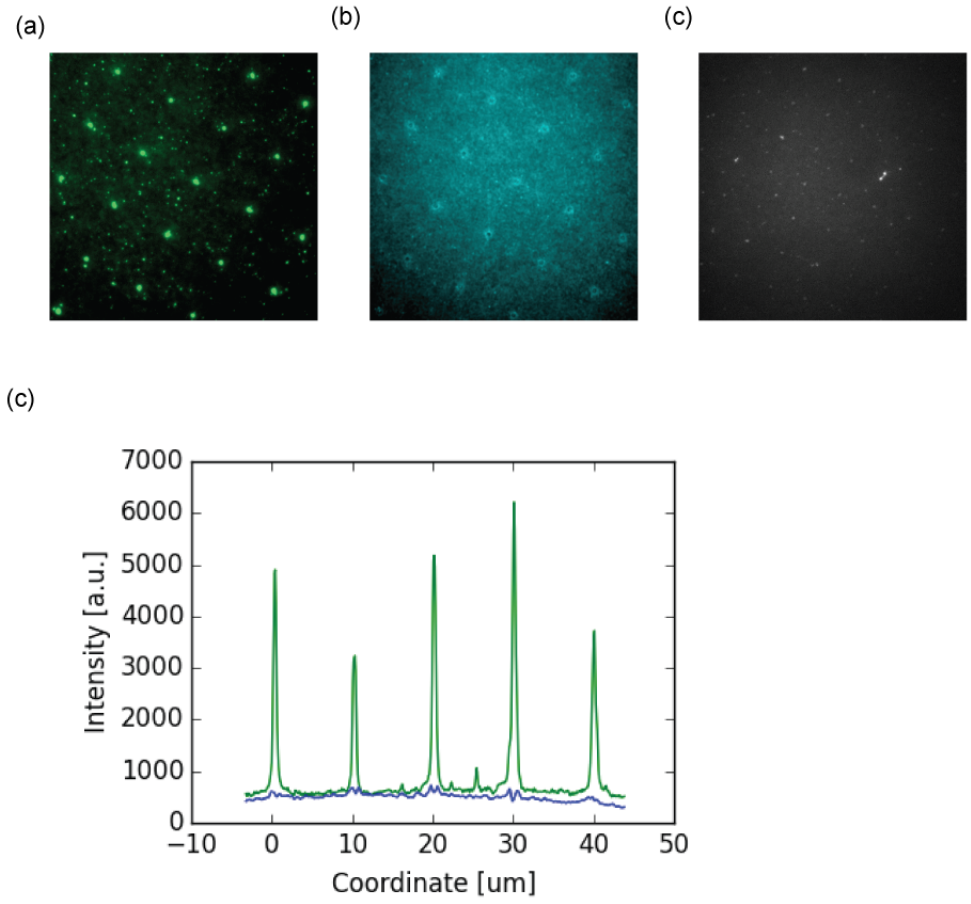

Figure 4.4: Accumulation of CHMP4B into the nano-hollows. The SLB is made of 81.995% POPC, 15% POPS, 3% PI3P, 0.005% DiD. (a) CHMP4B labeled with Atto 488 (CHMP4B-AT488), 8 minutes after adding ESCRT-II (100 nM), CHMP6 (200 nM), and CHMP4B (400 nM) (b) DiD in the SLB. (c) ALIX (a membrane-associated accessory protein in ESCRT machinery) labeled with Atto 594. (d) Line scan of fluorescence intensities of CHMP4B-AF488 (green) and DiD (blue) 8 minutes after the injection of CHMP4B. The intensities of the two channels are scaled arbitrarily so that the accumulation of CHMP4B and DiD can be compared.

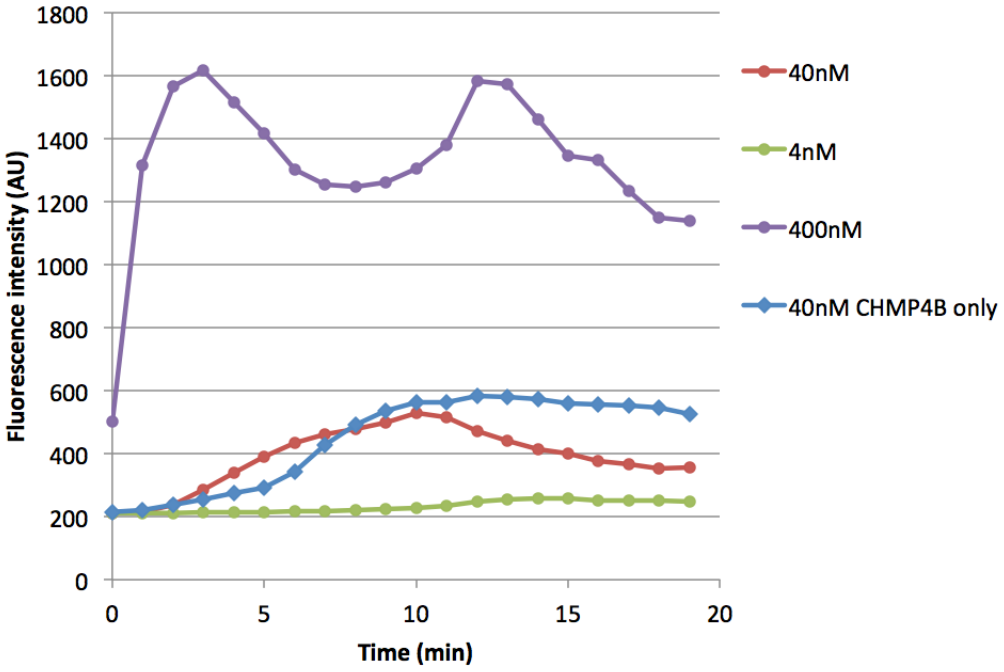

Figure 4.5: Fluorescence intensity change of CHMP4B at different concentrations over time. ESCRT-II (100 nM), CHMP6 (200 nM), varied concentrations of CHMP4B (green, red, purple). CHMP4B concentration: 4 nM (green), 40 nM (red), 400 nM (purple). CHMP4B 40 nM, without ESCRT-II and CHMP6 (blue)

Chapter 5

Future directions

In this Chapter, I will discuss possible interesting future directions that are based on the works presented in this dissertation.

5.1 Curvature-dependent regulation of T cell signaling

While we have investigated T cell signaling (Chapter 2 and 3) and ESCRT machinery (Chapter 4) in separate projects, there seems to be a connection between these two areas. Dustin and colleagues found that TSG-101, a component of the ESCRT-I complex that binds to ubiquitin, is required for cSMAC formation and dephosphorylation of proteins in the microcluster, which indicates the involvement of membrane budding and scission in the downregulation of T cell signaling at cSMAC.[158] Recently, Dustin, Stokes, and colleagues showed that TSG-101 dependent release of TCR-containing vesicles from the T cell occurs at the cSMAC, and this is a mechanism of downregulation of the T cell as well as signaling to the B cell, a counterpart of the T cell.[159] This idea of signaling extracellular vesicles is very new and exciting to the field of T cell signaling.

By forming a bump on the SLB, we could possibly "pre-form" curvature on the T cell membrane for the T cell to cause TCR vesicle fission in a controlled manner, which would be useful for understanding this newly found ESCRT-dependent T cell signaling at the cSMAC. Hollows of $\sim$100 nm can be made by FIB as in Chapter 4. Bumps of the size in the order of 100 nm could be made by lithography and reactive ion etching[160] (Figure 5.1(c)) or gold nanoparticles (Figure 5.1(d)). Gold nanodots originally prepared by block copolymer micelles is $\sim$ 10 nm in diameter, but the size of gold nanodots can grow bigger by applying GoldEnhance reagent (Figure 5.2).

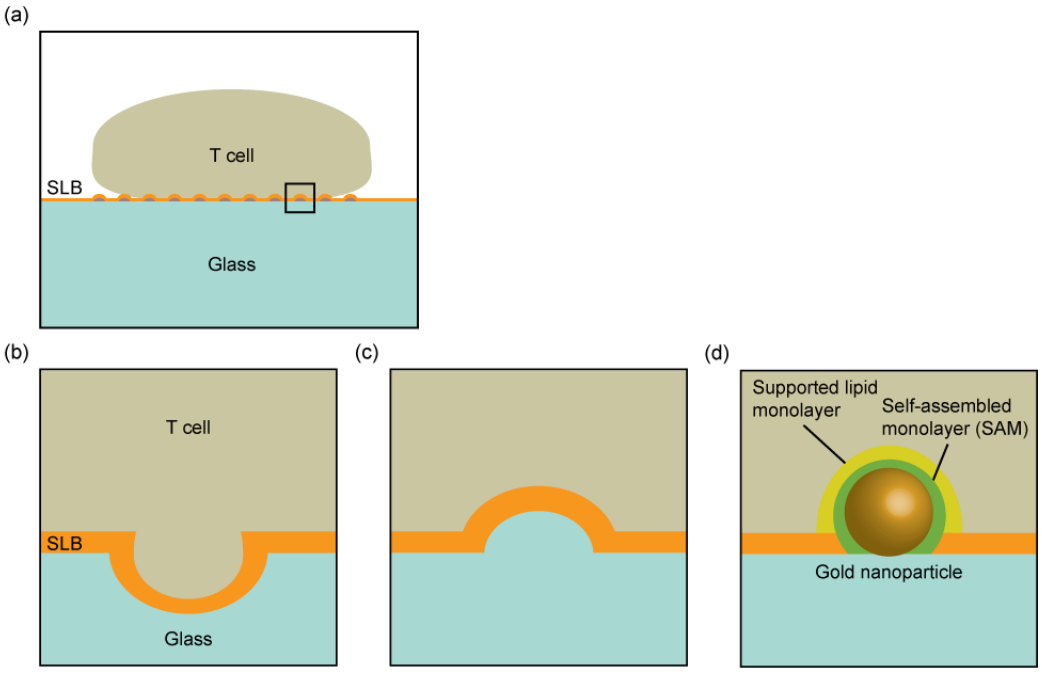

Figure 5.1: Schematic of nano-curvatures for the T cell. (a) T cell-substrate contact. Hollows can be made by (b) FIB as in Chapter 4. Bumps can be made on the glass surface by (c) a lithographic process or (d) gold nanoparticles coated with a self-assembled monolayer of alkanes. (b), (c), and (d) are a magnified view of a small rectangle in (a).

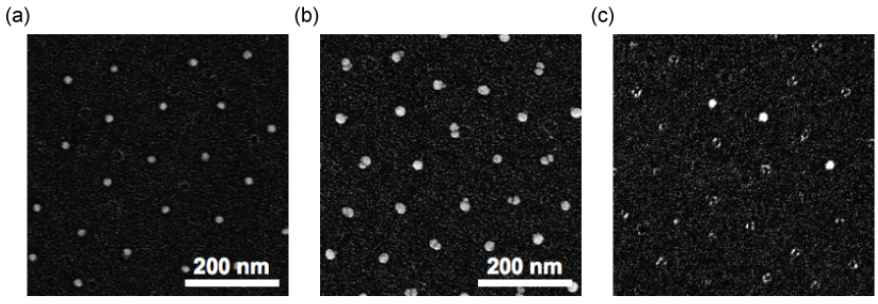

Figure 5.2: Growth of gold nanodots by GoldEnhance reagent. (a) Gold nanodots increased the size by the factor of 2.5 in area. (b) In some cases, gold nanodots are removed.

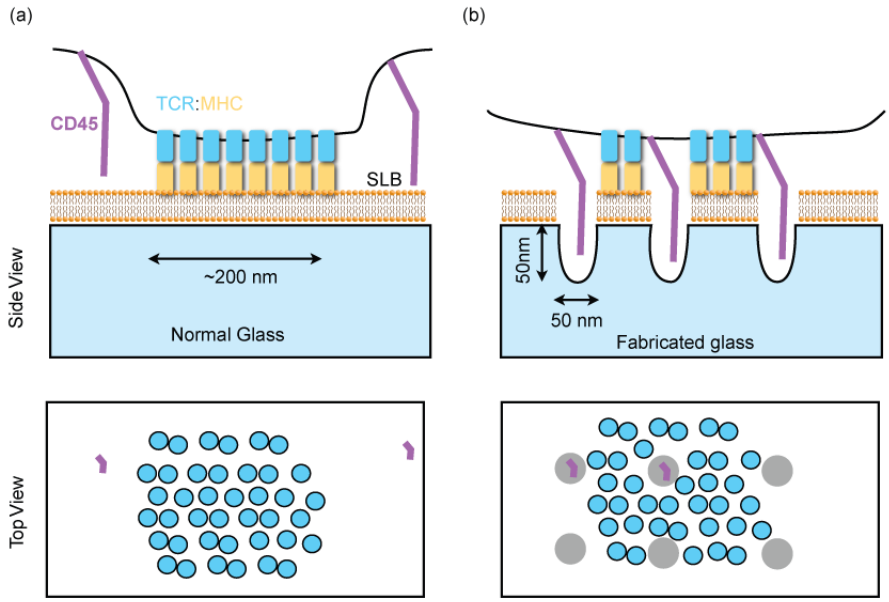

Figure 5.3: Schematic of "vertical spatial mutation". (a) TCR microclusters and CD45 on the ordinary, flat SLB. (b) CD45 can better colocalize with TCR microclusters without membrane distortion

5.2 SLB with holes for observation of steric effects of CD45

The kinetic segregation model states that steric exclusion of CD45, a phosphatase for TCR, from the dense cluster containing TCRs leads to stable phosphorylation and activation of the TCR.[161] Previous studies indicated that CD45 is excluded from TCR microclusters, and CD45 mutant with a truncated extracellular domain abolishes TCR phosphorylation and activation, and the TCR activation was rescued by using a CD45 mutant that has CD43 (an unrelated protein) extracellular region.[162] Another observation that supports the kinetic segregation model is that MHC that is extended on the side of the SLB activates TCR only weakly.[163]

As we have successfully made the array of nano-hollows on the glass surface as in Chapter 4, we can apply similar nano-hollows to studying kinetic segregation models. The CD45 can escape from the TCR microcluster yet stay in proximity of the TCR without disrupting the TCR microcluster by fitting into a FIB-fabricated "pocket" on the glass surface (Figure 5.3). Challenge would be to fabricate dense array of even smaller nano-hollows than made in Chapter 4. 7 nm resolution in FIB process is possible according to the specification of FEI Quanta FIB machine, and fabrication of desired dimensions ($\sim$50 nm) would be realistic.

Chapter 6

Concluding remarks

Combining quantitative fluorescence imaging with materials patterning technology, we investigated dynamic phenomena in T cells and ESCRT proteins.

In Chapter 2, we investigated the lateral transport of TCR microclusters on the T cell membrane under mechanical perturbation using gold nanodot arrays. The major finding that TCR microclusters can become very small such as the order of 30 nm and they are still active in signaling requires reconsideration of the nature and role of TCR microclusters, because microclusters with that small size cannot really make a microenvironment to exclude phosphatase. This nanodot array on the SLB can be used as a platform to manipulate microcluster transport, and it offers possibility for further investigation of TCR microclusters and other proximal signaling molecules such as CD80, CD45, etc.

In Chapter 3, we investigated the clustering dynamics of LAT with spatially localized stimulation to T cells. Interestingly, the T cells clearly showed LAT dynamics that was previously not clearly resolved, and this stimulated interesting questions about a mechanism of regulation of LAT signaling.

In Chapter 4, we investigated the dynamics of ESCRT assemblies on the SLB with nano-hollows. Geometry-sensitive accumulation of CHMP4B, a subunit of ESCRT-III, into the nano-hollows was observed, which indicates the curvature sensing function of CHMP4B and geometry-triggered polymerization of CHMP4B. This platform can be used further detailed kinetics study of ESCRTs in unprecedented precision in a massively parallel way taking advantage of the dense array of nano-hollows.

Throughout Chapter 2 and 3, we employed systematic image analysis approach that separates algorithm (scripts written in Python/Scipy, Fiji, etc.), data (fluorescence images), and parameters (cell image ROIs, intensity threshold, etc.) in order to deal with a large collection of image data in a consistent manner. Data sets and parameters are the only "source of

the truth", and the analysis results are always reproducible from these two. This approach enabled reusable data analysis: exploring huge datasets with various aspects was easy, manageable, and reproducible. Although the written algorithm in this dissertation was specialized for our specific aims, this concept of "reusable data analysis" should be useful for any project that explores big and complicated datasets.

References

[1] Sarah L. Gaffen and Kathleen D. Liu. Overview of interleukin-2 function, production and clinical applications. *Cytokine*, 28(3):109–123, November 2004.

[2] Banishree Saha, S. Jyothi Prasanna, Bhagawat Chandrasekar, and Dipankar Nandi. Gene modulation and immunoregulatory roles of interferonγ. *Cytokine*, 50(1):1–14, April 2010.

[3] Stephen J. Jenkins, Dominik Ruckerl, Graham D. Thomas, James P. Hewitson, Sheelagh Duncan, Frank Brombacher, Rick M. Maizels, David A. Hume, and Judith E. Allen. IL-4 directly signals tissue-resident macrophages to proliferate beyond homeostatic levels controlled by CSF-1. *The Journal of Experimental Medicine*, 210(11):2477–2491, October 2013.

[4] D.S. Goodsell. T-cell receptor. *RCSB Protein Data Bank*, March 2005.

[5] Jennifer E. Smith-Garvin, Gary A. Koretzky, and Martha S. Jordan. T cell activation. *Annual review of immunology*, 27:591–619, 2009.

[6] Robert T. Abraham and Arthur Weiss. Jurkat t cells and development of the t-cell receptor signalling paradigm. *Nature Reviews Immunology*, 4(4):301–308, 2004.

[7] M. A. Goldsmith, L. K. Bockenstedt, P. Dazin, and A. Weiss. Use of somatic cell mutants to study the signal transduction function of the t cell antigen receptor. *Advances in Experimental Medicine and Biology*, 254:25–33, 1989.

[8] Heonsik Choi, Sung-Yup Cho, Ronald H. Schwartz, and Kyungho Choi. Dual effects of sprouty1 on TCR signaling depending on the differentiation state of the t cell. *Journal of Immunology (Baltimore, Md.: 1950)*, 176(10):6034–6045, May 2006.

[9] Jin-Sung Chung, Irene Dougherty, Ponciano D. Cruz, and Kiyoshi Ariizumi. Syndecan-4 mediates the coinhibitory function of DC-HIL on t cell activation. *Journal of Immunology (Baltimore, Md.: 1950)*, 179(9):5778–5784, November 2007.

[10] Tatjana C Gust, Luisa Neubrandt, Claudia Merz, Khusru Asadullah, Ulrich Zügel, and Arne von Bonin. RNA interference-mediated gene silencing in murine t cells: in

vitro and in vivo validation of proinflammatory target genes. *Cell communication and signaling : CCS*, 6:3, August 2008.

[11] Paola Larghi, David J. Williamson, Jean-Marie Carpier, Stéphanie Dogniaux, Karine Chemin, Armelle Bohineust, Lydia Danglot, Katharina Gaus, Thierry Galli, and Claire Hivroz. VAMP7 controls t cell activation by regulating the recruitment and phosphorylation of vesicular lat at TCR-activation sites. *Nature Immunology*, 14(7):723–731, July 2013.

[12] Susan Swift, James Lorens, Philip Achacoso, and Garry P. Nolan. Rapid production of retroviruses for efficient gene delivery to mammalian cells using 293t cell–based systems. In *Current Protocols in Immunology*. John Wiley & Sons, Inc., 2001.

[13] Plat-e: an efficient and stable system for transient packaging of retroviruses. *, Published online: 13 June 2000; — doi:10.1038/sj.gt.3301206*, 7(12), June 2000.

[14] Ben N. G. Giepmans, Stephen R. Adams, Mark H. Ellisman, and Roger Y. Tsien. The fluorescent toolbox for assessing protein location and function. *Science*, 312(5771):217–224, April 2006.

[15] Bo Huang, Hazen Babcock, and Xiaowei Zhuang. Breaking the diffraction barrier: Super-resolution imaging of cells. *Cell*, 143(7):1047–1058, December 2010. WOS:000285625400004.

[16] Lothar Schermelleh, Rainer Heintzmann, and Heinrich Leonhardt. A guide to super-resolution fluorescence microscopy. *Journal of Cell Biology*, 190(2):165–175, July 2010. WOS:000280593300003.

[17] Qing Han, Elizabeth M. Bradshaw, Björn Nilsson, David A. Hafler, and J. Christopher Love. Multidimensional analysis of the frequencies and rates of cytokine secretion from single cells by quantitative microengraving. *Lab on a chip*, 10(11):1391–1400, June 2010.

[18] Alexis J. Torres, Rita Lucia Contento, Susana Gordo, Kai W. Wucherpfennig, and J. Christopher Love. Functional single-cell analysis of t-cell activation by supported lipid bilayer-tethered ligands on arrays of nanowells. *Lab on a chip*, 13(1):90–99, January 2013.

[19] Michael J. Berridge, Peter Lipp, and Martin D. Bootman. The versatility and universality of calcium signalling. *Nature Reviews Molecular Cell Biology*, 1(1):11–21, October 2000.

[20] David E Clapham. Calcium signaling. *Cell*, 80(2):259–268, January 1995.

[21] Boryana N. Manz, Bryan L. Jackson, Rebecca S. Petit, Michael L. Dustin, and Jay Groves. T-cell triggering thresholds are modulated by the number of antigen within

individual t-cell receptor clusters. *Proceedings of the National Academy of Sciences*, 108(22):9089–9094, May 2011.

[22] Masakatsu Yamashita, Motoko Kimura, Masato Kubo, Chiori Shimizu, Tomio Tada, Roger M. Perlmutter, and Toshinori Nakayama. T cell antigen receptor-mediated activation of the ras/mitogen-activated protein kinase pathway controls interleukin 4 receptor function and type-2 helper t cell differentiation. *Proceedings of the National Academy of Sciences*, 96(3):1024–1029, February 1999.

[23] Keishi Adachi and Mark M. Davis. T-cell receptor ligation induces distinct signaling pathways in naïve vs. antigen-experienced t cells. *Proceedings of the National Academy of Sciences*, 108(4):1549–1554, January 2011.

[24] Taichiro Tomida, Kenzo Hirose, Azusa Takizawa, Futoshi Shibasaki, and Masamitsu Iino. NFAT functions as a working memory of ca2+ signals in decoding ca2+ oscillation. *The EMBO Journal*, 22(15):3825–3832, August 2003.

[25] Maria-Cristina Seminario and Ronald L. Wange. Signaling pathways of d3-phosphoinositide-binding kinases in t cells and their regulation by PTEN. *Seminars in Immunology*, 14(1):27–36, February 2002.

[26] X. Wang, A. Gjörloff-Wingren, M. Saxena, N. Pathan, J. C. Reed, and T. Mustelin. The tumor suppressor PTEN regulates t cell survival and antigen receptor signaling by acting as a phosphatidylinositol 3-phosphatase. *Journal of Immunology (Baltimore, Md.: 1950)*, 164(4):1934–1939, February 2000.

[27] X. Shan, M. J. Czar, S. C. Bunnell, P. Liu, Y. Liu, P. L. Schwartzberg, and R. L. Wange. Deficiency of PTEN in jurkat t cells causes constitutive localization of itk to the plasma membrane and hyperresponsiveness to CD3 stimulation. *Molecular and Cellular Biology*, 20(18):6945–6957, September 2000.

[28] E. Astoul, C. Edmunds, D. A. Cantrell, and S. G. Ward. PI 3-k and t-cell activation: limitations of t-leukemic cell lines as signaling models. *Trends in Immunology*, 22(9):490–496, September 2001.

[29] Tak W. Mak, Josef M. Penninger, and Pamela S. Ohashi. Knockout mice: a paradigm shift in modern immunology. *Nature Reviews Immunology*, 1(1):11–19, 2001.

[30] Rémy Bosselut. Retroviral TCR gene transduction: 2a for two. *Nature Methods*, 3(3):162–164, 2006.

[31] Matthew L Bettini, Maria Bettini, and Dario A A Vignali. T-cell receptor retrogenic mice: a rapid, flexible alternative to t-cell receptor transgenic mice. *Immunology*, 136(3):265–272, July 2012.

[32] N Kahya, E I Pécheur, W P de Boeij, D A Wiersma, and D Hoekstra. Reconstitution of membrane proteins into giant unilamellar vesicles via peptide-induced fusion. *Biophysical Journal*, 81(3):1464–1474, September 2001.

[33] Kirsten Bacia, Christina G. Schuette, Nicoletta Kahya, Reinhard Jahn, and Petra Schwille. SNAREs prefer liquid-disordered over "raft" (liquid-ordered) domains when reconstituted into giant unilamellar vesicles. *Journal of Biological Chemistry*, 279(36):37951–37955, September 2004.

[34] David L. Richmond, Eva M. Schmid, Sascha Martens, Jeanne C. Stachowiak, Nicole Liska, and Daniel A. Fletcher. Forming giant vesicles with controlled membrane composition, asymmetry, and contents. *Proceedings of the National Academy of Sciences*, 108(23):9431–9436, June 2011.

[35] Thomas Wollert, Christian Wunder, Jennifer Lippincott-Schwartz, and James H. Hurley. Membrane scission by the ESCRT-III complex. *Nature*, 458(7235):172–177, March 2009.

[36] Thomas Wollert and James H. Hurley. Molecular mechanism of multivesicular body biogenesis by ESCRT complexes. *Nature*, 464(7290):864–869, April 2010.

[37] Winfried Römer, Ludwig Berland, Valérie Chambon, Katharina Gaus, Barbara Windschiegl, Danièle Tenza, Mohamed R. E. Aly, Vincent Fraisier, Jean-Claude Florent, David Perrais, Christophe Lamaze, Graça Raposo, Claudia Steinem, Pierre Sens, Patricia Bassereau, and Ludger Johannes. Shiga toxin induces tubular membrane invaginations for its uptake into cells. *Nature*, 450(7170):670–675, November 2007.

[38] Pierre Sens, Ludger Johannes, and Patricia Bassereau. Biophysical approaches to protein-induced membrane deformations in trafficking. *Current Opinion in Cell Biology*, 20(4):476–482, August 2008.

[39] Katarina Trajkovic, Chieh Hsu, Salvatore Chiantia, Lawrence Rajendran, Dirk Wenzel, Felix Wieland, Petra Schwille, Britta Brügger, and Mikael Simons. Ceramide triggers budding of exosome vesicles into multivesicular endosomes. *Science (New York, N.Y.)*, 319(5867):1244–1247, February 2008.

[40] Hirotami Matsuo, Julien Chevallier, Nathalie Mayran, Isabelle Le Blanc, Charles Ferguson, Julien Fauré, Nathalie Sartori Blanc, Stefan Matile, Jacques Dubochet, Rémy Sadoul, Robert G. Parton, Francis Vilbois, and Jean Gruenberg. Role of LBPA and alix in multivesicular liposome formation and endosome organization. *Science (New York, N.Y.)*, 303(5657):531–534, January 2004.

[41] R. E. Scott. Plasma membrane vesiculation: a new technique for isolation of plasma membranes. *Science (New York, N.Y.)*, 194(4266):743–745, November 1976.

[42] R. E. Scott and P. B. Maercklein. Plasma membrane vesiculation in 3t3 and SV3t3 cells. II. factors affecting the process of vesiculation. *Journal of Cell Science*, 35:245–252, February 1979.

[43] D. Holowka and B. Baird. Structural studies on the membrane-bound immunoglobulin e-receptor complex. 1. characterization of large plasma membrane vesicles from rat basophilic leukemia cells and insertion of amphipathic fluorescent probes. *Biochemistry*, 22(14):3466–3474, July 1983.

[44] Erdinc Sezgin, Hermann-Josef Kaiser, Tobias Baumgart, Petra Schwille, Kai Simons, and Ilya Levental. Elucidating membrane structure and protein behavior using giant plasma membrane vesicles. *Nature Protocols*, 7(6):1042–1051, June 2012.

[45] E. Sackmann. Supported membranes: Scientific and practical applications. *Science*, 271(5245):43–48, January 1996.

[46] Edward T. Castellana and Paul S. Cremer. Solid supported lipid bilayers: From biophysical studies to sensor design. *Surface Science Reports*, 61(10):429–444, November 2006.

[47] Ralf P. Richter, Rémi Bérat, and Alain R. Brisson. Formation of solid-supported lipid bilayers: an integrated view. *Langmuir*, 22(8):3497–3505, April 2006.

[48] Erdinc Sezgin and Petra Schwille. Model membrane platforms to study protein-membrane interactions. *Molecular Membrane Biology*, 29(5):144–154, August 2012.

[49] Y. Barenholz, D. Gibbes, B. J. Litman, J. Goll, T. E. Thompson, and F. D. Carlson. A simple method for the preparation of homogeneous phospholipid vesicles. *Biochemistry*, 16(12):2806–2810, June 1977.

[50] B.J. Frisken, C. Asman, and P.J. Patty. Studies of vesicle extrusion. *Langmuir*, 16(3):928–933, 2000.

[51] R. Nayar, M.J. Hope, and P.R. Cullis. Generation of large unilamellar vesicles from long-chain saturated phosphatidylcholines by extrusion technique. *BBA - Biomembranes*, 986(2):200–206, 1989.

[52] L. D. Mayer, M. J. Hope, and P. R. Cullis. Vesicles of variable sizes produced by a rapid extrusion procedure. *Biochimica et Biophysica Acta (BBA) - Biomembranes*, 858(1):161–168, June 1986.

[53] M. J. Hope, M. B. Bally, G. Webb, and P. R. Cullis. Production of large unilamellar vesicles by a rapid extrusion procedure. characterization of size distribution, trapped volume and ability to maintain a membrane potential. *Biochimica et Biophysica Acta (BBA) - Biomembranes*, 812(1):55–65, January 1985.

[54] S. J. Johnson, T. M. Bayerl, D. C. McDermott, G. W. Adam, A. R. Rennie, R. K. Thomas, and E. Sackmann. Structure of an adsorbed dimyristoylphosphatidylcholine bilayer measured with specular reflection of neutrons. *Biophysical Journal*, 59(2):289–294, February 1991.

[55] C. A. Keller, K. Glasmästar, V. P. Zhdanov, and B. Kasemo. Formation of supported membranes from vesicles. *Physical Review Letters*, 84(23):5443–5446, June 2000.

[56] V. P. Zhdanov and B. Kasemo. Comments on rupture of adsorbed vesicles. *Langmuir*, 17(12):3518–3521, June 2001.

[57] M. Grandbois, H. Clausen-Schaumann, and H. Gaub. Atomic force microscope imaging of phospholipid bilayer degradation by phospholipase a2. *Biophysical Journal*, 74(5):2398–2404, May 1998.

[58] Siwei Zhao, Arnold Chen, Alexander Revzin, and Tingrui Pan. Chapter 10 - stereomask lithography for multi-protein patterning. In Matthieu Piel Théry and Manuel, editors, *Methods in Cell Biology*, volume 119 of *Micropatterning in Cell Biology Part A*, pages 175–192. Academic Press, 2014.

[59] Jay T. Groves, Steven G. Boxer, and Harden M. McConnell. Electric field-induced reorganization of two-component supported bilayer membranes. *Proceedings of the National Academy of Sciences*, 94(25):13390–13395, December 1997.

[60] Jay T. Groves and Steven G. Boxer. Micropattern formation in supported lipid membranes. *Accounts of Chemical Research*, 35(3):149–157, March 2002.

[61] Kaspar D. Mossman, Gabriele Campi, Jay T. Groves, and Michael L. Dustin. Altered TCR signaling from geometrically repatterned immunological synapses. *Science (New York, N.Y.)*, 310(5751):1191–1193, November 2005.

[62] Niña C. Hartman, Jeffrey A. Nye, and Jay T. Groves. Cluster size regulates protein sorting in the immunological synapse. *Proceedings of the National Academy of Sciences of the United States of America*, 106(31):12729–12734, August 2009.

[63] Khalid Salaita, Pradeep M. Nair, Rebecca S. Petit, Richard M. Neve, Debopriya Das, Joe W. Gray, and Jay T. Groves. Restriction of receptor movement alters cellular response: physical force sensing by EphA2. *Science (New York, N.Y.)*, 327(5971):1380–1385, March 2010.

[64] Pradeep M Nair, Khalid Salaita, Rebecca S Petit, and Jay T Groves. Using patterned supported lipid membranes to investigate the role of receptor organization in intercellular signaling. *Nature protocols*, 6(4):523–539, April 2011.

[65] Lars Iversen, Hsiung-Lin Tu, Wan-Chen Lin, Sune M. Christensen, Steven M. Abel, Jeff Iwig, Hung-Jen Wu, Jodi Gureasko, Christopher Rhodes, Rebecca S. Petit,

Scott D. Hansen, Peter Thill, Cheng-Han Yu, Dimitrios Stamou, Arup K. Chakraborty, John Kuriyan, and Jay T. Groves. Molecular kinetics. ras activation by SOS: allosteric regulation by altered fluctuation dynamics. *Science (New York, N.Y.)*, 345(6192):50–54, July 2014.

[66] Jennifer S. Hovis and Steven G. Boxer. Patterning barriers to lateral diffusion in supported lipid bilayer membranes by blotting and stamping. *Langmuir*, 16(3):894–897, February 2000.

[67] Raghuveer Parthasarathy, Cheng-han Yu, and Jay T. Groves. Curvature-modulated phase separation in lipid bilayer membranes. *Langmuir*, 22(11):5095–5099, 2006.

[68] Theobald Lohmüller, Sara Triffo, Geoff P. O'Donoghue, Qian Xu, Michael P. Coyle, and Jay T. Groves. Supported membranes embedded with fixed arrays of gold nanoparticles. *Nano Letters*, 11(11):4912–4918, November 2011.

[69] Gregory L. Kenausis, Janos Vörös, Donald L. Elbert, Ningping Huang, Rolf Hofer, Laurence Ruiz-Taylor, Marcus Textor, Jeffrey A. Hubbell, and Nicholas D. Spencer. Poly(l-lysine)-g-poly(ethylene glycol) layers on metal oxide surfaces: attachment mechanism and effects of polymer architecture on resistance to protein adsorption†. *The Journal of Physical Chemistry B*, 104(14):3298–3309, April 2000.

[70] Uta Wattendorf and Hans P. Merkle. PEGylation as a tool for the biomedical engineering of surface modified microparticles. *Journal of Pharmaceutical Sciences*, 97(11):4655–4669, November 2008.

[71] Min Wu, David Holowka, Harold G. Craighead, and Barbara Baird. Visualization of plasma membrane compartmentalization with patterned lipid bilayers. *Proceedings of the National Academy of Sciences of the United States of America*, 101(38):13798–13803, September 2004.

[72] A. Grakoui, S. K. Bromley, C. Sumen, M. M. Davis, A. S. Shaw, P. M. Allen, and M. L. Dustin. The immunological synapse: a molecular machine controlling t cell activation. *Science (New York, N.Y.)*, 285(5425):221–227, July 1999.

[73] Samara L. Reck-Peterson, Nathan D. Derr, and Nico Stuurman. Imaging single molecules using total internal reflection fluorescence microscopy (TIRFM). *Cold Spring Harbor Protocols*, 2010(3):pdb.top73, March 2010.

[74] Erdinc Sezgin and Petra Schwille. Fluorescence techniques to study lipid dynamics. *Cold Spring Harbor Perspectives in Biology*, 3(11):a009803, November 2011.

[75] Jodi Gureasko, William J. Galush, Sean Boykevisch, Holger Sondermann, Dafna Bar-Sagi, Jay T. Groves, and John Kuriyan. Membrane-dependent signal integration by the ras activator son of sevenless. *Nature Structural & Molecular Biology*, 15(5):452–461, May 2008.

[76] Marta Bally, Kelly Bailey, Kaori Sugihara, Dorothee Grieshaber, Janos Vörös, and Brigitte Städler. Liposome and lipid bilayer arrays towards biosensing applications. *Small*, 6(22):2481–2497, November 2010.

[77] Torsten Wieprecht, Michael Beyermann, and Joachim Seelig. Thermodynamics of the coil-alpha-helix transition of amphipathic peptides in a membrane environment: the role of vesicle curvature. *Biophysical Chemistry*, 96(2-3):191–201, May 2002.

[78] Kenneth M. P. Taylor and Mark A. Roseman. Effect of cholesterol, fatty acyl chain composition, and bilayer curvature on the interaction of cytochrome b5 with liposomes of phosphatidylcholines. *Biochemistry*, 34(11):3841–3850, March 1995.

[79] Joëlle Bigay, Pierre Gounon, Sylviane Robineau, and Bruno Antonny. Lipid packing sensed by ArfGAP1 couples COPI coat disassembly to membrane bilayer curvature. *Nature*, 426(6966):563–566, December 2003.

[80] Tobias Baumgart, Samuel T. Hess, and Watt W. Webb. Imaging coexisting fluid domains in biomembrane models coupling curvature and line tension. *Nature*, 425(6960):821–824, October 2003.

[81] Aurélien Roux, Damien Cuvelier, Pierre Nassoy, Jacques Prost, Patricia Bassereau, and Bruno Goud. Role of curvature and phase transition in lipid sorting and fission of membrane tubules. *The EMBO Journal*, 24(8):1537–1545, April 2005.

[82] Rosemary Cornell and Svetla Taneva. Amphipathic helices as mediators of the membrane interaction of amphitropic proteins, and as modulators of bilayer physical properties. *Current Protein & Peptide Science*, 7(6):539–552, December 2006.

[83] Guillaume Drin, Jean-François Casella, Romain Gautier, Thomas Boehmer, Thomas U. Schwartz, and Bruno Antonny. A general amphipathic α-helical motif for sensing membrane curvature. *Nature Structural & Molecular Biology*, 14(2):138–146, February 2007.

[84] Brian J. Peter, Helen M. Kent, Ian G. Mills, Yvonne Vallis, P. Jonathan G. Butler, Philip R. Evans, and Harvey T. McMahon. BAR domains as sensors of membrane curvature: The amphiphysin BAR structure. *Science*, 303(5657):495–499, January 2004.

[85] Nikos S. Hatzakis, Vikram K. Bhatia, Jannik Larsen, Kenneth L. Madsen, Pierre-Yves Bolinger, Andreas H. Kunding, John Castillo, Ulrik Gether, Per Hedegård, and Dimitrios Stamou. How curved membranes recruit amphipathic helices and protein anchoring motifs. *Nature Chemical Biology*, 5(11):835–841, November 2009.

[86] Jannik Bruun Larsen, Martin Borch Jensen, Vikram K. Bhatia, Søren L. Pedersen, Thomas Bjørnholm, Lars Iversen, Mark Uline, Igal Szleifer, Knud J. Jensen, Nikos S.

Hatzakis, and Dimitrios Stamou. Membrane curvature enables n-ras lipid anchor sorting to liquid-ordered membrane phases. *Nature Chemical Biology*, 11(3):192–194, 2015.

[87] E. J. Ambrose. A surface contact microscope for the study of cell movements. *Nature*, 178(4543):1194–1194, November 1956.

[88] D. Axelrod. Cell-substrate contacts illuminated by total internal reflection fluorescence. *The Journal of Cell Biology*, 89(1):141–145, April 1981.

[89] Dinah Loerke, Beate Preitz, Walter Stühmer, and Martin Oheim. Super-resolution measurements with evanescent-wave fluorescence excitation using variable beam incidence. *Journal of Biomedical Optics*, 5(1):23, 2000.

[90] C. R. Monks, B. A. Freiberg, H. Kupfer, N. Sciaky, and A. Kupfer. Three-dimensional segregation of supramolecular activation clusters in t cells. *Nature*, 395(6697):82–86, September 1998.

[91] Kyeong-Hee Lee, Amy D. Holdorf, Michael L. Dustin, Andrew C. Chan, Paul M. Allen, and Andrey S. Shaw. T cell receptor signaling precedes immunological synapse formation. *Science (New York, N.Y.)*, 295(5559):1539–1542, February 2002.

[92] Rajat Varma, Gabriele Campi, Tadashi Yokosuka, Takashi Saito, and Michael L. Dustin. T cell receptor-proximal signals are sustained in peripheral microclusters and terminated in the central supramolecular activation cluster. *Immunity*, 25(1):117–127, July 2006. WOS:000239713000015.

[93] David R. Fooksman, Santosh Vardhana, Gaia Vasiliver-Shamis, Jan Liese, David A. Blair, Janelle Waite, Catarina Sacristán, Gabriel D. Victora, Alexandra Zanin-Zhorov, and Michael L. Dustin. Functional anatomy of t cell activation and synapse formation. *Annual Review of Immunology*, 28:79–105, 2010.

[94] Kaushik Choudhuri and Michael L Dustin. Signaling microdomains in t cells. *FEBS letters*, 584(24), December 2010.

[95] Maria-Cristina Seminario and Stephen C. Bunnell. Signal initiation in t-cell receptor microclusters. *Immunological Reviews*, 221:90–106, February 2008.

[96] P. Anton van der Merwe and Omer Dushek. Mechanisms for t cell receptor triggering. *Nature Reviews. Immunology*, 11(1):47–55, January 2011.

[97] Thomas R. Weikl and Reinhard Lipowsky. Pattern formation during t-cell adhesion. *Biophysical Journal*, 87(6):3665–3678, December 2004.

[98] Thomas R. Weikl, Mesfin Asfaw, Heinrich Krobath, Bartosz Różycki, and Reinhard Lipowsky. Adhesion of membranesviareceptor–ligand complexes: Domain formation, binding cooperativity, and active processes. *Soft Matter*, 5(17):3213–3224, August 2009.

[99] Niña G. Caculitan, Hiroyuki Kai, Eulanca Y. Liu, Nicole Fay, Yan Yu, Theobald Lohmüller, Geoff P. O'Donoghue, and Jay T. Groves. Size-based chromatography of signaling clusters in a living cell membrane. *Nano Letters*, 14(5):2293–2298, May 2014.

[100] Takashi Saito and Tadashi Yokosuka. Immunological synapse and microclusters: the site for recognition and activation of t cells. *Current Opinion in Immunology*, 18(3):305–313, 2006.

[101] Daniel D. Billadeau, Jeffrey C. Nolz, and Timothy S. Gomez. Regulation of t-cell activation by the cytoskeleton. *Nature Reviews Immunology*, 7(2):131–143, 2007.

[102] G. Campi, R. Varma, and M. L. Dustin. Actin and agonist MHC-peptide complex-dependent t cell receptor microclusters as scaffolds for signaling. *Journal of Experimental Medicine*, 202(8):1031–1036, October 2005. WOS:000232929500003.

[103] T. Yokosuka, K. Sakata-Sogawa, W. Kobayashi, M. Hiroshima, A. Hashimoto-Tane, M. Tokunaga, M. L. Dustin, and T. Saito. Newly generated t cell receptor microclusters initiate and sustain t cell activation by recruitment of zap70 and SLP-76. *Nature Immunology*, 6(12):1253–1262, December 2005. WOS:000233371900014.

[104] Michael L. Dustin and Jay T. Groves. Receptor signaling clusters in the immune synapse. *Annual Review of Biophysics*, 41(1):543–556, 2012.

[105] Wolfgang W. A. Schamel and Balbino Alarcón. Organization of the resting TCR in nanoscale oligomers. *Immunological Reviews*, 251(1):13–20, January 2013.

[106] Björn F Lillemeier, Manuel A Mörtelmaier, Martin B Forstner, Johannes B Huppa, Jay T Groves, and Mark M Davis. TCR and lat are expressed on separate protein islands on t cell membranes and concatenate during activation. *Nature Immunology*, 11(1):90–96, January 2010.

[107] Yan Yu, Nicole C. Fay, Alexander A. Smoligovets, Hung-Jen Wu, and Jay T. Groves. Myosin IIA modulates t cell receptor transport and CasL phosphorylation during early immunological synapse formation. *PLoS ONE*, 7(2), February 2012.

[108] Jay T. Groves, Nick Ulman, and Steven G. Boxer. Micropatterning fluid lipid bilayers on solid supports. *Science*, 275(5300):651–653, January 1997.

[109] Janosch Deeg, Markus Axmann, Jovana Matic, Anastasia Liapis, David Depoil, Jehan Afrose, Silvia Curado, Michael L. Dustin, and Joachim P. Spatz. T cell activation is determined by the number of presented antigens. *Nano Letters*, 13(11):5619–5626, 2013.

[110] Derfogail Delcassian, David Depoil, Dominika Rudnicka, Mengling Liu, Daniel M. Davis, Michael L. Dustin, and Iain E. Dunlop. Nanoscale ligand spacing influences receptor triggering in t cells and NK cells. *Nano Letters*, 13(11):5608–5614, 2013.

[111] Theobald Lohmüller, Qian Xu, and Jay T. Groves. Nanoscale obstacle arrays frustrate transport of EphA2-ephrin-a1 clusters in cancer cell lines. *Nano Letters*, 13(7):3059–3064, July 2013.

[112] Jovana Matic, Janosch Deeg, Alexander Scheffold, Itamar Goldstein, and Joachim P. Spatz. Fine tuning and efficient t cell activation with stimulatory aCD3 nanoarrays. *Nano Letters*, 13(11):5090–5097, November 2013.

[113] Wan-Chen Lin, Cheng-Han Yu, Sara Triffo, and Jay T. Groves. Supported membrane formation, characterization, functionalization, and patterning for application in biological science and technology. In *Current Protocols in Chemical Biology*. John Wiley & Sons, Inc., 2009.

[114] Khuloud Jaqaman, Dinah Loerke, Marcel Mettlen, Hirotaka Kuwata, Sergio Grinstein, Sandra L. Schmid, and Gaudenz Danuser. Robust single-particle tracking in live-cell time-lapse sequences. *Nature Methods*, 5(8):695–702, August 2008.

[115] Kaushik Choudhuri, David Wiseman, Marion H. Brown, Keith Gould, and P. Anton van der Merwe. T-cell receptor triggering is critically dependent on the dimensions of its peptide-MHC ligand. *Nature*, 436(7050):578–582, July 2005.

[116] Evan W. Newell, Lauren K. Ely, Andrew C. Kruse, Philip A. Reay, Stephanie N. Rodriguez, Aaron E. Lin, Michael S. Kuhns, K. Christopher Garcia, and Mark M. Davis. Structural basis of specificity and cross-reactivity in t cell receptors specific for cytochrome c-i-e(k). *Journal of Immunology (Baltimore, Md.: 1950)*, 186(10):5823–5832, May 2011.

[117] John R. James and Ronald D. Vale. Biophysical mechanism of t-cell receptor triggering in a reconstituted system. *Nature*, 487(7405):64–69, July 2012.

[118] Darrell J. Irvine, Marco A. Purbhoo, Michelle Krogsgaard, and Mark M. Davis. Direct observation of ligand recognition by t cells. *Nature*, 419(6909):845–849, October 2002.

[119] Geoff P. O'Donoghue, Rafal M. Pielak, Alexander A. Smoligovets, Jenny J. Lin, and Jay T. Groves. Direct single molecule measurement of TCR triggering by agonist pMHC in living primary t cells. *eLife*, 2:e00778, 2013.

[120] Yiyuan Yin, Xin Xiang Wang, and Roy A. Mariuzza. Crystal structure of a complete ternary complex of t-cell receptor, peptide–MHC, and CD4. *Proceedings of the National Academy of Sciences*, 109(14):5405–5410, April 2012.

[121] Juha P. Himanen, Laila Yermekbayeva, Peter W. Janes, John R. Walker, Kai Xu, Lakmali Atapattu, Kanagalaghatta R. Rajashankar, Anneloes Mensinga, Martin Lackmann, Dimitar B. Nikolov, and Sirano Dhe-Paganon. Architecture of eph receptor clusters. *Proceedings of the National Academy of Sciences*, 107(24):10860–10865, June 2010.

[122] Qian Xu, Wan-Chen Lin, Rebecca S. Petit, and Jay T. Groves. EphA2 receptor activation by monomeric ephrin-a1 on supported membranes. *Biophysical Journal*, 101(11):2731–2739, December 2011.

[123] W. Zhang, J. Sloan-Lancaster, J. Kitchen, R. P. Trible, and L. E. Samelson. LAT: the ZAP-70 tyrosine kinase substrate that links t cell receptor to cellular activation. *Cell*, 92(1):83–92, January 1998.

[124] Lakshmi Balagopalan, Nathan P. Coussens, Eilon Sherman, Lawrence E. Samelson, and Connie L. Sommers. The LAT story: A tale of cooperativity, coordination, and choreography. *Cold Spring Harbor Perspectives in Biology*, 2(8), August 2010.

[125] Romain Roncagalli, Michael Mingueneau, Claude Grégoire, Marie Malissen, and Bernard Malissen. LAT signaling pathology: an "autoimmune" condition without t cell self-reactivity. *Trends in Immunology*, 31(7):253–259, July 2010.

[126] J. Lin and A. Weiss. Identification of the minimal tyrosine residues required for linker for activation of t cell function. *The Journal of Biological Chemistry*, 276(31):29588–29595, August 2001.

[127] Rebekah R. Bartelt and Jon C. D. Houtman. The adaptor protein LAT serves as an integration node for signaling pathways that drive t cell activation. *Wiley Interdisciplinary Reviews: Systems Biology and Medicine*, 5(1):101–110, January 2013.

[128] M. Wittekind, C. Mapelli, B. T. Farmer, K. L. Suen, V. Goldfarb, J. Tsao, T. Lavoie, M. Barbacid, C. A. Meyers, and L. Mueller. Orientation of peptide fragments from sos proteins bound to the n-terminal SH3 domain of grb2 determined by NMR spectroscopy. *Biochemistry*, 33(46):13531–13539, November 1994.

[129] Jon C. D. Houtman, Hiroshi Yamaguchi, Mira Barda-Saad, Alex Braiman, Brent Bowden, Ettore Appella, Peter Schuck, and Lawrence E. Samelson. Oligomerization of signaling complexes by the multipoint binding of GRB2 to both LAT and SOS1. *Nature Structural & Molecular Biology*, 13(9):798–805, September 2006.

[130] Ambarish Nag, Michael I. Monine, James R. Faeder, and Byron Goldstein. Aggregation of membrane proteins by cytosolic cross-linkers: Theory and simulation of the LAT-grb2-SOS1 system. *Biophysical Journal*, 96(7):2604–2623, 2009.

[131] Ambarish Nag, Michael Monine, Alan S. Perelson, and Byron Goldstein. Modeling and simulation of aggregation of membrane protein LAT with molecular variability in the number of binding sites for cytosolic grb2-SOS1-grb2. *PloS One*, 7(3):e28758, 2012.

[132] Stephen C. Bunnell, David I. Hong, Julia R. Kardon, Tetsuo Yamazaki, C. Jane McGlade, Valarie A. Barr, and Lawrence E. Samelson. T cell receptor ligation induces the formation of dynamically regulated signaling assemblies. *The Journal of Cell Biology*, 158(7):1263–1275, September 2002.

[133] Eilon Sherman, Valarie Barr, Suliana Manley, George Patterson, Lakshmi Balagopalan, Itoro Akpan, Carole K. Regan, Robert K. Merrill, Connie L. Sommers, Jennifer Lippincott-Schwartz, and Lawrence E. Samelson. Functional nanoscale organization of signaling molecules downstream of the t cell antigen receptor. *Immunity*, 35(5):705–720, 2011.

[134] Marco A. Purbhoo, Hebin Liu, Stephane Oddos, Dylan M. Owen, Mark A. A. Neil, Sophie V. Pageon, Paul M. W. French, Christopher E. Rudd, and Daniel M. Davis. Dynamics of subsynaptic vesicles and surface microclusters at the immunological synapse. *Science Signaling*, 3(121):ra36, May 2010. WOS:000277564900002.

[135] Georges A. Azar, Fabrice Lemaitre, Ellen A. Robey, and Philippe Bousso. Subcellular dynamics of t cell immunological synapses and kinapses in lymph nodes. *Proceedings of the National Academy of Sciences of the United States of America*, 107(8):3675–3680, February 2010. WOS:000275130900072.

[136] Stephen C. Bunnell, Andrew L. Singer, David I. Hong, Berri H. Jacque, Martha S. Jordan, Maria-Cristina Seminario, Valarie A. Barr, Gary A. Koretzky, and Lawrence E. Samelson. Persistence of cooperatively stabilized signaling clusters drives t-cell activation. *Molecular and Cellular Biology*, 26(19):7155–7166, October 2006.

[137] Jon C. D. Houtman, Mira Barda-Saad, and Lawrence E. Samelson. Examining multiprotein signaling complexes from all angles. the use of complementary techniques to characterize complex formation at the adapter protein, linker for activation of t cells. *FEBS Journal*, 272(21):5426–5435, November 2005.

[138] Natsuko Tanimura, Masakazu Nagafuku, Yasuko Minaki, Yukio Umeda, Fumie Hayashi, Junko Sakakura, Akiko Kato, Douglas R. Liddicoat, Masato Ogata, Toshiyuki Hamaoka, and Atsushi Kosugi. Dynamic changes in the mobility of LAT in aggregated lipid rafts upon t cell activation. *The Journal of Cell Biology*, 160(1):125–135, January 2003.

[139] Adam D. Douglass and Ronald D. Vale. Single-molecule microscopy reveals plasma membrane microdomains created by protein-protein networks that exclude or trap signaling molecules in t cells. *Cell*, 121(6):937–950, June 2005.

[140] Akihiro Kusumi, Hiroshi Ike, Chieko Nakada, Kotono Murase, and Takahiro Fujiwara. Single-molecule tracking of membrane molecules: plasma membrane compartmentalization and dynamic assembly of raft-philic signaling molecules. *Seminars in Immunology*, 17(1):3–21, February 2005.

[141] Bridget S. Wilson, Janet R. Pfeiffer, Zurab Surviladze, Elizabeth A. Gaudet, and Janet M. Oliver. High resolution mapping of mast cell membranes reveals primary and secondary domains of fcϵRI and LAT. *The Journal of Cell Biology*, 154(3):645–658, August 2001.

[142] Travis J. Crites, Kartika Padhan, James Muller, Michelle Krogsgaard, Prabhakar R. Gudla, Stephen J. Lockett, and Rajat Varma. TCR microclusters pre-exist and contain molecules necessary for TCR signal transduction. *Journal of Immunology*, 193(1):56–67, July 2014. WOS:000338438900010.

[143] Lakshmi Balagopalan, Valarie A. Barr, and Lawrence E. Samelson. Endocytic events in TCR signaling: focus on adapters in microclusters. *Immunological Reviews*, 232:84–98, November 2009. WOS:000271057600008.

[144] David J Williamson, Dylan M Owen, Jérémie Rossy, Astrid Magenau, Matthias Wehrmann, J Justin Gooding, and Katharina Gaus. Pre-existing clusters of the adaptor lat do not participate in early t cell signaling events. *Nature Immunology*, 12(7):655–662, June 2011.

[145] Lakshmi Balagopalan, Valarie A. Barr, Robert L. Kortum, Anna K. Park, and Lawrence E. Samelson. Cutting edge: cell surface linker for activation of t cells is recruited to microclusters and is active in signaling. *Journal of Immunology (Baltimore, Md.: 1950)*, 190(8):3849–3853, April 2013.

[146] Michael Dustin. Faculty of 1000 evaluation for pre-existing clusters of the adaptor lat do not participate in early t cell signaling events. Technical report, September 2011.

[147] Helena Soares, Ricardo Henriques, Martin Sachse, Leandro Ventimiglia, Miguel A. Alonso, Christophe Zimmer, Maria-Isabel Thoulouze, and Andrés Alcover. Regulated vesicle fusion generates signaling nanoterritories that control t cell activation at the immunological synapse. *The Journal of Experimental Medicine*, 210(11):2415–2433, October 2013.

[148] C. K. Yee, M. L. Amweg, and A. N. Parikh. Membrane photolithography: Direct micropatterning and manipulation of fluid phospholipid membranes in the aqueous phase using deep-UV light. *Advanced Materials*, 16(14):1184–1189, July 2004.

[149] James H. Hurley and Phyllis I. Hanson. Membrane budding and scission by the ESCRT machinery: it's all in the neck. *Nature Reviews Molecular Cell Biology*, 11(8):556–566, August 2010. WOS:000280201100012.

[150] Daniel P. Nickerson, Matthew West, Ryan Henry, and Greg Odorizzi. Regulators of vps4 ATPase activity at endosomes differentially influence the size and rate of formation of intralumenal vesicles. *Molecular Biology of the Cell*, 21(6):1023–1032, March 2010.

[151] Daniel P. Nickerson, Matthew West, and Greg Odorizzi. Did2 coordinates vps4-mediated dissociation of ESCRT-III from endosomes. *The Journal of Cell Biology*, 175(5):715–720, December 2006.

[152] S. E. Rieder, L. M. Banta, K. Köhrer, J. M. McCaffery, and S. D. Emr. Multilamellar endosome-like compartment accumulates in the yeast vps28 vacuolar protein sorting mutant. *Molecular Biology of the Cell*, 7(6):985–999, June 1996.

[153] Monika Bajorek, Heidi L. Schubert, John McCullough, Charles Langelier, Debra M. Eckert, William-May B. Stubblefield, Nathan T. Uter, David G. Myszka, Christopher P. Hill, and Wesley I. Sundquist. Structural basis for ESCRT-III protein autoinhibition. *Nature Structural & Molecular Biology*, 16(7):754–762, July 2009.

[154] Ricardo Pires, Bettina Hartlieb, Luca Signor, Guy Schoehn, Suman Lata, Manfred Roessle, Christine Moriscot, Sergei Popov, Andreas Hinz, Marc Jamin, Veronique Boyer, Remy Sadoul, Eric Forest, Dmitri I. Svergun, Heinrich G. Göttlinger, and Winfried Weissenhorn. A crescent-shaped ALIX dimer targets ESCRT-III CHMP4 filaments. *Structure (London, England: 1993)*, 17(6):843–856, June 2009.

[155] Suman Lata, Guy Schoehn, Ankur Jain, Ricardo Pires, Jacob Piehler, Heinrich G. Gottlinger, and Winfried Weissenhorn. Helical structures of ESCRT-III are disassembled by VPS4. *Science (New York, N.Y.)*, 321(5894):1354–1357, September 2008.

[156] Phyllis I. Hanson, Robyn Roth, Yuan Lin, and John E. Heuser. Plasma membrane deformation by circular arrays of ESCRT-III protein filaments. *The Journal of Cell Biology*, 180(2):389–402, January 2008.

[157] Ian Fyfe, Amber L. Schuh, J. Michael Edwardson, and Anjon Audhya. Association of the endosomal sorting complex ESCRT-II with the vps20 subunit of ESCRT-III generates a curvature-sensitive complex capable of nucleating ESCRT-III filaments. *Journal of Biological Chemistry*, 286(39):34262–34270, September 2011.

[158] Santosha Vardhana, Kaushik Choudhuri, Rajat Varma, and Michael L. Dustin. Essential role of ubiquitin and TSG101 protein in formation and function of the central supramolecular activation cluster. *Immunity*, 32(4):531–540, April 2010.

[159] Kaushik Choudhuri, Jaime Llodrá, Eric W. Roth, Jones Tsai, Susana Gordo, Kai W. Wucherpfennig, Lance C. Kam, David L. Stokes, and Michael L. Dustin. Polarized release of t-cell-receptor-enriched microvesicles at the immunological synapse. *Nature*, advance online publication, February 2014.

[160] Chong Xie, Lindsey Hanson, Yi Cui, and Bianxiao Cui. Vertical nanopillars for highly localized fluorescence imaging. *Proceedings of the National Academy of Sciences*, 108(10):3894–3899, March 2011.

[161] Simon J. Davis and P. Anton van der Merwe. The kinetic-segregation model: TCR triggering and beyond. *Nature Immunology*, 7(8):803–809, 2006.

[162] Claudine Irles, Antony Symons, Frédérique Michel, Talitha R. Bakker, P. Anton van der Merwe, and Oreste Acuto. CD45 ectodomain controls interaction with GEMs

and lck activity for optimal TCR signaling. *Nature Immunology*, 4(2):189–197, February 2003.

[163] Kaushik Choudhuri, David Wiseman, Marion H. Brown, Keith Gould, and P. Anton van der Merwe. T-cell receptor triggering is critically dependent on the dimensions of its peptide-MHC ligand. *Nature*, 436(7050):578–582, July 2005.

[164] Jeff Bezanson, Alan Edelman, Stefan Karpinski, and Viral B. Shah. Julia: A fresh approach to numerical computing. *arXiv:1411.1607 [cs]*, November 2014.

[165] Jeff Bezanson, Stefan Karpinski, Viral B. Shah, and Alan Edelman. Julia: A fast dynamic language for technical computing. *arXiv:1209.5145 [cs]*, September 2012.

[166] Jeff Bezanson, Jiahao Chen, Stefan Karpinski, Viral Shah, and Alan Edelman. Array operators using multiple dispatch: A design methodology for array implementations in dynamic languages. In *Proceedings of ACM SIGPLAN International Workshop on Libraries, Languages, and Compilers for Array Programming*, ARRAY'14, pages 56:56–56:61, New York, NY, USA, 2014. ACM.

Appendix A

Consideration on image processing platforms

There are various platforms that are convenient quantitative analysis of fluorescence images of cells and visualization of the analysis results. Among those, I discuss Fiji/ImageJ, Matlab. Numpy/Scipy, and Julia below.

Fiji/ImageJ

This free, cross-platform software is arguably the most comprehensive platform for image processing with a large collection of built-in and third party image processing functions available. Scripting allows you to use virtually all functions of Fiji. Jython (a variant of Python running on Java environment), JRuby, JavaScript, etc. are supported for scripting.

The disadvantage is that there are not many resources you can find online. You will also have to translate the API JavaDoc to each language when you use Fiji APIs in the script. In addition, Fiji lacks a graph drawing capability. Full-scale numerical computation is tricky.

Matlab

Matlab is a language and execution environment with a powerful set of matrix calculation capabilities. As digital images are represented as matrix, Matlab has a long history of use in biological imaging study. It has been used by many papers on biological image processing algorithms, including u-track software[114] we used in Chapter 2. Matlab has a convenient GUI of a variable inspector and debugger, which are completely missing in all the other platforms described here. A few disadvantages of Matlab are: (1) Matlab functions are very poor for common tasks other than numerical data processing, e.g. file I/O, string operations, etc. (2) Language syntax and design are outdated, and I believe ergonomics of the language (i.e. programmer productivity) is lower than

modern languages such as Python and Ruby.

Matlab has DipImage (http://www.diplib.org/), a package for biological image processing. DipImage appears to be powerful, although I was not able to install it on my Mac.

Numpy/Scipy (Python)

Numpy is a numerical computation library in Python to offer a matrix computation capability. Numpy's matrix API resembles Matlab. The original version of Numpy, named Numeric, was first released in 1995. Scipy is a scientific computation library that works on top of Numpy. The core of these libraries is written in C and fast. There are many online resources of Numpy/Scipy, which suggests it has a large user base. The biggest advantage of using Python is that there is a huge amount of resources online to solve common issues. Matplotlib on Python is a graph drawing library that can be used seamlessly with Numpy.

Julia

Julia is an emerging scientific computing language (open-sourced in 2012).[164–166] It runs very fast, and the language design is clean, easy-to-use, and modern. Julia has a big momentum in library development driven by an open-source community, as there are >500 libraries available at the central repository. The disadvantages are: (1) There is still a very limited set of libraries for image processing. (2) The language and libraries are still changing very rapidly, which causes problems in maintainability of old code.

Appendix B

Scripts for image analysis

The following scripts are also available at:
https://github.com/hirokai/Dissertation/tree/master/tex/code.

Listing B.1: Line scan of LAT intensity (Fiji Jython macro)

```
# Fiji Jython macro

# Dependencies should be copied to $FIJI_ROOT/scripts folder.
# (1) Microjson: https://github.com/phensley/microjson
# Copy is here: https://gist.github.com/hirokai/2fc4353cf6b28e5d2aac
# (2) hiroutil.py: https://gist.github.com/hirokai/77779cdade6d33d0702b

from ij import IJ
from ij.gui import Line, ProfilePlot
import csv
import os

# http://fiji.sc/Jython_Scripting#Importing_other_.py_scripts_.28modules
    .29
from sys import path
from java.lang.System import getProperty

# extend the search path by $FIJI_ROOT/scripts
path.append(getProperty('fiji.dir') + '/scripts')

import microjson
from hiroutil import *

# base = '/Volumes/Groves/Scope 7/'
base = '/Volumes/MacintoshHD/Google Drive/Groves/Scope 7/'
tsv_path = base + '20150214 LAT-EGFP T cells on PLL-PEG-biotin pattern
    TCR labeled/process/20150214 LAT-EGFP T cells on PLL-PEG-biotin - Line
     scan of images.tsv'
```

```
out_path_base = base + '20150214 LAT-EGFP T cells on PLL-PEG-biotin
    pattern TCR labeled/process/linescan/20150214 linescan'


def parse_row(row):
    vs = row[0:2]+map(mayint,row[2:13])
    if len(row) > 13:
        xys = filter(lambda v: v is not None, map(mayint,row[13:]))
        vs = vs + ([xys] if len(xys) > 0 else [None])
    else:
        vs = vs + [None]
    return vs


def process(name, folder, ch, frm, to, interval, w, h, x, y, xs, ys):
    frames = to - frm + 1 # Or custom number of frames.
    in_path = '%s20150214 LAT-EGFP T cells on PLL-PEG-biotin pattern TCR
        labeled/%s'%(base,folder)
    imp = read_sequence(in_path)
    take_slices(imp,range(3-ch,1000,2)[frm-1:to])
    remove_scale(imp)
    crop(imp,w,h,x,y)

    IJ.run(imp,"Green" if ch == 1 else "Red","");
    imp.setTitle(folder + '_' + ("Green" if ch == 1 else "Red"))
    vs = transpose(map_slices(linescan_poly(xs,ys),imp))

    out_path = out_path_base + '_' + name + '_' + ("Green" if ch == 1
        else "Red") + '.tsv'
    out_path_condition = out_path_base + '_' + name + '_' + ("Green" if
        ch == 1 else "Red") + '_condition.tsv'

    write_tsv(out_path, vs)

    metadata_path = os.path.join(in_path,'metadata.txt')
    f = open(metadata_path,'r')
    json_data = f.read()
    f.close()
    obj = microjson.from_json(json_data)
    uuid = obj['Summary']['UUID']
    write_tsv(out_path_condition,
        [['Image folder', 'UUID', 'Name', 'Subfolder',
        'ch', 'Frame start', 'Frame end', 'Crop X', 'Crop Y', 'Crop W', '
            Crop H',
        'Line xs', 'Line ys'],
        [in_path, uuid, name, folder, ch, frm, to, x, y, w, h,
            ';'.join(map(str,xs)),';'.join(map(str,ys))]])


def do_set(count,prev_args,fc, folder, x, y, w, h, frm,to,interval,x1,y1,
    x2,y2,xys):
```

```
    print(x)
    if x is None:
        fc, folder, x, y, w, h = prev_args
    else:
        prev_args = fc, folder, x, y, w, h
    name = folder.replace('/','_') + str(count)
    count += 1
    xs = [x1,x2]+ (xys[0::2] if xys else [])
    ys = [y1,y2]+ (xys[1::2] if xys else [])
    process(name, folder, 1,frm,to,interval,w,h,x,y,xs,ys)
    process(name, folder, 2,frm,to,interval,w,h,x,y,xs,ys)
    return count,prev_args


def main():
    datasets = map(parse_row, load_tsv(tsv_path))
    count = 1
    prev_args = None
    for ds in datasets:
        print(ds)
        count,prev_args = do_set(count,prev_args,*ds)

main()
print('Done.')
```

Listing B.2: Time-lapse line scan of LAT intensity (Python with Matplotlib)

```
# plot_linescan.py: Standalone (not Fiji) script

import matplotlib.pyplot as plt
from pylab import axes
import numpy as np
import csv
import os

base = '/Volumes/Groves/Scope 7'
folder_of_date = '20150214 LAT-EGFP T cells on PLL-PEG-biotin pattern TCR
    labeled'

# Line scan results were generated by linescan.fiji.py
datasets = [
    # file name, output name, interval, [vmin,vmax] (optional)
    ['20150214 linescan_03 FC3_01 cells_1_Pos81_Green','FC3 Pos8_1_LAT'
       ,46,None]
    , ['20150214 linescan_03 FC3_01 cells_1_Pos81_Red','FC3 Pos8_1_TCR'
       ,46,None]
]


for ds in datasets:
    name = ds[0]
```

```
    csv_path = os.path.join(base, folder_of_date, 'process/linescan/',
       name+'.tsv')
    vs = []

    with open(csv_path,'rU') as f:
        reader = csv.reader(f,delimiter='\t')
    #   times = map(float,reader.next())
        for row in reader:
            vs.append(map(float,row))

    vs = np.array(vs)
    interval = ds[2]
    duration = interval*(len(vs[0])-1)
    times = np.arange(0,duration+interval,interval)
    linelength = 0.143 * len(vs) # Checked on 2/23/2015. See "20150223
       Scope 7 pixel calibration" spreadsheet.
    aspect = 7

    plt.xlabel('Time [sec]')
    plt.ylabel('Coordinate [um]')
    if ds[3]:
        plt.imshow(vs, aspect=aspect, interpolation='bilinear', extent
           =[0,17*(len(vs[0])-1),0,linelength],vmin=ds[3][0],vmax=ds
           [3][1])
    else:
        plt.imshow(vs, aspect=aspect, interpolation='bilinear', extent
           =[0,17*(len(vs[0])-1),0,linelength])
    out_path = os.path.join(base, folder_of_date, 'process/linescan/', ds
       [1]+'.png')
    plt.savefig(out_path)
#   plt.show()
```

Listing B.3: Utility functions for common image processing tasks (Fiji Jython macro). This also exemplifies how to use Fiji APIs from Jython. The latest version of the source code is hosted at https://github.com/hirokai/FijiScriptingTools

```
# hiroutil.py

from ij import ImageStack, IJ


def load_stack(w,h,paths):
    stk = ImageStack(w,h)
    for path in paths:
        ip = IJ.openImage(path).getProcessor()
        stk.addSlice(ip)
    return stk


# Loading a tab-separate file (TSV) with n skipping rows.
# n (>= 1) must be put in the first column in the first row.
def load_tsv(path):
```

```
    import csv
    f = open(path,'rU')
    rows = []
    reader = csv.reader(f,delimiter='\t')
    skipping = int(reader.next()[0])
    for _ in range(skipping-1):
        reader.next()
    for row in reader:
        rows.append(row)
    f.close()
    return rows


def write_tsv(path,rows):
    import csv
    f = open(path,'wb')
    print('Writing: %s'%path)
    writer = csv.writer(f,delimiter='\t')
    for row in rows:
        writer.writerow(row)
    f.close()


def read_sequence(path):
    from ij.plugin import FolderOpener
    return FolderOpener().openFolder(path)


# imp: ImagePlus
# slices: a list of slice indices (1-based)
def remove_slices(imp,slices):
    stk = imp.getStack()
    slices = sorted(slices, reverse=True)
    num_slices = stk.getSize()
    for s in slices:
        if s <= num_slices:
            stk.deleteSlice(s)
    return imp


# imp: ImagePlus
# slices: a list of slice indices (1-based)
def take_slices(imp,slices):
    stk = imp.getStack()
    num_slices = stk.getSize()
    slices = diff(range(1,num_slices+1), slices)
    slices = sorted(slices, reverse=True)
    remove_slices(imp,slices)
    return imp
```

```
def map_slices(func,imp,slices=None):
    stk = imp.getStack()
    num_slices = stk.getSize()
    if slices is None:
        slices = range(1,num_slices+1)
    res = []
    for s in slices:
        imp.setSlice(s)
        res.append(func(imp))
    return res


def linescan(x1,y1,x2,y2):
    from ij.gui import Line,ProfilePlot
    def f(imp):
        line = Line(x1,y1,x2,y2)
        imp.setRoi(line)
        vs = ProfilePlot(imp).getProfile()
        imp.killRoi()
        return vs
    return f


def linescan_poly(xs,ys):
    def f(imp):
        from ij.gui import Line, Roi, ProfilePlot, PolygonRoi
        if len(xs) > 1:
            print(xs,ys)
            line = PolygonRoi(xs,ys,len(xs),Roi.POLYLINE)
            imp.setRoi(line)
        else:
            line = Line(xs[0],ys[0],xs[1],ys[1])
            imp.setRoi(line)
        vs = ProfilePlot(imp).getProfile()
        imp.killRoi()
        return vs
    return f


def remove_scale(imp):
    IJ.run(imp,"Set Scale...", "distance=0 known=0 pixel=1 unit=pixel");


def crop(imp,w,h,x,y):
    IJ.run(imp,"Specify...", "width=%d height=%d x=%d y=%d"%(w,h,x,y))
    IJ.run(imp,"Crop","")
    return imp


#
# List functions
```

```
#

def transpose(xss):
    return [list(i) for i in zip(*xss)]


def diff(a, b):
    b = set(b)
    return [aa for aa in a if aa not in b]


#
# Utility
#


def mayint(s):
    try:
        r = int(s)
    except:
        r = None
    return r
```